Toward a sustainable future: Investigating the nanocrystalline structure and properties of C-(N)-A-S-H gels.

Theodosios Dimitrasopoulos

May 2017

Submitted in partial fulfillment

of the requirements for the degree of

Bachelor of Science in Engineering

Department of Civil and Environmental Engineering

Princeton University

Abstract

The dire need for sustainability and environmental protection, as well as the recent environmental degradation around the planet, makes increasing efforts towards alternative binder systems in concrete a necessary step in tackling one of the biggest sources of CO_2 emissions worldwide. The nanocrystalline structure of calcium (-sodium) aluminosilicate hydrate (C-(N)-A-S-H) gels and their occurrence in various alkali-activated cements has been contested in past decades. Various claims have been made about the similarities between calcium silicate hydrate in ordinary Portland cement (OPC) systems and such gels, but the differences in the nano-scale structures as well as their chemical properties cannot be overlooked. In this investigation, a combination of X-ray diffraction (XRD), pair distribution function analysis (PDF), attenuated total reflectance (ATR) - Fourier transform infrared spectrometry (FTIR) and thermogravimetric analysis (TGA) was deployed to offer a more holistic understanding of the structural properties of gels. It is shown that C-(N)-A-S-H follows well-ordered patterns in short-ranges, and sodium (in the form of an alkaline solution) is catalytic for the definition of the nanocrystalline structure over time. The elucidation of such similarities and differences can influence the macroscale material properties of the gels, such as durability and weather resistance of alkali-activated cements.

Contents

List of Figures

Acknowledgments

I would like to extend my most sincere gratitude to the following individuals and institutions, without whose support and patience I would not have managed to be where I am today:

To my family Ευαγγελία, Τατιάνα, Σίσσυ, Σάκη, Φένια, Κώστα, Αντώνη and Βέτα. They managed to see to my success from 5000 miles away, a truly admirable accomplishment for which I owe them my life.

To my advisor, Claire White. She introduced me to the study of materials my sophomore year as my professor and then guided me through this colossal task with immense patience and wisdom. It is my greatest pleasure to have met and worked with such an exciting and excitable presence, and to have made a friend in the process.

To Terrace F. Club, without which my time in college would be of very little value. An institution of its own accord, Terrace was crucial to my well-being and helped me form friendships and have conversations that will last a lifetime. I gave my life to her, and that is

still not enough. Thank you mother. FOOD=LOVE

To my confidantes, partners in crime and the best friends I have made who shaped my character to the core; Bennett, thank you for always being the positive force of the crew, without whose snarky and witty humor we'd all be doomed; David, thank you for being my true brother, one and the same, an equal; Kafkas, thank you for being the voice of reason in unreasonable situations, the wisest of all and the one who sees through every situation I didn't have the foresight and ability to comprehend; Kei, thank you for your showing me patience and dedication to your work and the people you love; Nicholas, I thank you for your presence and dedication to the passions that we share. You eloquence, logic and beautiful sarcasm among many other traits made you an inspirational figure in my life and one that will always be in ingrained in my memory. You have all helped me become who I am today. I am forever grateful for your friendship and will always be by your side.

To Emma, the first person I met here who proved to be one of my closest friends. No matter the distance, we'll always be together. Thank you for always being there for me and seeing me at my best and worst with the same compassion, kindness and understanding.

To all my fellow Greeks, who made me feel like home in a land so different and bizarre. I am forever in your debt. *Σας αγαπώ!*

To Natalia Chen, the fiercest, wisest woman I know, who I will idolize for the rest of my life;

To Caitlin Miller: thank you for letting me be part of your exciting life, I can't wait to see what the future holds for us in Manhattan and beyond;

To Benjamin Gallo: thank you for all the late nights, the intellectual conversations and your company even since freshman year;

To Yankia Ned: thank you for your empathy, selflessness and shining glamor that perpetually radiate outwards;

To Joe Bonacci, a truly compassionate friend whose good conversation I will always savor. Thank you for showing me what it means to be a human.

and finally, Nadeem Demian, thank you for offering me the gift of your company. I feel extremely lucky to have met you this year. It is an honor and a privilege to have shared my time with you and I hope our lives will forever be linked long after we leave Princeton.

0

Introduction

ADVERSE ENVIRONMENTAL CONDITIONS in conjunction with the slow detachment of government entities from issues of sustainability and environmental protection call for increasing efforts and advocacy towards alternative binder systems in concrete construction, a decisive step in tackling one of the biggest sources of CO_2 emissions worldwide. The use of

supplementary cementitious materials (SCMs) can contribute to the reduction of ordinary Portland cement (OPC) content from concrete mixes, but are limited by the supersaturated solution's ability to activate the SCM[19]. Use of alkali activated materials (AAMs) in place of such mixes however is a promising direction in increasing their efficacy[19].

The presence of sodium- and aluminum- enriched calcium silicate hydrate i.e. C-(N)-A-S-H (a main reaction product in AAMs) introduces more complex thermodynamic and chemical performances[34].As elucidated in detail in Lodeiro et al.[19], aluminate species potentiate the polymerization process via formation of tetrahedra between silicate units[19]. Also, alkalis play a crucial role in the 3-dimensional nature of C-(N)-A-S-H gels, since the aluminum-induced tetrahedra are more densely linked, ultimately leading to faster and more efficient dissolution of the aluminosilicate in the binder[19]. Therefore understanding this phase can even lead to higher performance materials, as opposed to only more sustainable ones.

The C-(N)-A-S-H phase is extremely complex to study, and careful manipulation along with high-accuracy equipment is needed to identify the nanocrystalline structures within the disordered gel. In addition, the significant differences in the structure of ordinary Portland cement (OPCs) make the identification of the common grounds between them necessary. Despite its complex nature, C-(N)-A-S-H is heavily studied and numerous investigations have taken place to characterize it. However, these investigations disagree with

each other on numerous occasions, mainly due to non-holistic investigations i.e. performing measurements with only one technique or allowing for multiple unconstrained parameters[34]. Therefore, a more encapsulating investigation that yields complementing results can offer insight on the exact nanonanocrystalline structure and chemical properties of the gel. In this investigation, X-ray diffraction and pair distribution function analysis cross-referenced with thermogravimetric analysis and attenuated total reflectance-Fourier transform infrared spectrometry (ATR-FTIR) was deployed in order to understand the molecular structure, the influence of NaOH and aluminum in the mix and the changes incurred on the whole structure across a 3-month span. It is hypothesized that alkali activation initiates changes in the nanonanocrystalline structure very early on (as soon as 10 days after mixing) and that changes incurred in the atomic arrangement of the C-(N)-A-S-H gel due to the introduction of alkali and aluminum is derived logically from its less complex counterparts i.e. N-A-S-H (sodium-only-substituted C-S-H gel), C-A-S-H (aluminum-only-substituted C-S-H gel) and C-S-H. To further elucidate on the latter, it is expected that C-(N)-A-S-H gels will be expressing structural similarities to the aforementioned phases, and their differences will be the second main topic of this investigation, along with the influence of age on the samples.

1

Literature Review

1.1 Introduction to Cement Chemistry

Calcium Silicates offer a vast range of intricacies (Table 1.2) in their structural morphology[4]. This umbrella term includes all crystalline structures that occur naturally within the mix by the hydration of tricalcium silicate (C_3S) or β—dicalcium silicate ($\beta - C_2S$) at ap-

proximately 75% of the total Portland cement[4]. Table 1.1 shows the conventions used to represent the various phases we will be discussing[32]; The following is the reaction process of production of Ordinary Portland Cement (OPC) is estimated to generate $5 - 8\%$ of the total humanmade greenhouse gas emissions globally[33].

The French chemist Henry Louis Le Chatelier first elaborated the hydration process in cement[32]. It starts with dissolution where, the cement releases ions into the water mix[32]. The resulting ionic H_2O mix is called the pore solution, which contains highly soluble ions from C_3S and $C_3\mathcal{A}$ that increase as the cement and water are combined[32]. Precipitation occurs when the mix is supersaturated, and the main precipitates are the hydration products, which are control the main properties of concrete (such as strength, porosity etc.). Precipitation also relieves the supersaturation of the mix, thus allowing more ions to be introduced. In this manner, ions dissolve in water and new hydration products (different from the starting chemicals) precipitate in a continuous process mediated by the pore solution as necessary[32].

The hydration process can successfully take place in limited amounts of water[13]. The supersaturated solution aforementioned also contains alkali concentrations, an effect outlined and demonstrated experimentally by Longuet et al., by extracting pore fluid and measuring its alkalinity, which ranged from $0.1 - 1\mathcal{M}$[20]. Some alkali also end up binding with cement paste consituents and changing the internal nanocrystalline structure of the material[13]. In

Table 1.1: Basic Cement Chemistry Notation

Oxide form	Notation
CaO	C
SiO2	S
Al2O3	A
Fe2O3	F
SO3	S
H2O	H

Table 1.2: Various Cement minerals and products during mix binding and gel formation

Chemical Name	Chemical Formula	Oxide Formula	Cement Notation
Tricalcium Silicate	Ca_3SiO5	$3CaO.SiO_2$	C_3S
Dicalcium Silicate	Ca_2SiO_4	$2CaO.SiO_2$	C_2S
Tricalcium Aluminate	$Ca_3Al_2O_6$	$3CaO.Al_2O_3$	C_3A
Tetracalcium Aluminoferrite	Ca_2AlFeO_5	$4CaO.Al_2O_3.Fe_2O_3$	C_4AF
Calcium hydroxide	$Ca(OH)_2$	$CaO.H_2O$	CH
Calcium sulfate dihydrate	$CaSO_4.2H_2O$	$CaO.SO_3.2H_2O$	CSH_2
Calcium oxide	CaO	CaO	C
Calcium Silicate Hydrate	H_2CaO_4Si	$0.6 - 2.0CaO \cdot SiO2 \cdot 0.9 - 2.5H_2O$	C-S-H

the case of alkali-activated binders therefore, the introduction of sodium or potassium allows for interesting properties such as chemical (acid) resistance and high-temperature resistance, along with reductions in CO_2 emissions[26,5].

1.2 Existing Literature

Existing literature covering C-(N)-A-S-H gels focuses on specific aspects of the structure and chemical composition of the material and research that tested multiple parameters at once using a range of instruments is rather limited. Papers covering a singular

aspect of the gel were used to determine the exact chemical composition of the samples synthesized in this study and the literature covering multiple parameters of the C-(N)-A-S-H gels were used to justify the acquired results. L'Hôpital et al.[21] investigate the aluminum uptake of C-S-H gels in the presence and absence of alkalis, in which they provided a Ca/Si ratio of 1.0 and an Al/Si ratio of 0.33. They observed formation of C-A-S-H gels at Al/Si $\leqslant$0.1 and an increase in the free aluminum present in the mix and its subsequent incorporation in the C-A-S-H gel. Additionally, the formation of additional phases such as katoite, stratlingite, AH_3 and other AFm phases limited the aluminum uptake in the C-S-H gel to a ratio of Al/Si $\approx$ 0.1. The addition of alkali in the C-A-S-H mix limited the uptake even further, to Al/Si $\approx$ 0.23, a behavior compatible with other studies of C-A-S-H gels of higher alkalinity forming in Portland cements[1]. L'Hôpital et al.[17] also tested the alkali uptake in C-A-S-H gels of molar Ca/Si and Al/Si ratios of 0.6 - 1.6 and 0 or 0.05 respectively over a 12-month course, and observe how alkalinity affects the nanostructural evolution of the gel. Most notably, there were no significant differences in the uptake of sodium vs. potassium, which ultimately stops at 91 days[17]. L'Hôpital et al thus introduce upper limits in mix design while also delineating a new one, namely one that covers much higher alkalinity and a different combination of molar Ca/Si and Al/Si ratios. Lodeiro et al.[18] introduced higher alkalinity in their experiment, with a 10M NaOH solution to maintain a pH of 13 throughout testing. They performed FTIR analysis -also included in this study- as a means

of quantifying Si interconnectivity in the samples. Different amounts of 8M NaOH was introduced in the samples and characterized with Fourier transform IR spectroscopy[18]. A very important finding, namely the linear relationship between carbonation and alkalinity of samples sheds light on CO_2 peaks appearing in older samples in the series, despite the careful manipulation and transfer in N_2 environments. Kobayashi and Uno[16] exhaustively investigated the carbonation of concrete in relation to alkali content using fast-rate carbonation environments, and their 1990 finding confirms that alkalinity in the mix leads to higher levels of carbonation in concrete. The following describes the exact mechanism of carbonation, suggestive of a close relation with the pore structure in the mix[16]:

$$Ca(OH)_2 + CO_2 = CaCO_3 + H_2O \tag{1.1}$$

or, if rewritten using the ions responsible for the carbonation:

$$Ca^{2+} + CO_3^{2-}(orHCO_3^-) \rightarrow CaCO_3 \tag{1.2}$$

Finally, Black et al.[3] explore the effects of carbonation of C-S-H gels using Raman spectroscopy and X-ray diffraction. The novelty of the experiment is in the subsequent result, in which they concluded that the type and extent of carbonation are tied to the CaO/SiO2 (Ca/Si) ratio of the original samples[3]. Calcium carbonate crystallizes, over time, to give pri-

marily vaterite at Ca/Si$\geq$0.67 and aragonite at Ca/Si$\leqslant$0.50[3](not relevant in this study). C-A-S-H phases with Ca/Si ratios $\geq$0.75 proved to be the most resistant to carbonation[3], which was incorporated in the current experiment. With that in mind, significant steps to prevent carbonation of samples were taken, such as N_2 glovebox environments during handling and transfer of materials and the use of N_2 gas for the sample atmosphere during thermogravimetric analysis.

Calcium silicate hydrate (C-S-H) is the largest cement reaction product by volume, occupying 50% of the total paste[32]. The continuous matrix of gel spreads across the entire cement paste and forms tiny pores in its main body called gel pores[32]. The ability of C-S-H to contribute to the overall strength of cement can be observed on the nanometer-scale structures it forms[32]. And, at that scale, the intricacy of the structures makes understanding the exact mechanisms a daunting task.

The alkaline activation of silica- and alumina- rich materials is less understood than that of slag since research has not been ongoing for as long as the latter[8]. A mechanism suggested by Glukhovsky in 1994 proposing a 3-stage reaction:

- destruction-coagulation: OH^- ions in the alkaline activator break the Si-O-Si bonds[8]. This process yields silanol (-Si-OH) and sialate ($-Si-O^-$) species[8]. The alkaline cations neutralize the charges and the formation of $Si?O?^?Na^+$ bonds prevents the reversion to siloxane (Si?O?Si)[8].

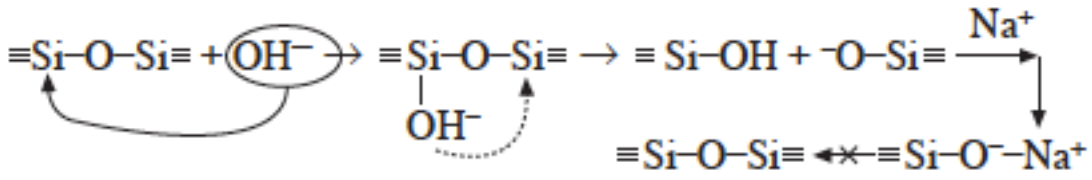

Figure 1.1: Destruction-coagulation schematic. Adapted from [7].

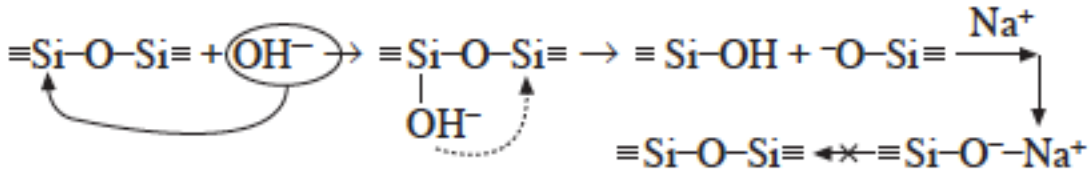

Figure 1.2: Destruction-coagulation schematic. Adapted from [7].

- coagulation-condensation: Coagulation of structures occurs via accumulation of ionic species that brings the disaggregated products closer together[8]. Monomeric silica forms dimers via new Si-O-Si bond formation, which gives rise to silica polymers (all assisted by OH^- catalysis[8]. These clusters subsequently grow into larger structures called colloids[8]. Finally, the aluminates assist the polymerization process, replacing silicon tetrahedra[8].

- condensation-crystallization: This stage is dominated by further product precipitation, by nature of particles being present in the initial solid phase[8].

However, this model was revised by Palomo et al. and then Fernandez-Jimenez et al in 2005 and it described the alkaline activation of fly ash based on zeolite synthesis[8]. The two stages in this process are as follows:

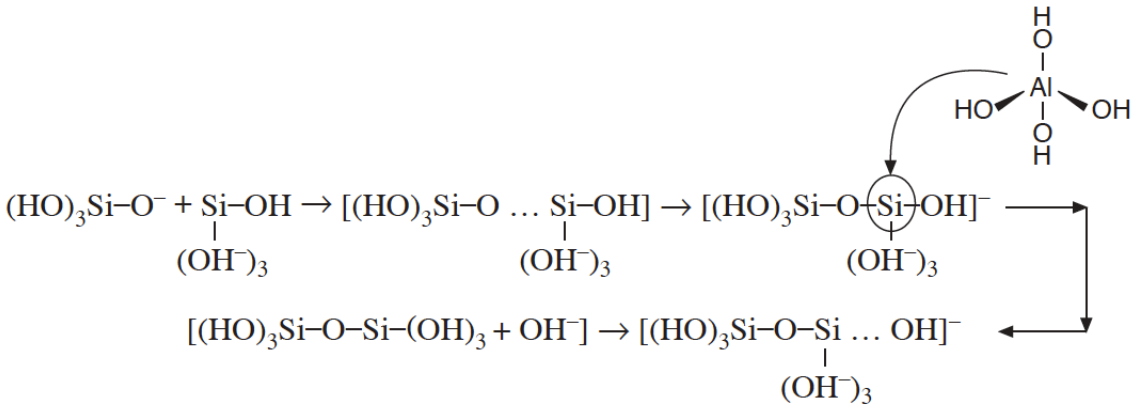

Figure 1.3: Coagulation-condensation schematic. Adapted from [7].

1. nucleation or the dissolution of the aluminates via polymerization(covering both stages in the Glukhovsky model)[8];

2. growth of crystals when nuclei reach a critical point. The alkaline activation of fly ash yields an amorphous matrix of an aluminosilicate gel called N?A?S?H gel[8], also known as alkaline inorganic polymer (AIP)[8]. Its silicon and aluminium tetrahedra are randomly distributed in a 3-dimensional structure[8].

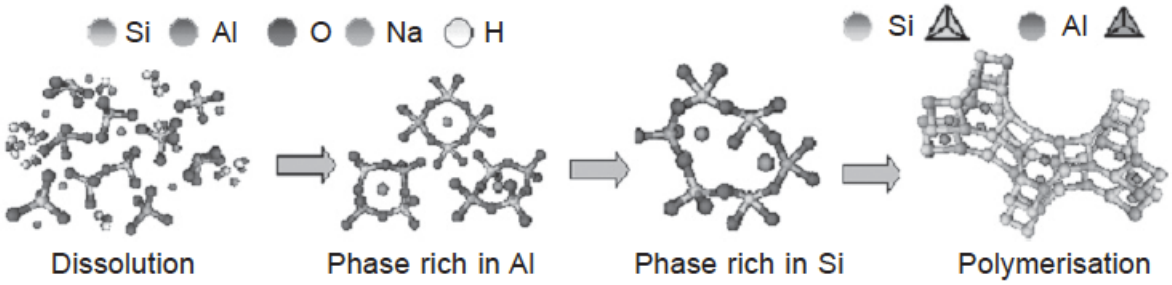

Figure 1.4: Model of N-A-S-H gel formation, proposed by Fern?ndez-Jim?nez et al. , 2005b and revised by Shi et al., 2011. Adapted from [7].

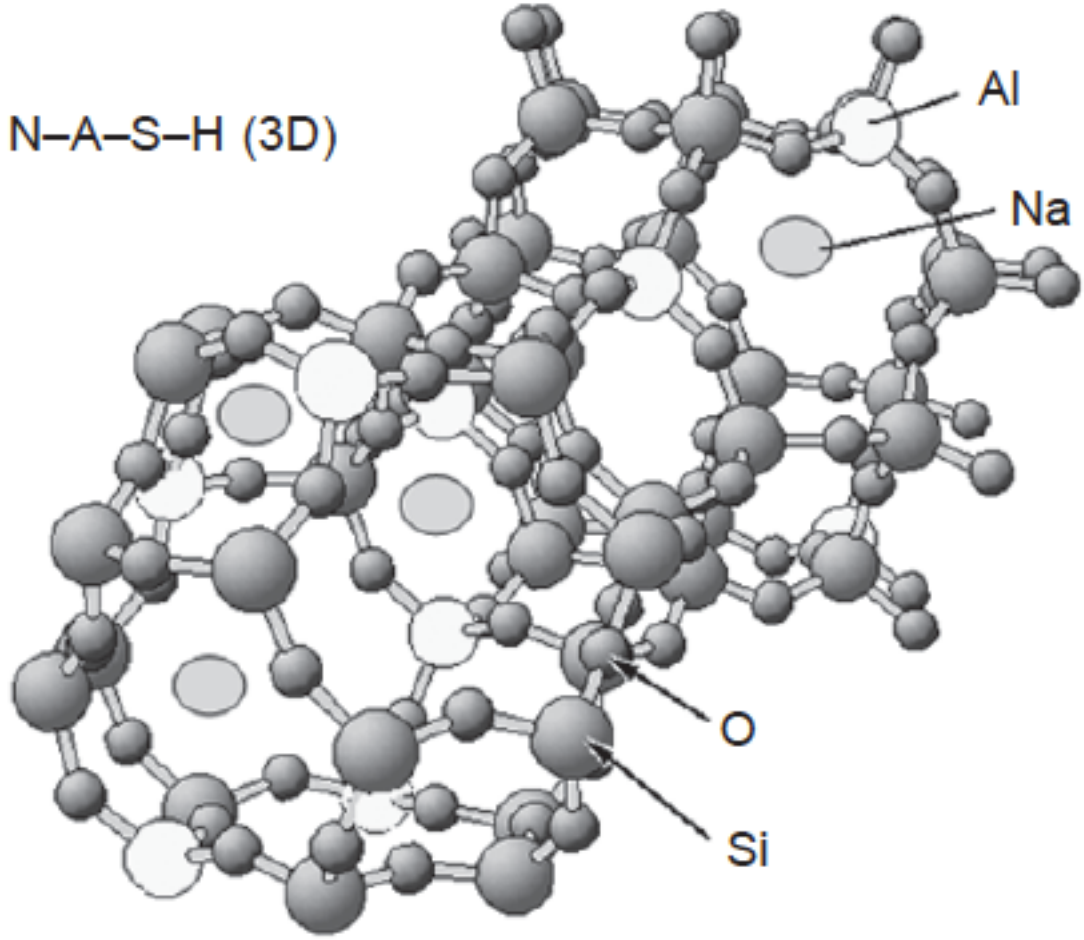

Figure 1.5: Molecular structure of N-A-S-H gel. Adapted from [7].

Finally, the main reaction product forming in slag-based alkaline cements is an aluminium-containing calcium silicate hydrate (C-A-S-H gel)[8]. This gel is reminiscent of the reaction products observed in Portland cement hydration, but with a lower Ca/Si ratio[8]. C-A-S-H gel ratios usually range from 0.9 to 1.2[8].

The final study that informed the FTIR processes followed in the current investigation is the exploration of the compatibility between C-S-H and N-A-S-(H) gels as products of Portland Cement hydration and alkali activation of fly ash respectively[10]. And, as with other research investigating the effects of alkalinity on the gels, the pH level was found to play a determinant role in both C-S-H and N-A-S-(H) gel synthesis, with C-S-H gel forming at pH≥11 and N-A-S-(H) gel at pH≥12[10].

With regards to alkali-aluminum interrelationships in the formation of the alkali-activated binders in question, Lodeiro et al.[19] further investigated the simultaneous addition of alkali and aluminum and their interrelated effects on the silica connectivity of the gels. It was shown that silicate polymerization increases by both alkalinity and aluminum addition in the samples and introduces a crystalline calcium aluminosilicate precipitate[19]. However, the sole addition of aluminum and its effects on the structure of C-S-H was not investigated independently of alkalinity changes. Sun et al[31] investigate the role of Al in C-S-H gels using X-ray diffraction, compositional analysis, and 29Si and 27Al MAS NMR spectroscopy on an Al-substituted tobermorite-type C-A-S-H gel. They found that the various coordinations of Al, namely Al[4], Al[5], and Al[6] coordinations contributes to the structural properties of the gel(Fig. 1.6); more specifically Al[4] forms in the drierkette aluminumsilicate chains and Al[5] and Al[6] in the interlayers of the structure[31].

In a more time-based, serial manner, White et. al[36] (2013) investigate the evolution of

metakaolin-based geopolymers in the early stages of gel formation using X-ray distribution function analysis. The method aforementioned sheds light in the specific atom-atom correlation in the gel matrix and its interaction with free elements in the mix under different chemical compositions and alkalinity. The short-scale structural changes of the different chemical systems during the alkali-activation reaction involve both the incorporation of free silica and calcium in the evolving morphology[36]. As an extension to the research above, White et al.[37] determined the short-scale bonding and nano-crystalline structures present in hydrated tricalcium silicate (C_3S), blended C_3S-slag and alkali-activated slag, that illustrated the difference between CSH gels from C_3S and more importantly, C-(N)-A-S-H gel in slags. This provides validity in the study of synthetically-derived gels as a potential replacement for conventional OPC cements, since the differences are actively being investigated and outlined using techniques such as tomography/microdiffraction combinations, post-processed with PDF analysis[37]. Additionally, the elucidation on the impact of mix design provided by the research above indirectly creates the area of study of C-(N)-A-S-H gels that has not been fully investigated i.e. precise alkalinity levels at both extremes. Finally, the density of the data provided by PDF analysis is covered in length and is presented as a main tool for investigating the relationships expounded above.

Even though all of the research above concerns itself with the exact chemical composition and evolution of the gels over time, the precise structure and geometry of the gel

and the pores bridging them is of equal importance. Provis et al.[27] explore the pore network and microstructural characteristics in three dimensions using X-ray microtomography (μCT), using a synchrotron beamline instrument. They found out that increases in slag content and sample age increase tortuosity and reduce porosity, particularly notable in samples with $\geq$ 50% slag content, which is correlated to the presence of a space-filling calcium (alumino)silicate gel[27]. The domination of space-filling C-A-S-H gels occurs within a $25\% \leqslant p \leqslant 50\%$ window, and samples with less than 25% slag content experienced a domination of N-A-S-(H) gels, which do not chemically bind water and induce a smaller degree of pore network obstruction[27].

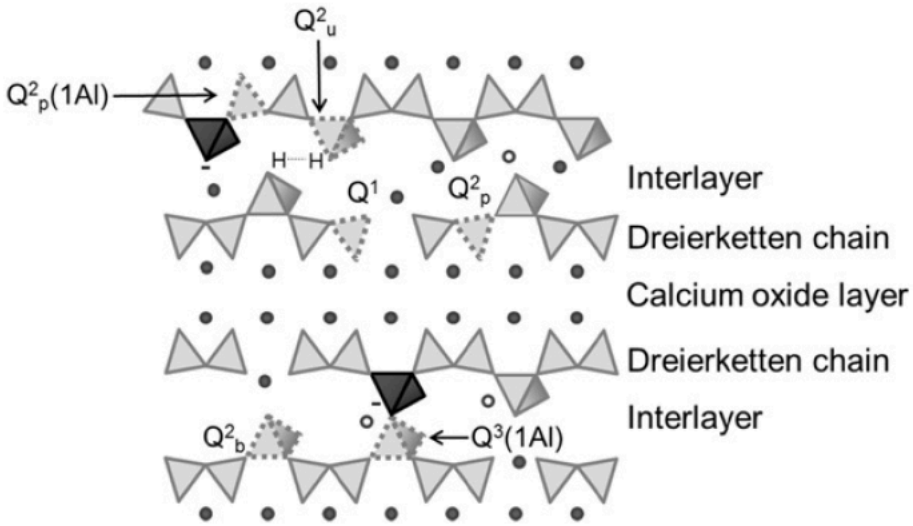

Figure 1.6: Structure of C-A-S-H. Grey circle calcium ion; Empty circle species in the interlayer (water or alkali); Light grey tetrahedra SiO_4, dark grey tetrahedra AlO_4^-; $-$: negative charge (compensated by proton, calcium or other cations). $Q^n_{(mAl)}$ n indicates the numbers of Si neighbors and the number of aluminum neighbours, b: bridging position, p: pairing position.Used notation system from [5].

2

Materials & Methods; Background Theory

2.1 Background theory

2.1.1 X-Ray Diffraction

X-ray diffraction is an ideal analytical technique to characterize crystalline, fine-grained materials[30]. The individual cement phases yielded from the analysis offer insight in the crystal

structural properties of the material under investigation. The crystalline structure diffracts X-rays and produces an XRD pattern of peaks and valleys at specific diffraction angles[30]. The diffraction angle is determined via symmetry and sizing of the unit cell using Bragg's Law,

$$n\lambda = 2dsin\vartheta \tag{2.1}$$

where n is an integer and λ is the wavelength of the incident wave, ϑ is the scattering angle and d is the interplanar distance between Specifically with regards to cements, whether anhydrous or hydrated are present in the material[30]. Therefore, this technique determines the various peaks that appear in the data are indicative of various phases present in the mix[30]. However, this alone is extremely insightful in understanding the exact nanocrystalline structure of the materials and potentially improve upon it.

All of the above are practical considerations based on a concise theoretical model that allows for the implementation of the method using modern, state-of-the-art machinery. Further investigations into improving the measurement tools will allow for more precision and clarity in the results presented in Chapter 4.

2.1.2 Pair Distribution Function Analysis

The pair distribution function (PDF) G(r) (Eq. 2.2) is obtained via a sine Fourier transform of the total scattering function S(Q), with Q being the momentum transfer (Eq. 2.3)[35,7].

$$G(r) = 2/\pi \int_{Q=Q_{min}}^{Q=Q_{max}} Q[S(Q) - 1]sin(Qr)dQ \tag{2.2}$$

$$Q = \frac{4\pi sin\vartheta}{\lambda} \tag{2.3}$$

PDF data is typically obtained using synchrotron radiation due to the need for a high Q_{max}.

2.1.3 Thermogravimetric Analysis

Thermogravimetric analysis is used to identify the amount of bound water and portlandite in the mix and thus follow the reaction of Portland cement or to benchmark the reactivity of supplementary cementitious materials (SCM's)[30]. Its ability to detect X-ray amorphous hydrates (which would not show up in a typical X-ray diffraction measurement due to their lack of a long-range structure) such as $C-S-H$ or AH_3 makes it a suitable complementary method to other measurements such as X-ray diffraction above[30]. The TGA measurement is strongly dependent on the exact conditions present at the time of the experiment, such as

the pan used, the heating vessel, the heat rate, the gas environment etc. This makes it difficult to replicate TGA experiments from one lab in another, but with enough accuracy the results can be replicated within the same lab for multiple samples (as is the case in this investigation).

2.1.4 Attenuated Total Reflectance and Fourier Transform IR Spectroscopy

FTIR Spectroscopy is an extremely useful technique in identifying the kinds of molecules and atomic arrangements present in the sample and their exact amounts. In the same way that TGA uses heat and XRD X-rays, FTIR uses *light*.

Light or electromagnetic radiation is composed of the electric and magnetic vectors (electric and magnetic waves propagating at 90° from each other. The beam hits an interferometer and splits into two paths 4 and 10*cm* and then recombines into a single outgoing beam that is interpreted by the light receiver (Fig 2.1)[29]. More specifically with regards to attenuated total reflectance (used in this investigation), the instrument is based on internal reflectance as shown in Fig. 2.2[29].

Table 2.1: Weight losses and molecular weights for CO_2 and H_2O of relevant cementitious phases [30]

Name	Formula	MẆ (g/mol)	H_2O loss (g/mol)	H_2O (wt.%)	CO_2 loss (g/mol)
Gypsum	CsH_2	172	36	20.9	
Hemihydrate	$CsH_{0.5}$	145	9	6.2	
Anhydrite	Cs	136			
Portlandite	CH	74	18	24.3	
Calcite	Cc	100		44	
Aragonite	Cc	100		44	
Vaterite	Cc	100		44	
Magnesite	Mc	84	44	52.2	
Dolomite	CcMc	184	88	47.7	
High-Ca	C-S-H	C1.5SH2	180	36	20
Low-Ca	C-S-H	CSH1.5	140	27	19.3
Ettringite	$C_6As_3H_{32}$	1255	576	45.9	
Thaumasite	C_3SscH_{15}	623	270	43.4	44
Monosulfate	C_4AsH_{12}	623	216	34.7	
Monocarbonate	C_4AcH_{11}	568	198	34.9	44
Hemicarbonate	$C_4Ac_{0.5}H_{12}$	564	216	38.3	22
Friedel's salt	$C_4ACl_2H_{10}$		561	180	32.1
Kuzel's salt	$C_4ACls_{0.5}H_{12}$		610	216	35.4
Stratlingite	C_2ASH_8	418	144	34.5	
Hydrotalcite	M_4AH_{10}	443	180	40.6	
	C_4AH_{19}	669	342	51.2	
	C_4AH_{13}	560	234	41.8	
Katoite	C_3AH_6	378	108	28.6	
	$C_2AH_{7.5}$	349	135	38.7	
	CAH_{10}	338	180	53.3	
Aluminium hydroxide	AH_3	156	54	34.6	

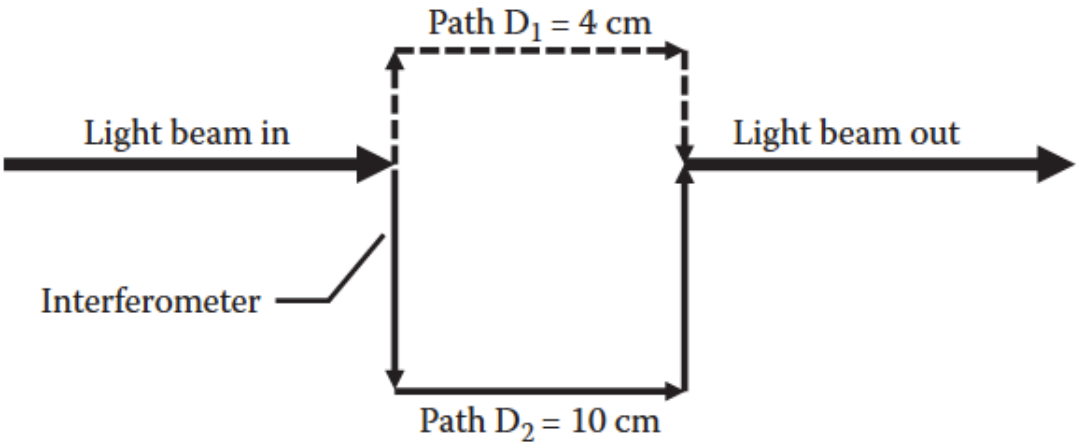

Figure 2.1: Simplified schematic of an interferometer. Adapted from [23].

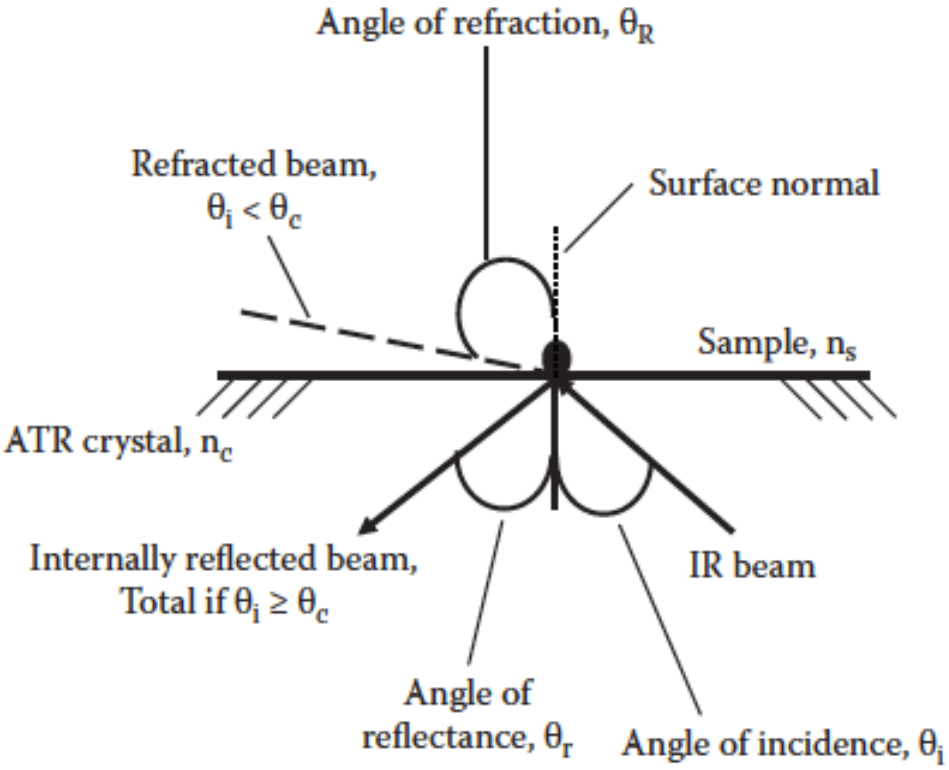

Figure 2.2: Simplified schematic of an internal reflection instrument. ϑ_c is the critical angle. Total internal reflectance takes place when $n_s < n_c$ and $\vartheta_i > \vartheta$[29]. Adapted from [23].

The critical angle ϑ_c mentioned above can be calculated in the following manner:

$$\vartheta_c = sin^{-1}(\frac{n_s}{n_c}) \tag{2.4}$$

The critical angle for diamond is n=2.42 and the material angle will be influencing exactly how much light will penetrate the sample and return back to the receiver, as illustrated in Fig. 2.3.

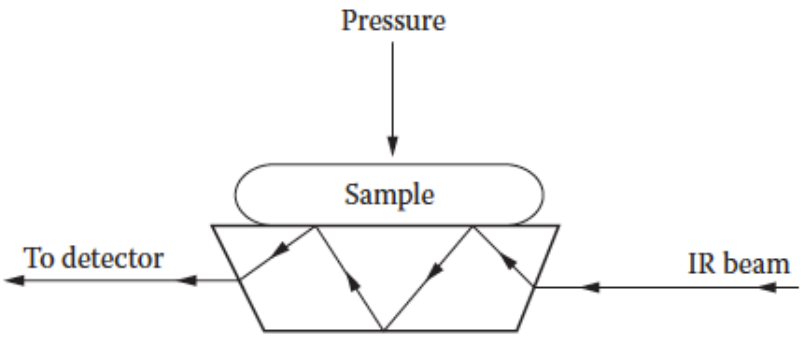

Figure 2.3: Simplified schematic of an ATR crystal. Adapted from [23].

The depth of penetration (Eq. 2.5) contains the final wavenumber W, which is what shows up on a typical ATR-FTIR graph and what is the most important piece of quantitative information in the result.

$$DP = \frac{1}{[2\pi W_n(sin^2\vartheta - n^2 s_c)]^{0.5}} \tag{2.5}$$

Where, DP = Depth of penetration, W = Wavenumber, n_c = Refractive index of ATR crystal, "θ= Angle of incidence and $n_{sc} = \frac{n_{sample}}{n_{crystal}}$

2.2 Materials & Methods

The samples were mixed in an inert environment (N_2 glove box to minimize CO_2 contamination) using a high-accuracy scale to measure the exact quantities of the ingredients

for each sample. Namely, 0.355g of fumed silica powder (SiO_2, 0.2-0.3nm average particle size), 0.263g of calcium hydroxide ($Ca(OH)_2$, 96.0% purity) and 0.049g of sodium aluminate powder ($NaAlO_2$, technical, anhydrous; Composition: 50-56% Al (Al_2O_3) and 40-45% Na (Na_2O)) were used for the 0.5M along with 0.255g, 0.377g and 0.035g of the same ingredients in that order for the 5M samples. NaOH pellets (ACS reagent of 97.0% purity) and distilled H2O were used to create the NaOH solution that was prepared separately and added to each of the sample containers after the main ingredients were mixed. More specifically, 30g of solution were added to each of the sample containers after the NaOH bottle dissolved and cooled down.

Preparation of samples: The ingredients were added in 10z, wide mouth PP bottles (Fisherbrand®) in the order aforementioned and sealed with laboratory film (Parafilm®) to minimize CO_2 infiltration in the mix. The bottles were then placed on an orbital shaker platform that was running for the entirety of the experiment (3 months) at 300 rpm, with samples taken out on the 4, 10-day and 1,2 and 3-month marks. The solids were then separated from the supernatants using two qualitative filter papers (5.5 cm size, VWR®) placed in a porcelain Buchner filter (CoorsTek®60240 Buchner Funnels, Ceramic, 87 mL, 8chr/cs) atop a Erlenmeyer vacuum flask (VWR®, 1000mL with No. 8 stopper) and treated for 2 minutes or until the solids were dry. Finally, they would be left to dry further in the N2 glovebox for five days and then capped and transferred to the appropriate vessels for testing.

The following table summarizes the samples that were measured: (the naming system is as follows: $[sampleidentificationnumber]_[Ca/Siratio]_[alkalinity]$. The Al/Si ratio was not incorporated into the naming system since it is the same across all samples. SiO_2, $NaAlO_2$ and $Ca(OH)_2$ refer to the amount added in each sample in g, NaOH is the final amount of NaOH solution added in each sample in mL & H_2O & NaOH (s) are the amounts required to create a large batch of NaOH, which was subsequently divided into individual 30mL batches for each sample.

Table 2.2: Stoichiometric ratios of the various C-(N)-A-S-H gels analyzed in this thesis.

	Ca/Si	Al/Si	NaOH(M)	SiO_2	$Ca(OH)_2$	$NaAlO_2$	NaOH(mL)	H_2O	NaOH (s)
1a_0.6_0.5M	0.6	0.1	0.5	0.355	0.263	0.049	30	240	4.8
1b_0.6_5M	0.6	0.1	5	0.355	0.263	0.049	30	240	48
1c_1.2_0.5M	1.2	0.1	0.5	0.255	0.377	0.035	30	240	4.8
1d_1.2_5M	1.2	0.1	5	0.255	0.377	0.035	30	240	48
2a_0.6_0.5M	0.6	0.1	0.5	0.355	0.263	0.049	30	240	4.8
2b_0.6_5M	0.6	0.1	5	0.355	0.263	0.049	30	240	48
2c_1.2_0.5M	1.2	0.1	0.5	0.255	0.377	0.035	30	240	4.8
2d_1.2_5M	1.2	0.1	5	0.255	0.377	0.035	30	240	48
3a_0.6_0.5M	0.6	0.1	0.5	0.355	0.263	0.049	30	240	4.8
3b_0.6_5M	0.6	0.1	5	0.355	0.263	0.049	30	240	48
3c_1.2_0.5M	1.2	0.1	0.5	0.255	0.377	0.035	30	240	4.8
3b_1.2_5M	1.2	0.1	5	0.255	0.377	0.035	30	240	48
4a_0.6_0.5M	0.6	0.1	0.5	0.355	0.263	0.049	30	240	4.8
4b_0.6_5M	0.6	0.1	5	0.355	0.263	0.049	30	240	48
4c_1.2_0.5M	1.2	0.1	0.5	0.255	0.377	0.035	30	240	4.8
4d_1.2_5M	1.2	0.1	5	0.255	0.377	0.035	30	240	48
5a_0.6_0.5M	0.6	0.1	0.5	0.355	0.263	0.049	30	240	4.8
5b_0.6_5M	0.6	0.1	5	0.355	0.263	0.049	30	240	48
5c_1.2_0.5M	1.2	0.1	0.5	0.255	0.377	0.035	30	240	4.8
5d_1.2_5M	1.2	0.1	5	0.255	0.377	0.035	30	240	48
6a_0.6_0.5M	0.6	0.1	0.5	0.355	0.263	0.049	30	240	4.8
6b_0.6_5M	0.6	0.1	5	0.355	0.263	0.049	30	240	48
6a_1.2_0.5M	1.2	0.1	0.5	0.255	0.377	0.035	30	240	4.8
6a_1.2_5M	1.2	0.1	5	0.255	0.377	0.035	30	240	48
7a_0.6_0.5M	0.6	0.1	0.5	0.355	0.263	0.049	30	240	4.8
7b_0.6_5M	0.6	0.1	5	0.355	0.263	0.049	30	240	48
7c_1.2_0.5M	1.2	0.1	0.5	0.255	0.377	0.035	30	240	4.8
7d_1.2_5M	1.2	0.1	5	0.255	0.377	0.035	30	240	48
8a_0.6_0.5M	0.6	0.1	0.5	0.355	0.263	0.049	30	240	4.8
8b_0.6_5M	0.6	0.1	5	0.355	0.263	0.049	30	240	48
8c_1.2_0.5M	1.2	0.1	0.5	0.255	0.377	0.035	30	240	4.8
8d_1.2_5M	1.2	0.1	5	0.255	0.377	0.035	30	240	48

The characterization of C-(N)-A-S-H gels was carried out as follows:

1. Thermogravimetric analysis (TGA) to acquire data on the water content of the samples. This was performed by heating the samples to 1000 °C using a ramp rate of 10 °C/min in a N2 environment. A PerkinElmer Pyris 1 Thermogravimetric analyzer was used, along with a platinum pan and approximately 10mg of each sample for every run. In between runs, the pan was washed using demineralized water and ethanol and stored in a drying oven at 150°.

2. X-ray diffraction data from the Bruker Advance D8 XRD and the Advanced Photon Source at Argonne National Laboratory, to acquire data on the crystalline phases that exist in the samples at different times in the evolution of the gel; The samples were placed in 1mm diameter, 2 inch length polyimide capillaries for analysis, after they were dried in a N_2 gas glove box for an additional five days at the end of their respective growth period. With regards to the data extracted at Argonne, a detector plate at 168mm from the sample was collecting the scattered X-rays from the source. The data conversion from 2-D to 1-D was via the Fit2D software and a CeO_2 capillary mounted on the first slot of the sample changer for calibration purposes[35,12,11].

3. For the laboratory-based XRD measurements (Bruker Advance D8), the samples were measured using an Ag-radiation source (wavelength of 0.56 Å) and a parallel geometry setup for data collection. A Göbel mirror was employed along with Soller

slits (on the primary and secondary path) and an exit slit of 1.2mm on the primary path. The sample was loaded and aligned on a goniometer head, and was rotated at a speed of 60 rotations/min during measurement. The secondary path divergence slit was set to be fully open (at 6mm), and a Lynxeye detector was used to collect the data.

4. Pair Distribution Function Analysis using the XRD diffraction data obtained from the Advanced Photon Source at Argonne National Laboratory in Chicago. Samples were mounted on 28-slot sample changers ("cassettes") in the following manner:

   (a) Finely ground powder was placed in polyimide capillaries;

   (b) epoxy-sealed on both ends and cleaned from any areas that will make contact with the beamline;

   (c) the capillaries were trimmed to 19 mm.

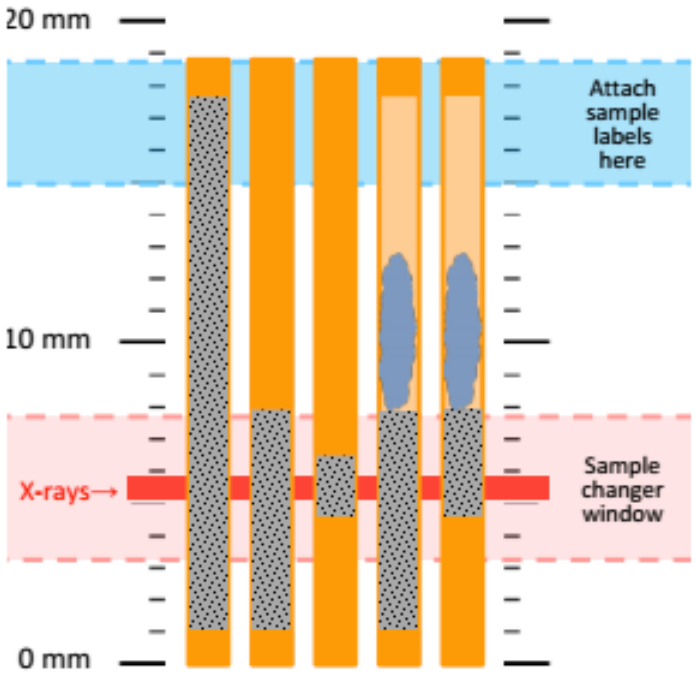

Figure 2.4: Best practices for capillary loading to yield maximal signal from the beamline[6]. Refer to Appendix A for full capillary loading practices at 11_*ID_B*.

Data reduction were executed using PDFgetX2, with a value for $Q_{max} = 20\text{Å}^{-1}$

5. Attenuated Total Reflectance in conjunction with Fourier Transform Infrared Spectroscopy (ATR-FTIR) to shed light on the extent of the silica connectivity in the samples during various stages of evolution. A PerkinElmer Frontier FT-IR Spectrometer with a Universal ATR Sampling Accessory was used, with a N2 gas flow to purge the instrument and thus enable the detection of water content and carbonate phases in the material. A total of approximately 20mg of each sample were pressed under 40 instrument pressure units to create the ideal conditions for a 32- pass scan up to

500Hz. The sample was in the form of a very soft solid.

3

Results & Discussion

As described in the Materials and Methods chapter, the main techniques used to investigate the effects of time and alkalinity in the silicate structure and general morphology of the gel were Attenuated Total Reflectance Spectroscopy (ATR) to investigate the level of silica interconnectivity, X-Ray Diffraction to acquire the crystalline structure

of the material in different phases in time and Thermogravimetric Analysis to determine the amounts of water present in the samples and the density of the structure itself (which appears as weight loss at higher temperatures in the graphs below). Individually, the tests showed significant changes in the morphology of the gel, but the results from the three different tests synergize in order to give a more complete picture of the gel's structure.

3.1 ATR Spectroscopy

The time series involved a 4-, 10- day and 1-, 2- and 3- month intervals for four combinations of Ca/Si ratios and alkalinity. The 700-1200 cm_{-1} band for the 4-day results of the early day formation of the gel (Figure 3.1 or A.1) shows a shift of the main peak, attributed to $Si - O$ stretching vibrations[9] to lower frequencies, with an increase in alkalinity (samples 1b and 1d). The bands of the 0.5M gels (samples 1a and 1c) are wider and centered at higher frequencies i.e. $\approx 960cm^{-1}$ and $\approx 950cm^{-1}$ for samples 1a and 1c respectively, which points to a higher SiO_2 content and polymerization in the crystalline structure[9,14,38]. Q^3 and Q^4 sites (Q^0,Q^1,Q^2,Q^3 and Q^4 is notation used in ^{29}Si-nuclear magnetic resonance spectroscopy for silica with four oxygens attached to it and the superscripts 0-4 indicate the number of silica units attached via the oxygen to individual silica atoms[2]) are theorized to exist in the sample, given the high levels of polymerization that take place in the latter pair of samples[9]. This is likely due to the presence of unreacted silica fume, which is predominantly Q^4 On

the other hand, the high-alkali samples show Si-O peaks at lower frequencies, indicating the complete dissolution of silica fume and aluminum in the structure[9], which can be assigned to stretching vibrations of Q^2 tetrahedra bonds[38]. The structures utilize the availability of calcium content in the mix in this higher alkalinity environment more, and subsequently lower the degree of polymerization[9,24,38]. To further prove this, it is worth noting the difference in samples 1b and 1d, where the latter has a higher Ca/Si ratio and thus exhibits a smaller degree of connectivity i.e. higher $\frac{Q^4}{Q^2}$ than the former (and across all samples of this age, given the highest alkalinity and Ca/Si ratio introduced in the experiment). This also explains why the band for sample 1c exhibits a much higher degree of polymerization than 1a (purely in terms of the Ca/Si ratio present in the mix). The results for the 10-day and 1- and 2-month samples also exhibit similar trends (See appendix A, A.3, A.5, A.7. Namely, the lower alkalinity samples exhibit a higher degree of polymerization (due to unreacted silica fume present) and its relationship with Ca/Si is also inversely proportional(Fig. 3.2, 3.3 and 3.4). However, the 3-month samples (Figure 3.5 or A.9) show a translation of the curves to a lower frequency range at $\approx 750 - 830 Hz$. A proposed model Macphee suggests that the aging of alkali-activated binder gels containing Ca could potentially lead to higher polymerization levels[22,23], which could sufficiently explain the above observation. Nonetheless, the behavior of the gels across the various Ca/Si-alkalinity combinations is the same as with the previous time steps.

Another disturbance is also observed at $\approx$ 810 – 820cm^{-1}, which corresponds to carbonate C-O bond stretching vibrations[9] (Fig. 3.1, 3.2, 3.3, 3.4). Hence, carbonation of the samples could not be completely avoided using the method outlined in chapter 2.

Looking at the full ATR-FTIR curves of the samples, we observe various band differences between samples across the 500-4000cm^{-1} spectrum. Table 3.1 summarizes the intensities of the different bands at various intervals across the spectrum[15], one that is consistent across all sample ages. At 2800cm^{-1} the curves for the higher alkalinity samples (1-5b and 1-5d) experience a drop in the transmission levels, when compared to the curves for the lower alkalinity samples (1-5a and 1-5c). This 2800cm^{-1} band corresponds to the introduction of sodium through the NaOH solution in the binder[25].

Table 3.1: AFt/AFm phases [15], with band intensity (s=strong; m=medium; l=low) from [7]

AFt/AFm phases	Wave-number(cm^{-1})									
	O-H			O-H, H_2O in capilaries	C-O, $[CO_3]$ 2-	S-O, $[SO_4]$ 2-	Si-O	Al-O		
Ettringite $Ca6Al_2(SO_4)_3(OH)_{12}$ / $26H_2O$	N/A	3637m	N/A	3413m, 1680- 1640m	N/A	1115s, 617m	N/A	857l	N/A	537m
Mono-Carboaluminate $Ca_4Al_2(CO_3)(OH)_{12}$ / $5H_2O$	3676m	3624m	3543m	3363m, 3005m, 1650l	1363s	N/A	N/A	953m	669l	535s
Hemi-Carboaluminate $Ca_4Al_2(CO_3)_{0.5}(OH)_{13}$ / $5.5H_2O$	3676m	3642m, 3624m	3544m	3367- 3007m, 1645l	1354s	N/A	N/A	954m	671l	537s
Mono-sulfoaluminate $Ca_4Al_2(SO_4)(OH)_{12}$ / $6H_2O$	3672m	N/A	3549m	3423s, 1650m	1380l	1150m	N/A	N/A	579m	535s
C_4AH_{13} ; $Ca_4Al_2(OH)_{14}$ / $6H_2O$	3673m	N/A	3541m	3490m, 1641l	1383l	N/A	N/A	N/A	667l	522s
C_3AH_6 (Hydrogarnet) ; $Ca_3Al_2(OH)_{12}$	3660m	N/A	N/A	N/A	N/A	N/A	N/A	810l	N/A	537s
C_2ASH_8 (Strätlingite) ; $Ca_2Al_2SiO_2(OH)_{10}$ / $2.2.5H_2O$	3669l	N/A	N/A	3442m, 1652l	N/A	N/A	1050s, 452s	951s	N/A	524s

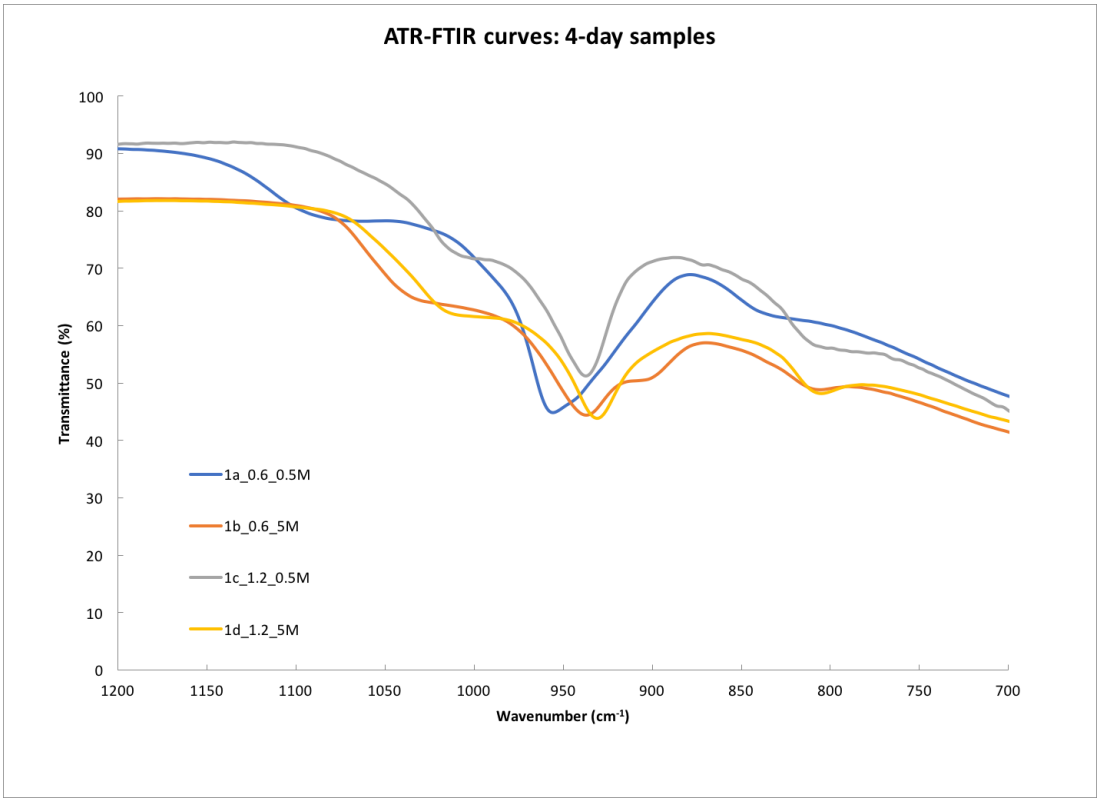

Figure 3.1: ATR curve detail of the silica band for 4-day C-N-A-S-H gel samples. The sample names follow the system: [timestep number and series letter]_[Ca/Si ratio]_[alkalinity].

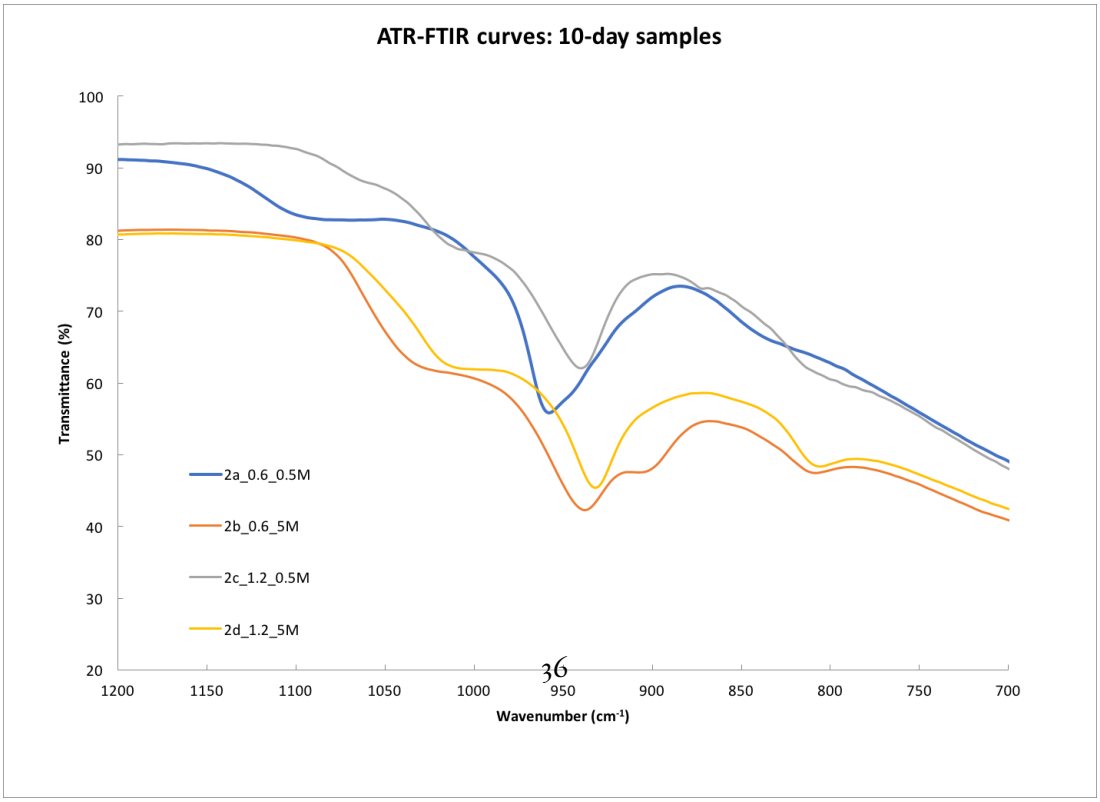

Figure 3.2: ATR curve detail of the silica band for 10-day C-N-A-S-H gel samples.

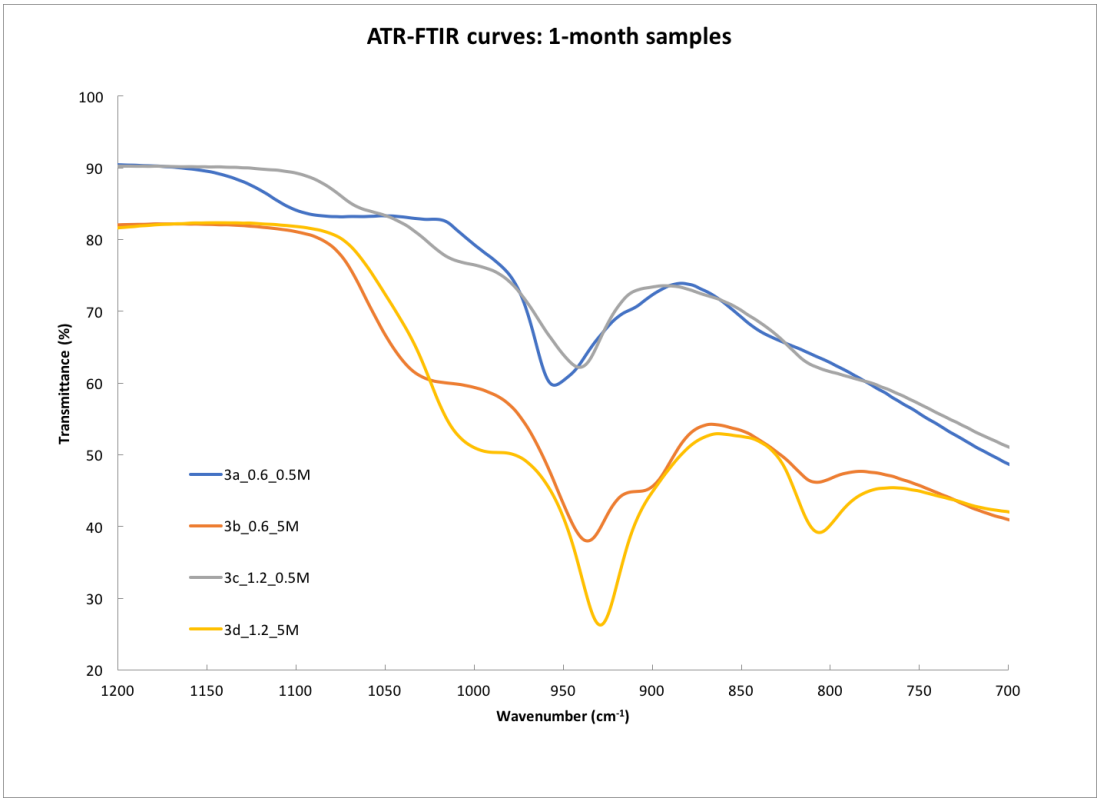

Figure 3.3: ATR curves of 1-month C-N-A-S-H gel samples.

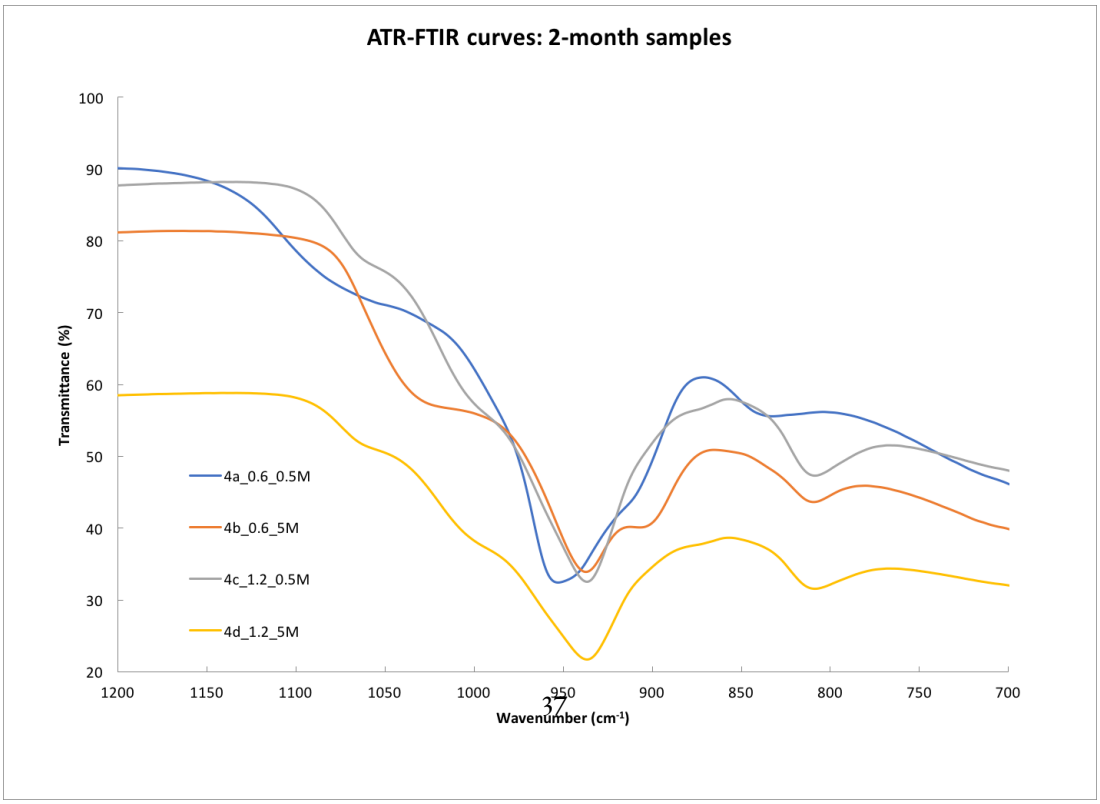

Figure 3.4: ATR curve detail of the silica band for 2-month C-N-A-S-H gel samples.

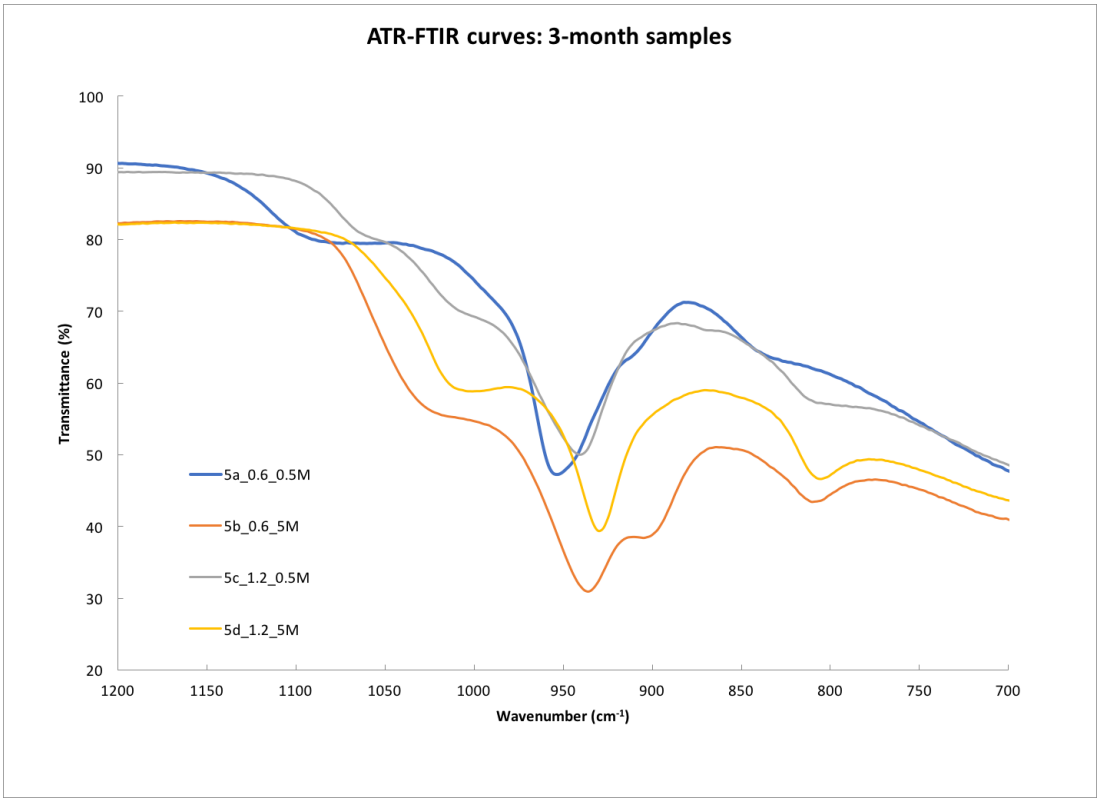

Figure 3.5: ATR curve detail of the silica band for 3-month C-N-A-S-H gel samples.

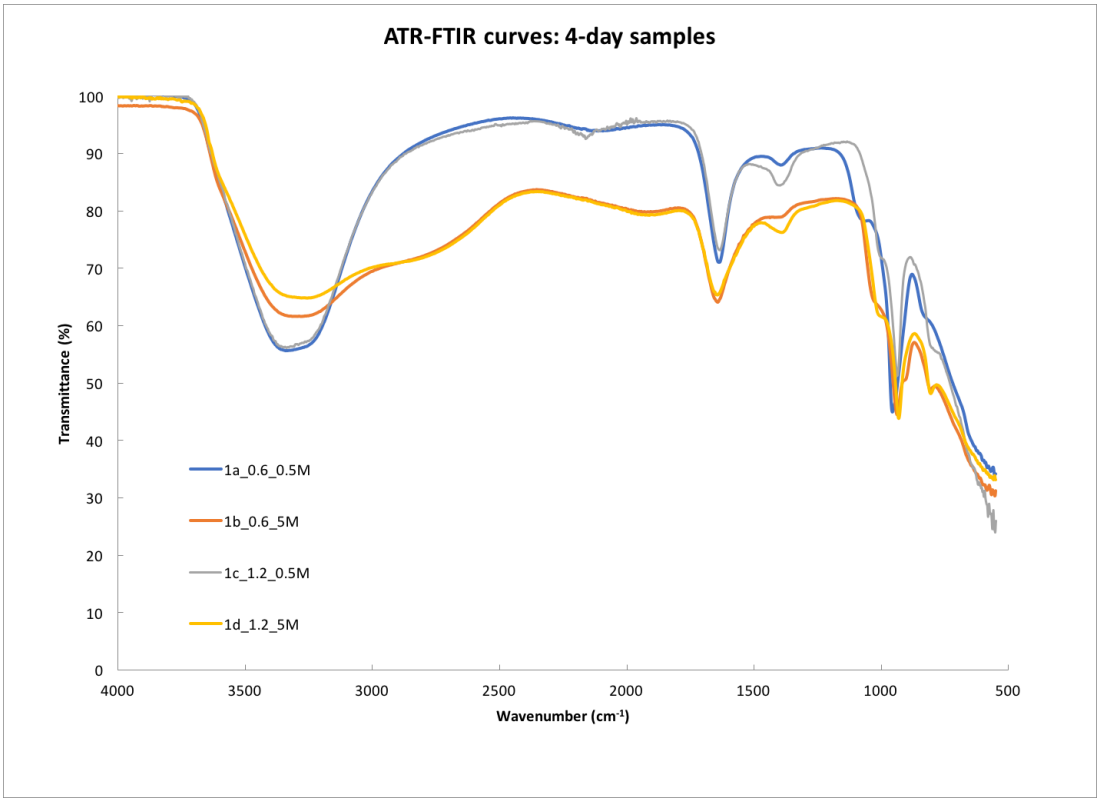

Figure 3.6: Full spectrum ATR curves of 10-day C-N-A-S-H gel samples.

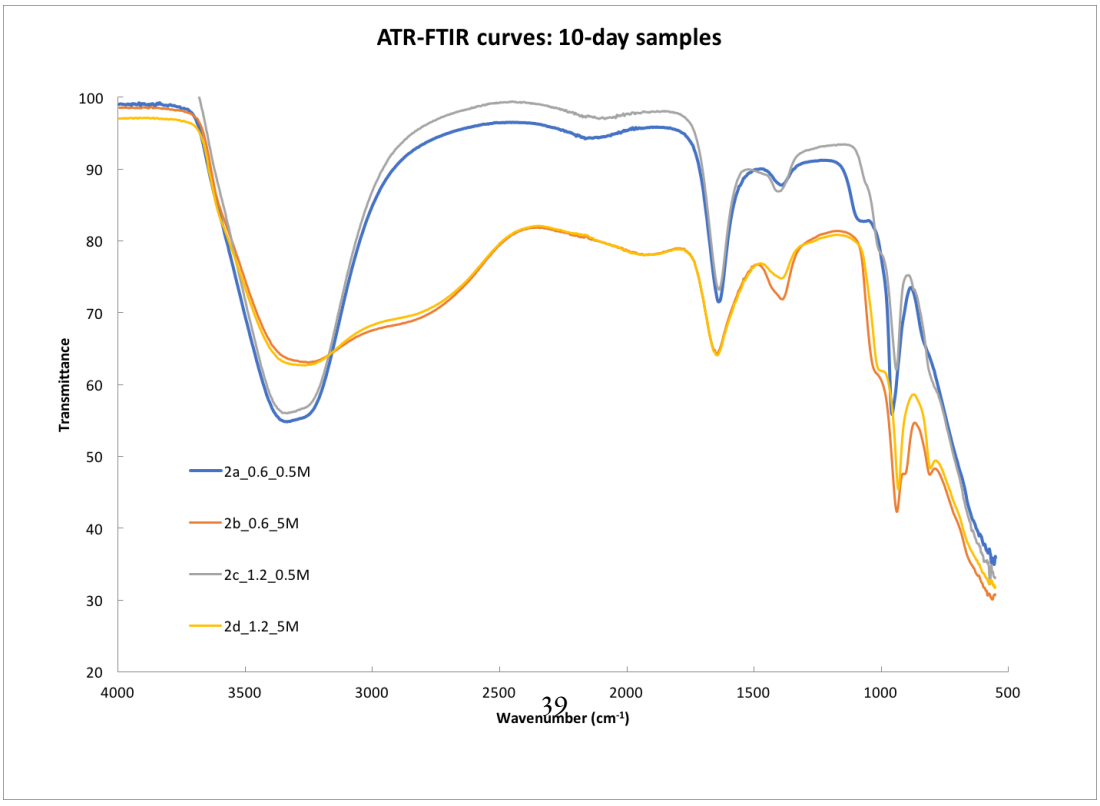

Figure 3.7: Full spectrum ATR curves of 10-day C-N-A-S-H gel samples.

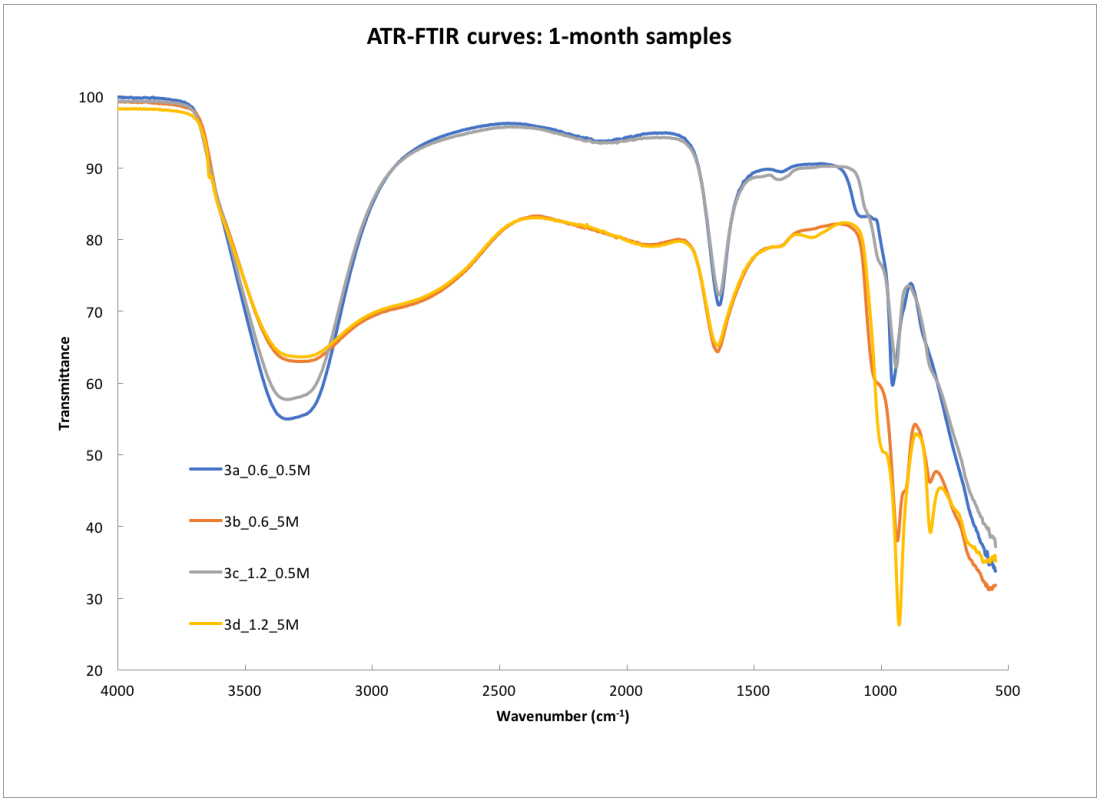

Figure 3.8: ATR curves of 1-month C-N-A-S-H gel samples.

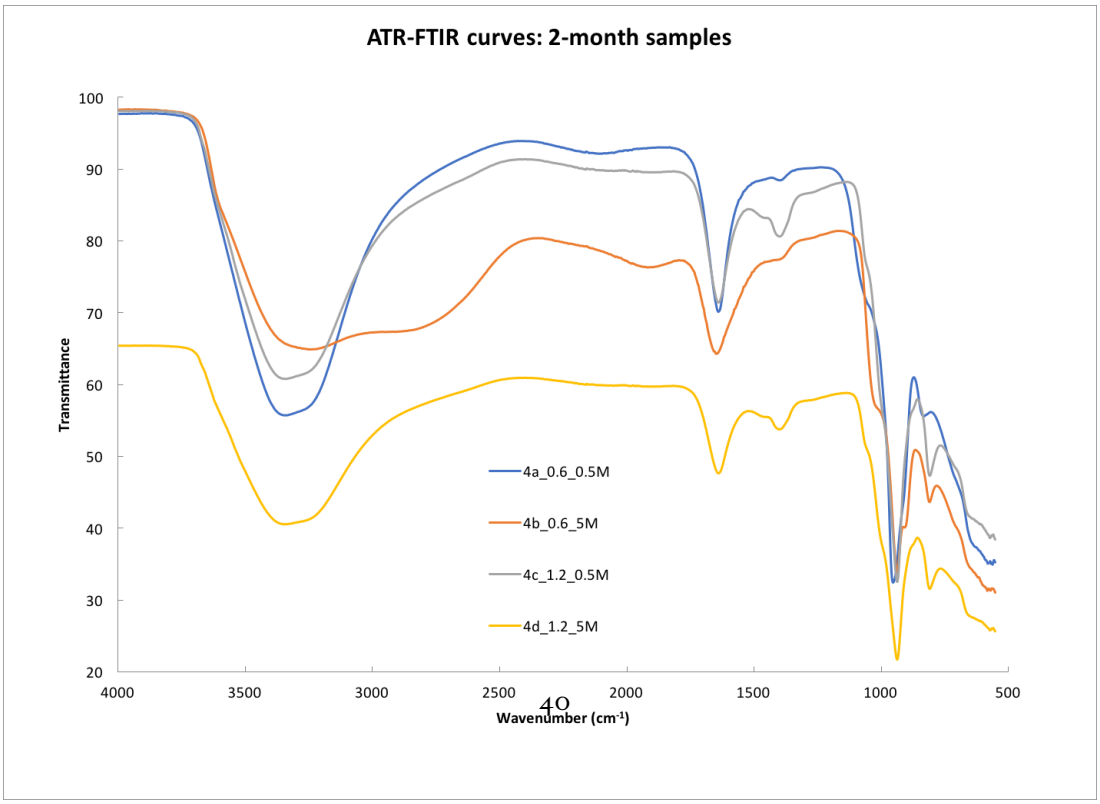

Figure 3.9: Full spectrum ATR curves of 2-month C-N-A-S-H gel samples.

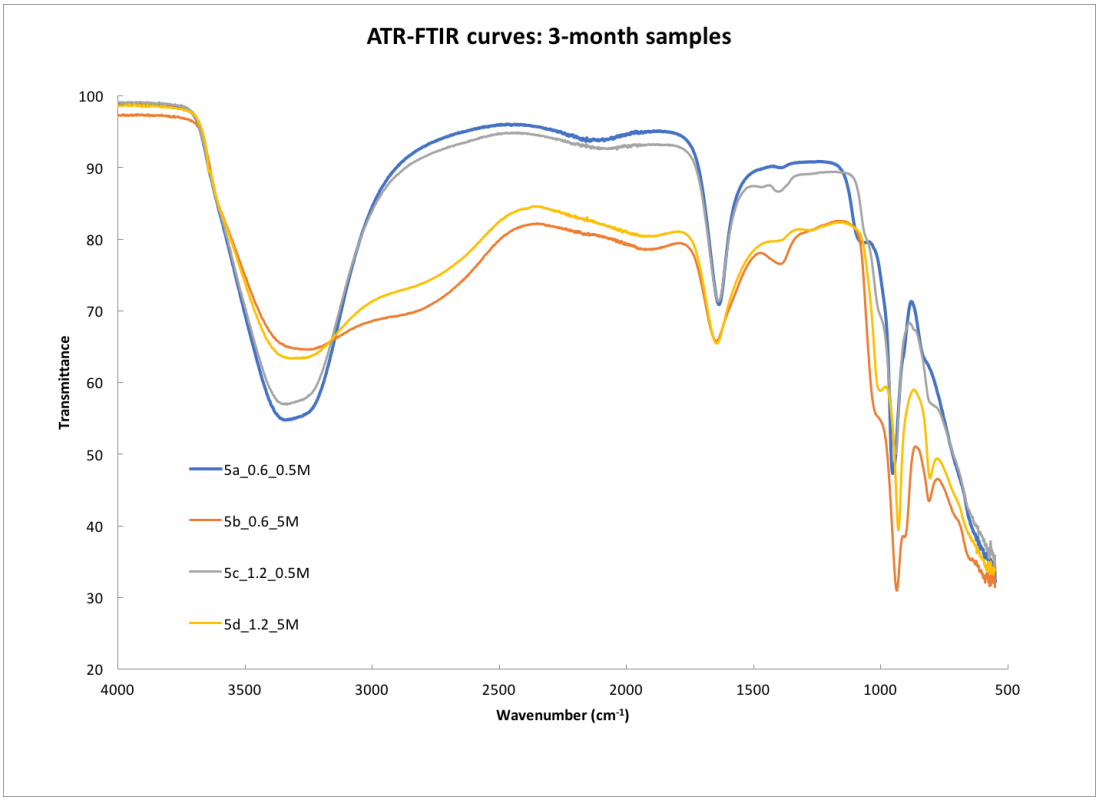

Figure 3.10: Full spectrum ATR curves of 3-month C-N-A-S-H gel samples.

3.2 X-Ray Diffraction

The X-Ray Diffraction results cover an important °2ϑ range that gives us valuable information on the crystalline phases and their evolution over time. Using the Bruker DIFFRAC.SUITE EVA analysis software on the 4-day curve for sample $1d\_1.2\_5M$ (chosen first since it exhibits a strong diffracting response), we identify the first peak at a 2ϑ of 6.5° as portlandite (in the form of $Ca(OH)_2$). The most intense signal appears at $\approx$ 10.5° over a whole degree (10 – 11°2ϑ), corresponding to a nanocrystalline phase of C-S-H ($CaO \cdot SiO_2 \cdot H_2O$ $C-S-H$)

visible at those angles. The amount of this C-S-H phase is driving the height of the peak i.e. the more intense it is, the higher the amount of the particular phase is diffracting, thus leading to a more pronounced curve. Similarly, the peaks appearing at $\approx$ 11.5°, $\approx$ 17.5°, $\approx$ 19.5°, $\approx$ 21° and $\approx$ 23° all correspond to calcium silicate hydrate ($CaO{\cdot}SiO_2{\cdot}H_2O\ C{-}S{-}H$) at different °2$\vartheta$. The peak at $\approx$ 12.3°2ϑ also corresponds to a portlandite phase (in the same form of $Ca(OH)_2$). Samples 1*a*_0.5_0.5*M*, 1*b*_0.6_5*M* and 1*c*_1.2_0.5*M* express similar trends, but the peaks aforementioned are much subtler and in most of them give a weaker signal. For example, the $\approx$ 6.5° peak appears as a short hump of relative intensity shorter than 0.3 units. This indicates that portlandite did not form under the specified conditions. The same applies to the $\approx$ 17.5° peak. Finally, the trends elucidated above are evident across all time steps, but their relative intensity changes. This is due to the phases developing further with time in terms of quantity. The signals that were lower than the distinct peaks in sample 1*d*_1.2_5*M* i.e. samples 1*a*_0.5_0.5*M*, 1*b*_0.6_5*M* and 1*c*_1.2_0.5*M* remained similar in the low peaks that they exhibited or intensified slightly with time.

An interesting effect observed was also the creation of "shoulders" next to distinct peaks. This is an instrumental anomaly present in the Bruker 8 XRD model used to make the measurements. More specifically, the X-ray emitter possesses both $AgKa_1$ and $AgKa_2$ wavelengths, and the slight difference between the angles of diffraction creates the "mirroring" effect that is observed across the diffraction results.

3.3 Pair Distribution Function Analysis

The detailed X-ray PDF's for two samples with Ca/Si ratio of 1.0 and alkalinities of 0.5M and 5M are shown in Fig.3.11. Fig. 3.13 presents features at large r values ($r \geq$ 10Å) and confirms that the substances are nanocrystalline, as opposed to amorphous[37]. This means that the atomic structure can roughly be described using the bulk crystalline structure (periodic unit cell) using a nanospaced shape function[37]. In the case of an amorphous material, in order to be eligible for analysis using a shape function, the data would have to be truncated below 10Å, impossible for a nanosized particle[37].

The peaks below $\approx$ 1Å are termination errors or imperfections in the correction data[37,7]. As mentioned in White et al.[37], the gel is amorphous above 8Å (Fig. 3.12 and 3.13) and since there are no atom-atom correlation past that region, the amorphous phases yield no spiking in the graph[7]. That is, the range $6 \leqslant r \leqslant 40$Å will be unchanged in terms of the nanocrystalline order of the C-(N)-A-S-H gel[35,7]. The importance of the medium range ordering of the samples is evident by the intense peaks and fluctuations as a result of changes in the alkalinity of the mix. More specifically, we see reductions in the interatomic distances in the $Si-O$, $Ca-O$, $O-O$, $Si-Si$, $Si-Ca$, and $Ca-Ca$ peaks (Fig. 3.11). X-ray PDF analysis is the ideal option in this case because the calcium (alumino)silicate framework structure is dominated by scattering of heavier elements present in the gel, namely Ca and Si[35].

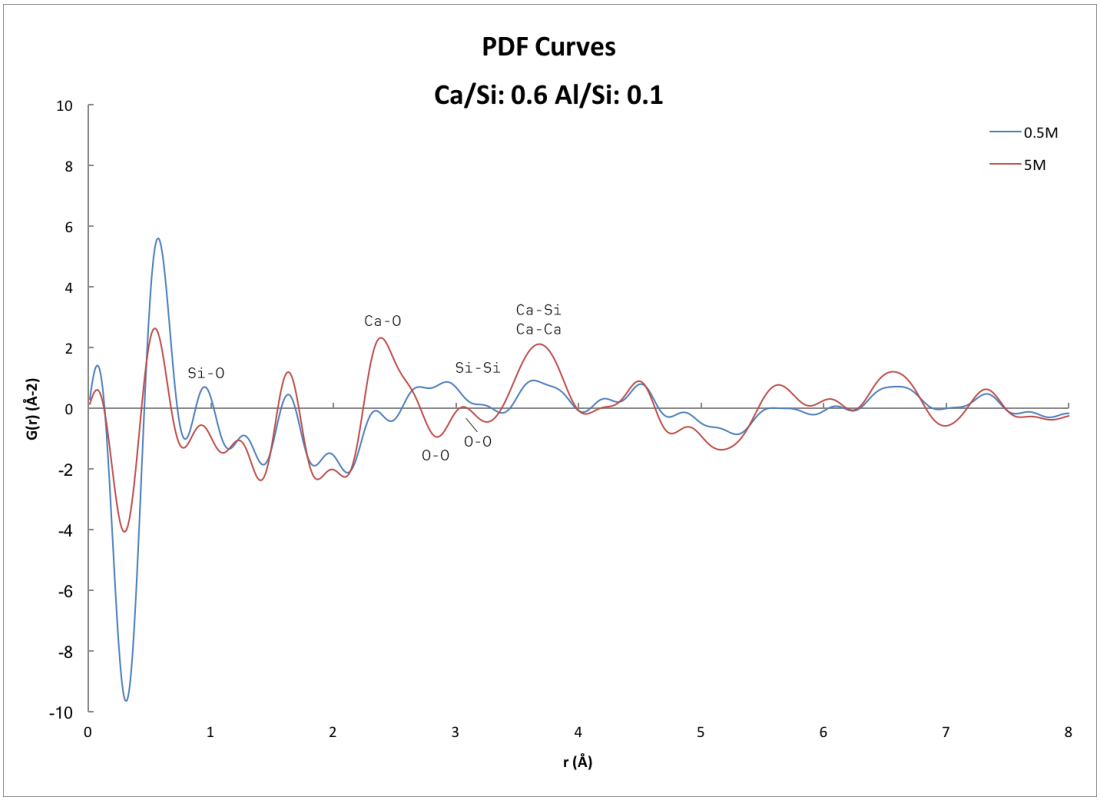

Figure 3.11: Detail of X-ray PDF's for samples of low and high alkalinity and fixed Ca/Si and Al/Si ratios.

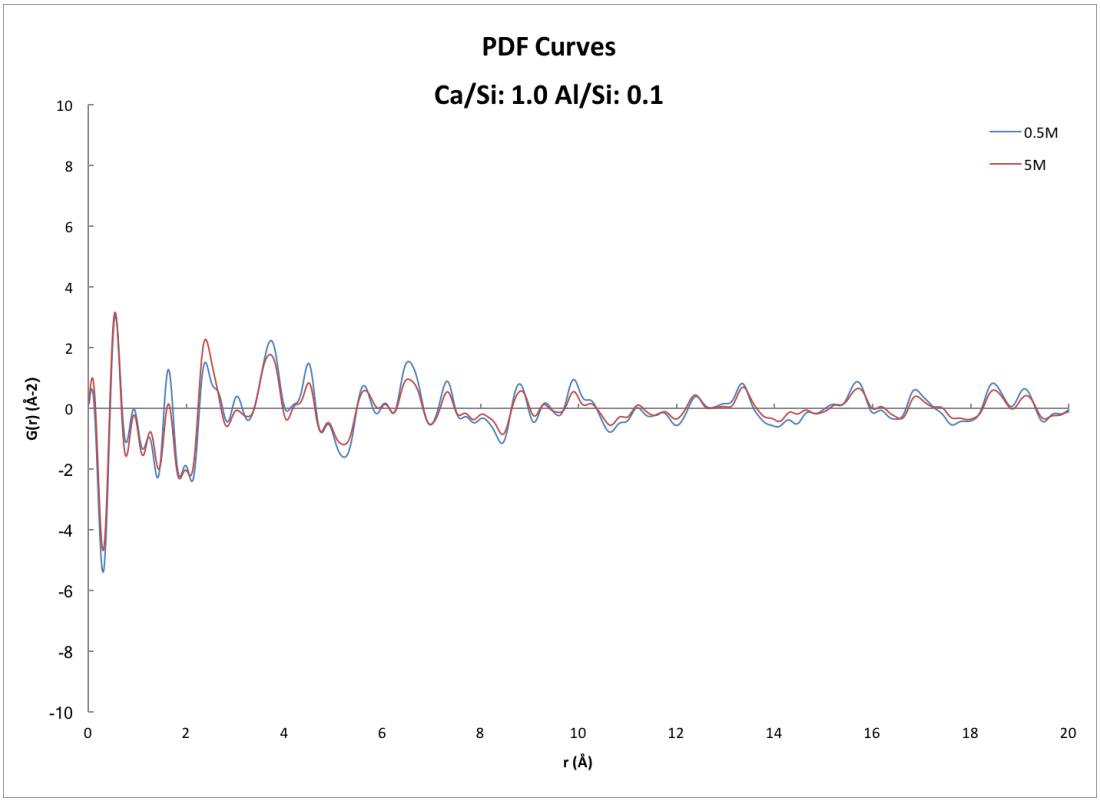

Figure 3.12: Half-spectrum X-ray PDF's for samples of low and high alkalinity and fixed Ca/Si and Al/Si ratios.

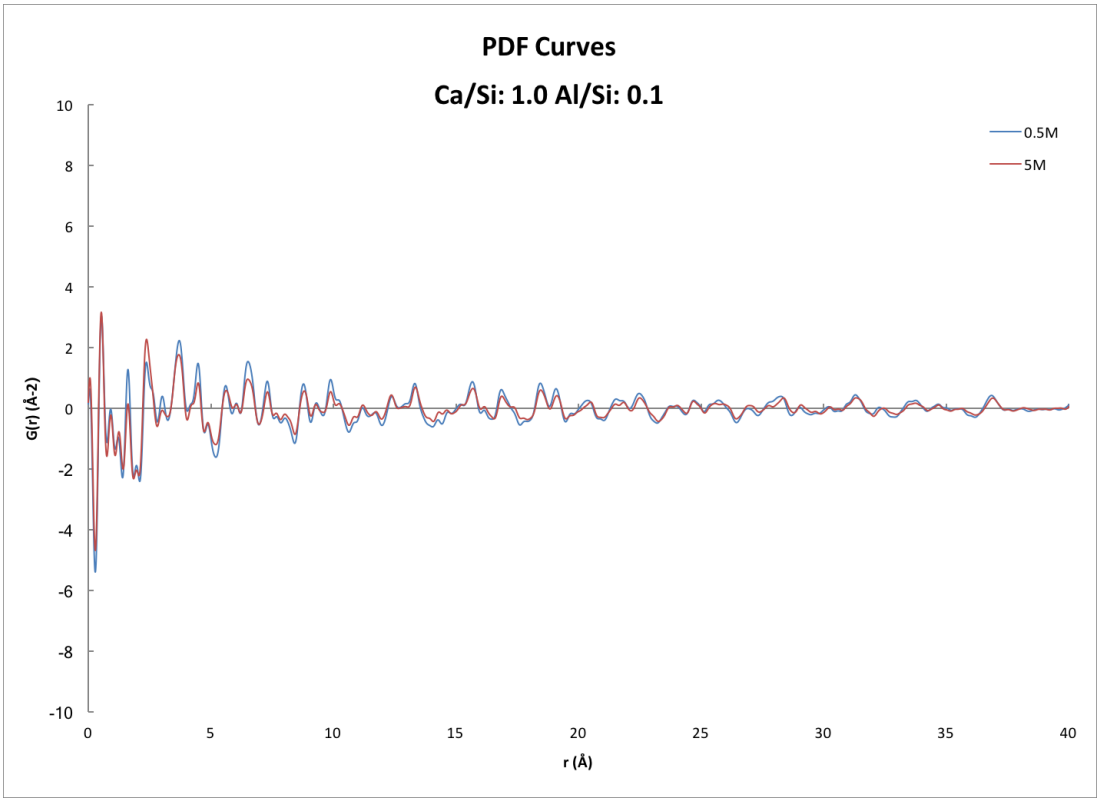

Figure 3.13: Full X-ray PDF's for samples of low and high alkalinity and fixed Ca/Si and Al/Si ratios.

3.4 Thermogravimetric Analysis

Thermogravimetric Analysis is used to determine the amount of water in the sample and also the degree of densification of the gel morphology by nature of the temperatures at which the water escapes the matrix. In the 4-day sample curves (Fig. 3.14, the higher alkalinity samples i.e. $1b\_0.6\_5\mathcal{M}$ and $1d\_1.2\_5\mathcal{M}$ experience the most intense weight loss percentage that starts at $\approx 100°C$ and ends at $\approx 200°C$, while the samples with lower alkalinity experience the same effect until $\approx 180°C$. At those temperatures, the volatilization of H_2O

at various states of absorption in the mix[28] is the most important process driving the weight loss. As reported in Rivera et al[28], the rapid weight loss at $\approx$ 50°C is tied to loss of free H_2O and the gradual loss at $\approx$ 450°C is attributed to dehydration of the $Ca(OH)_2$ and additional loss of H_2O in the interlayer region, pores and other regions of the C-S-H gel with chemically bound water[28]. It is evident across the curves of all time steps that the high alkalinity samples i.e. 1$-$5b_0.6_5$\mathcal{M}$ and 1$-$5d_1.2_5$\mathcal{M}$ lose a smaller percentage of their weight in volatilization of H_2O, by nature of containing less H_2O in the matrix between $\approx$ 100°C and $\approx$ 450°C. The higher alkalinity samples lose $\approx$ 60% of their initial weight with much smaller fluctuations across all time steps. On the other hand, the lower alkalinity samples exhibit a higher variance in the final weight percentage left in the pan and the weight loss is always more significant (with the exception of sample 1a_0.6_0.5$\mathcal{M}$, which drops down to 40% before stabilizing). By nature of the higher alkalinity samples containing less bound and free H_2O in solution and safely assuming that by the end of the experiment, when the analyzer has reached 1000°C all of the H_2O content has evaporated, the weight loss difference between the two is justified.

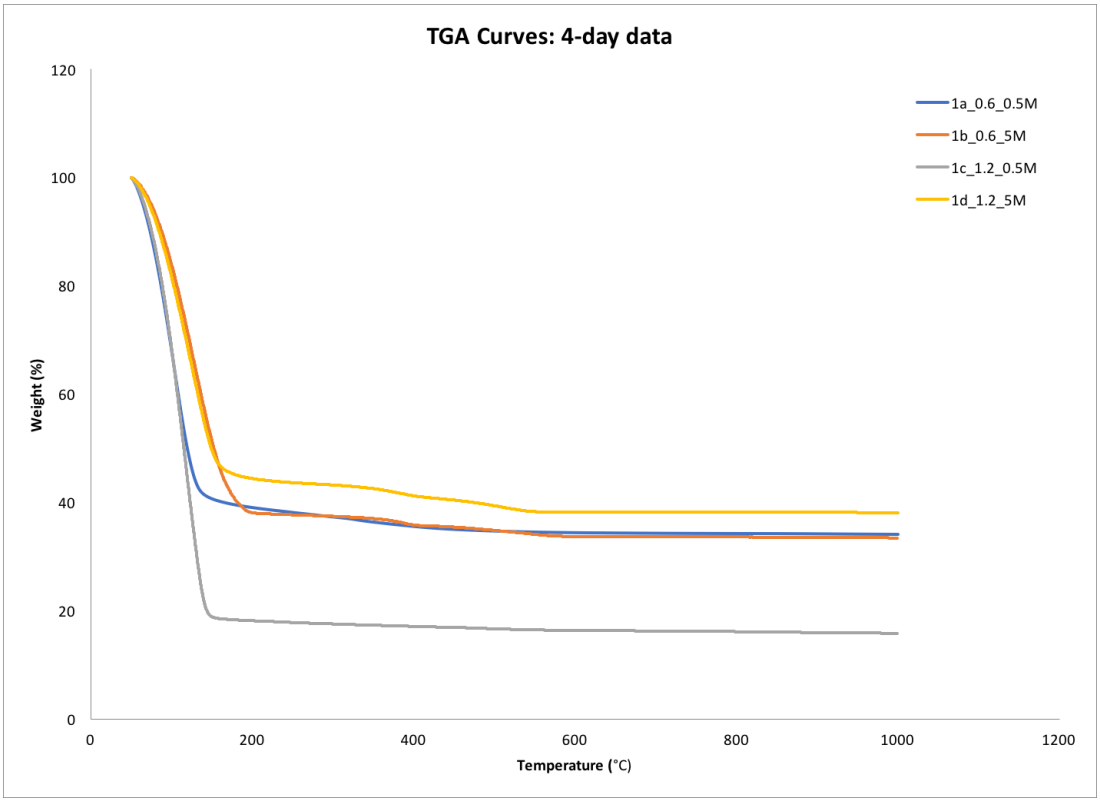

Figure 3.14: TGA curves of 4-day C-N-A-S-H gel samples.

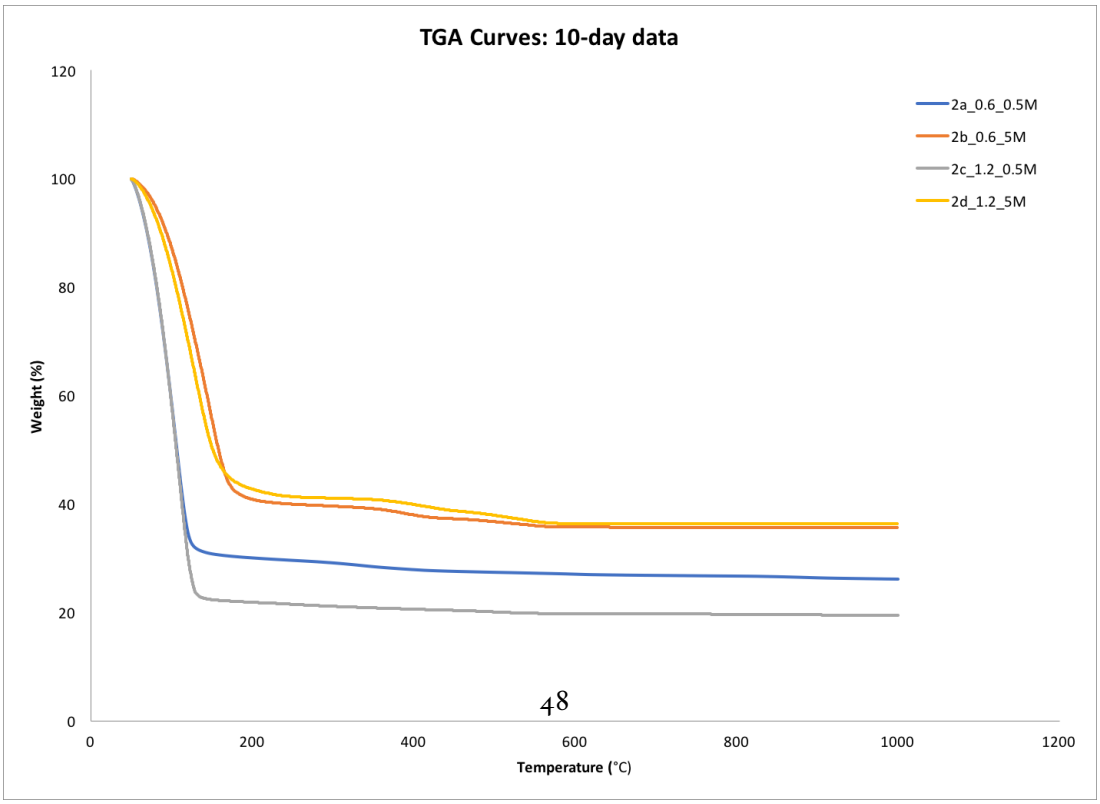

Figure 3.15: TGA curves of 10-day C-N-A-S-H gel samples.

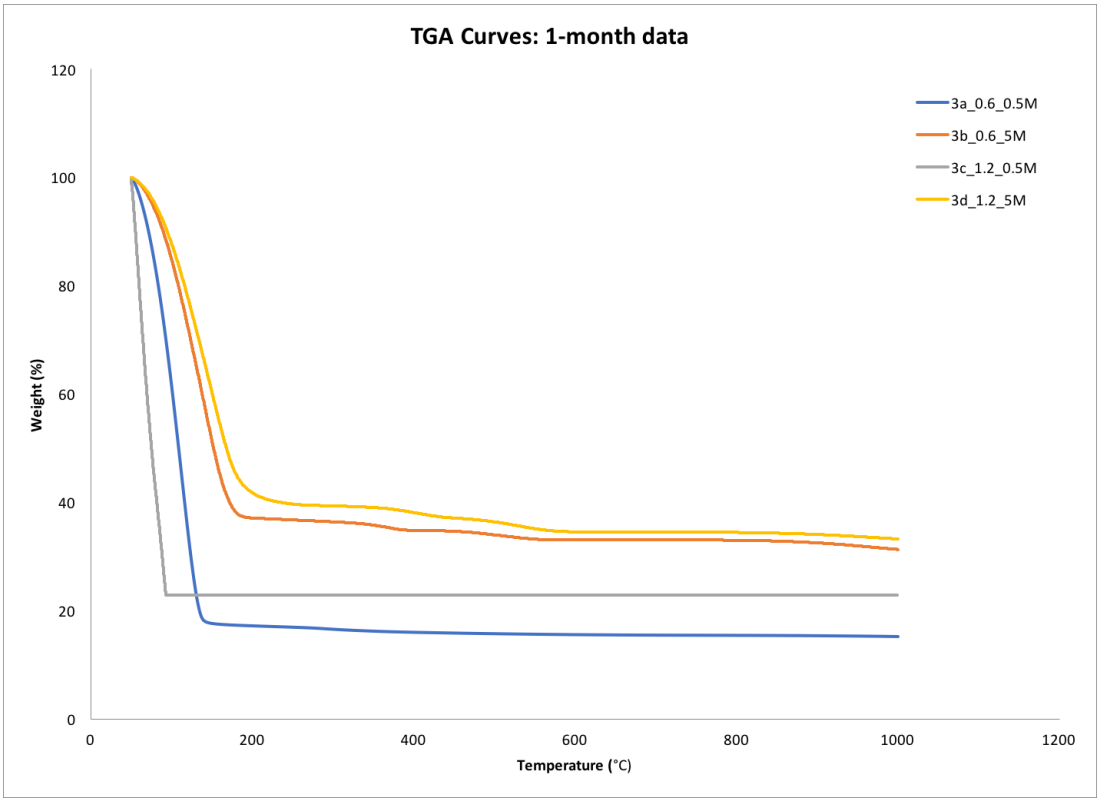

Figure 3.16: TGA curves of 1-month C-N-A-S-H gel samples.

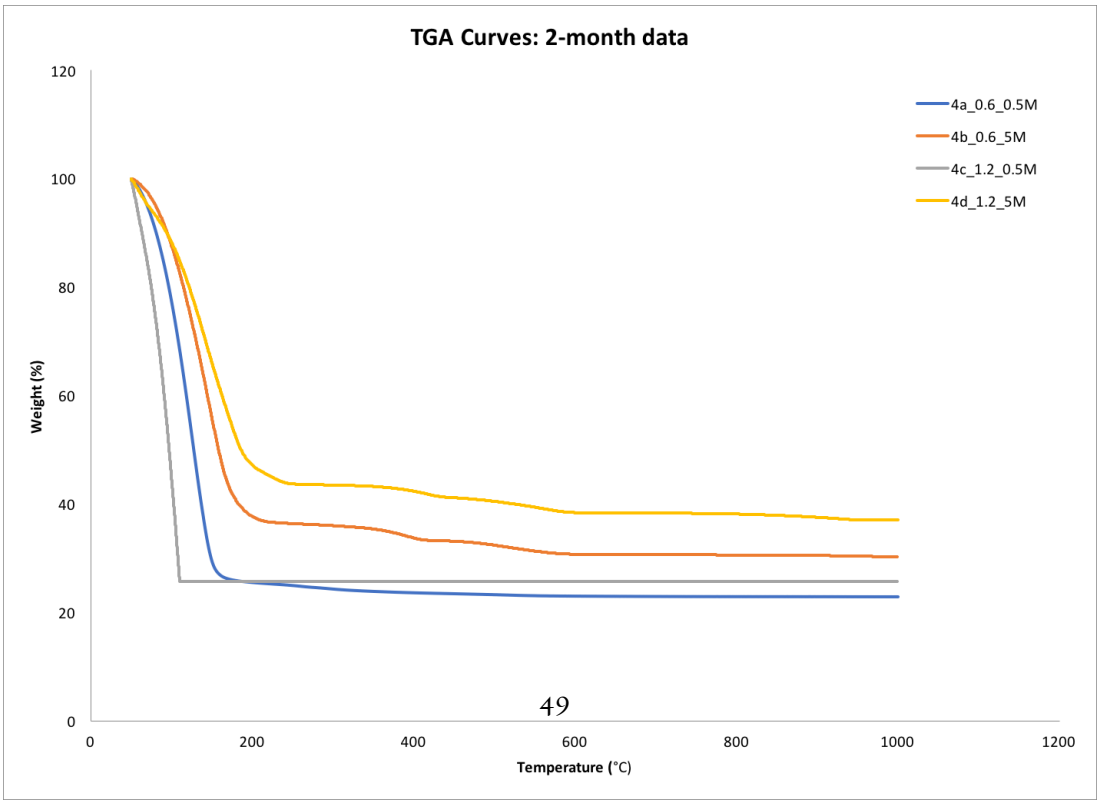

Figure 3.17: TGA curves of 2-month C-N-A-S-H gel samples.

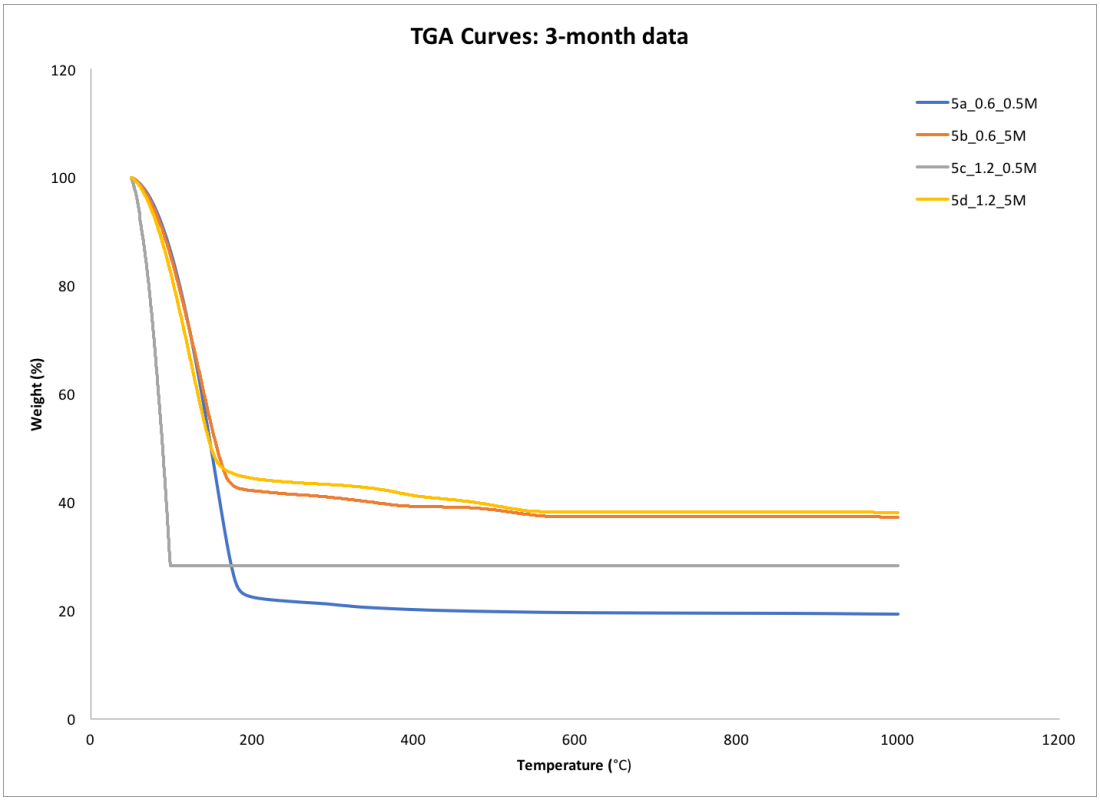

Figure 3.18: TGA curves of 3-month C-N-A-S-H gel samples.

4

Conclusion

The primary objective of this investigation was to synthesize C-(N)-A-S-H gels of various alkalinities and explore their nanocrystalline structure and properties. The changes in alkalinity introduced differences in the composition and behavior of the constituents in the samples.

4.1 Conclusions

In summary:

- C-S-H and portlandite phases increase with higher alkalinities.
- the atom-atom distances in the various formed phases decreases with alkalinity, leading to a denser morphology
- Silica interconnectivity increases within the nanocrystalline structure.
- Highly alkaline samples contain less H_2O as shown in the TGA experiments.
- There is a strong presence of unreacted silica fume in the matrix at Q^4.
- The methods outlined in chapter 2 did not fully allow for complete carbonation prevention. More rigorous methods of transfer and handling should be established to eliminated C-O bands in ATR-FTIR and other measurements.
- From the XRD measurements we conclude that atom-atom relation $\geq$ 8 are nonexistent due to the amorphous nature of the gel at longer-range structures.

4.2 Future work

The realm of C-(N)-A-S-H gel research is open for more additions and further expansion. This investigation followed a holistic approach and tackled a wide range of questions sur-

rounding the nanocrystalline structure of the gel. More advanced methods of preventing carbonations of the samples can be incorporated in future iterations of the work. More advanced X-ray diffraction setups can also be incorporated to yield higher resolution XRD graphs (such as the ones obtained at Argonne National Laboratory but for the entire range of samples measured) and thus a more complete understanding of the individual phases present in the structure. Finally, additional techniques such as ^{29}-NMR spectroscopy in addition to the aforementioned techniques can offer more insight in the exact Si sites and their behavior over time.

Bibliography

[1] Morten Daugaard Andersen, Hans J. Jakobsen, and Jørgen Skibsted. Incorporation of aluminum in the calcium silicate hydrate (c–s–h) of hydrated portland cements: a high-field 27al and 29si mas nmr investigation. *Inorganic Chemistry*, 42(7): 2280–2287, 2003. doi: 10.1021/ic020607b. URL http://dx.doi.org/10.1021/ic020607b. PMID: 12665361.

[2] David J. Belton, Olivier Deschaume, and Carole C. Perry. An overview of the fundamentals of the chemistry of silica with relevance to biosilicification and technological advances. *FEBS Journal*, 279(10):1710–1720, 2012. ISSN 1742-4658. doi: 10.1111/j.1742-4658.2012.08531.x. URL http://dx.doi.org/10.1111/j.1742-4658.2012.08531.x.

[3] Leon Black, Chris Breen, Jack Yarwood, Krassimir Garbev, Peter Stemmermann, and Biliana Gasharova. Structural features of c–s–h(i) and its carbonation in air—a raman spectroscopic study. part ii: Carbonated phases. *Journal of the American Ce-*

ramic Society, 90(3):908–917, 2007. ISSN 1551-2916. doi: 10.1111/j.1551-2916.2006.01429.x. URL http://dx.doi.org/10.1111/j.1551-2916.2006.01429.x.

[4] Jeffrey J. Chen, Jeffrey J. Thomas, Hal F.W. Taylor, and Hamlin M. Jennings. Solubility and structure of calcium silicate hydrate. *Cement and Concrete Research*, 34(9): 1499 – 1519, 2004. ISSN 0008-8846. doi: http://doi.org/10.1016/j.cemconres.2004.04.034. URL http://www.sciencedirect.com/science/article/pii/S000888460400211X. H. F. W. Taylor Commemorative Issue.

[5] J. Davidovits. *Geopolymer chemistry and applications*. Institue Geopolymere, Saint-Quentin, 2008.

[6] X-Ray Science Division. High-throughput pair distribution function measurements at 11-id-b, 2014.

[7] T Egami and S.J.L Billinge. Underneath the bragg peaks. *Materials Today*, 6 (6):57 –, 2003. ISSN 1369-7021. doi: http://doi.org/10.1016/S1369-7021(03)00635-7. URL http://www.sciencedirect.com/science/article/pii/S1369702103006357.

[8] I. Garcia-Lodeiro, A. Palomo, and A. Fernández-Jiménez. 2 - an overview of the chemistry of alkali-activated cement-based binders. In F. Pacheco-Torgal, J.A. Labrincha, C. Leonelli, A. Palomo, and P. Chindaprasirt, editors, *Handincollec-*

tion of Alkali-Activated Cements, Mortars and Concretes, pages 19 – 47. Woodhead Publishing, Oxford, 2015. ISBN 978-1-78242-276-1. doi: http://doi.org/10.1533/9781782422884.1.19. URL http://www.sciencedirect.com/science/incollection/pii/B9781782422761500022.

[9] Ines García-Lodeiro, A. Fernández-Jiménez, M. Teresa Blanco, and Angel Palomo. Ftir study of the sol–gel synthesis of cementitious gels: C–s–h and n–a–s–h. *Journal of Sol-Gel Science and Technology*, 45(1):63–72, 2008. ISSN 1573-4846. doi: 10.1007/s10971-007-1643-6. URL http://dx.doi.org/10.1007/s10971-007-1643-6.

[10] Lauren Gomez-Zamorano, Magdalena Balonis, Bartu Erdemli, Narayanan Neithalath, and Gaurav Sant. C–(n)–s–h and n–a–s–h gels: Compositions and solubility data at 25°c and 50°c. *Journal of the American Ceramic Society*, pages n/a–n/a, 2017. ISSN 1551-2916. doi: 10.1111/jace.14715. URL http://dx.doi.org/10.1111/jace.14715.

[11] A. P. Hammersley. *FIT2D V9.129 Reference Manual V3.1*, volume 1. ESRF Internal Report, 1998.

[12] A. P. Hammersley, S. O. Svensson, M. Hanfland, A. N. Fitch, and D. Hausermann. Two-dimensional detector software: From real detector to idealised image

or two-theta scan. *High Pressure Research*, 14(4-6):235–248, 1996. doi: 10.1080/08957959608201408. URL http://dx.doi.org/10.1080/08957959608201408.

[13] Sung-Yoon Hong and F.P. Glasser. Alkali binding in cement pastes: Part i. the c-s-h phase. *Cement and Concrete Research*, 29(12):1893 – 1903, 1999. ISSN 0008-8846. doi: http://doi.org/10.1016/S0008-8846(99)00187-8. URL http://www.sciencedirect.com/science/article/pii/S0008884699001878.

[14] Sung-Yoon Hong and F.P Glasser. Alkali sorption by c-s-h and c-a-s-h gels: Part ii. role of alumina. *Cement and Concrete Research*, 32(7):1101 – 1111, 2002. ISSN 0008-8846. doi: http://doi.org/10.1016/S0008-8846(02)00753-6. URL http://www.sciencedirect.com/science/article/pii/S0008884602007536.

[15] M. Horgnies, J. J. Chen, and C. Bouillon. Overview about the use of fourier transform infrared spectroscopy to study cementitious materials. *WIT Transactions on Engineering Science*, 77(3):251–262, 2013. URL https://www.witpress.com/elibrary/wit-transactions-on-engineering-sciences/77/24712.

[16] Kazusuke Kobayashi and Yuichi Uno. Influence of alkali on carbonation of concrete, part 2 - influence of alkali in cement on rate of carbonation of concrete -. *Cement and Concrete Research*, 20(4):619 – 622, 1990. ISSN 0008-8846. doi: http://dx.doi.

org/10.1016/0008-8846(90)90104-6. URL http://www.sciencedirect.com/science/article/pii/0008884690901046.

[17] E. L'Hôpital, B. Lothenbach, K. Scrivener, and D.A. Kulik. Alkali uptake in calcium alumina silicate hydrate (c-a-s-h). *Cement and Concrete Research*, 85:122 – 136, 2016. ISSN 0008-8846. doi: http://doi.org/10.1016/j.cemconres.2016.03.009. URL http://www.sciencedirect.com/science/article/pii/S0008884616303088.

[18] I. García Lodeiro, D.E. Macphee, A. Palomo, and A. Fernández-Jiménez. Effect of alkalis on fresh c–s–h gels. {FTIR} analysis. *Cement and Concrete Research*, 39(3): 147 – 153, 2009. ISSN 0008-8846. doi: http://doi.org/10.1016/j.cemconres.2009.01.003. URL http://www.sciencedirect.com/science/article/pii/S0008884609000039.

[19] I. García Lodeiro, A. Fernández-Jimenez, A. Palomo, and D.E Macphee. Effect on fresh c-s-h gels of the simultaneous addition of alkali and aluminium. *Cement and Concrete Research*, 40(1):27 – 32, 2010. ISSN 0008-8846. doi: http://doi.org/10.1016/j.cemconres.2009.08.004. URL http://www.sciencedirect.com/science/article/pii/S0008884609002051.

[20] P. Longuet, L. Burglen, and A. Zelwer. La phase liquide du ciment hydraté. *Revue des Materiaux et Construction*, 676(1):35–41, 1973.

[21] E. L'Hôpital, B. Lothenbach, G. Le Saout, D. Kulik, and K. Scrivener. Incorporation of aluminium in calcium-silicate-hydrates. *Cement and Concrete Research*, 75:91 – 103, 2015. ISSN 0008-8846. doi: http://doi.org/10.1016/j.cemconres.2015.04.007. URL http://www.sciencedirect.com/science/article/pii/S0008884615001131.

[22] D. E. Macphee, E. E. Lachowski, and F. P. Glasser. Polymerization effects in c-s-h: implications for portland cement hydration. *Advances in Cement Research*, 1(3):131–137, 1988. doi: 10.1680/1988.1.3.131. URL http://dx.doi.org/10.1680/1988.1.3.131.

[23] Donald E. Macphee, Karen Luke, Fred P. Glasser, and Eric E. Lachowski. Solubility and aging of calcium silicate hydrates in alkaline solutions at 25°c. *Journal of the American Ceramic Society*, 72(4):646–654, 1989. ISSN 1551-2916. doi: 10.1111/j.1151-2916.1989.tb06189.x. URL http://dx.doi.org/10.1111/j.1151-2916.1989.tb06189.x.

[24] H. Matsuyama and J. F. Young. Effects of ph on precipitation of quasi-crystalline calcium silicate hydrate in aqueous solution. *Advances in Cement Research*, 12(1):29–33, 2000. doi: 10.1680/adcr.2000.12.1.29. URL http://dx.doi.org/10.1680/adcr.2000.12.1.29.

[25] Jean-Joseph Max and Camille Chapados. Subtraction of the water spectra from infrared spectra of acidic and alkaline solutions. *Applied Spectroscopy*, 52(7):963–969, 1998. doi: 10.1366/0003702981944788. URL http://dx.doi.org/10.1366/0003702981944788.

[26] Duxson P, Provis JL, Lukey G. C., and J. S. J. vanDeventer. The role of inorganic polymer technology in the development of 'green concrete'. *Cement and Concrete Research*, 12(37):1590–1597, 2007.

[27] John L. Provis, Rupert J. Myers, Claire E. White, Volker Rose, and Jannie S.J. van Deventer. X-ray microtomography shows pore structure and tortuosity in alkali-activated binders. *Cement and Concrete Research*, 42(6):855 – 864, 2012. ISSN 0008-8846. doi: http://doi.org/10.1016/j.cemconres.2012.03.004. URL http://www.sciencedirect.com/science/article/pii/S0008884612000579.

[28] O.G. Rivera, W.R. Long, C.A. Weiss Jr., R.D. Moser, B.A. Williams, K. Torres-Cancel, E.R. Gore, and P.G. Allison. Effect of elevated temperature on alkali-activated geopolymeric binders compared to portland cement-based binders. *Cement and Concrete Research*, 90:43 – 51, 2016. ISSN 0008-8846. doi: http://doi.org/10.1016/j.cemconres.2016.09.013. URL http://www.sciencedirect.com/science/article/pii/S0008884615300405.

[29] B. C. Smith. *Fundamentals of Fourier transform infrared spectroscopy*. CRC Press, 2011. ISBN 9781420069297.

[30] RUBEN SNELLINGS. *X-ray powder diffraction applied to cement*. CRC Press, 2017/04/15 2015. ISBN 978-1-4987-3865-1. doi: doi:10.1201/b19074-5. URL http://dx.doi.org/10.1201/b19074-5.

[31] G.K. Sun, J. Francis Young, and R. James Kirkpatrick. The role of al in c–s–h: Nmr, xrd, and compositional results for precipitated samples. *Cement and Concrete Research*, 36(1):18 – 29, 2006. ISSN 0008-8846. doi: http://doi.org/10.1016/j.cemconres.2005.03.002. URL http://www.sciencedirect.com/science/article/pii/S0008884605000840.

[32] Jeff Dr. Thomas and Hamlin Dr. Jennings. Introduction to cement chemistry, 2008. URL http://iti.northwestern.edu/cement/monograph/Monograph3_2.html.

[33] Jannie S. J. van Deventer, John L. Provis, Peter Duxson, and David G. Brice. Chemical research and climate change as drivers in the commercial adoption of alkali activated materials. *Waste and Biomass Valorization*, 1(1):145–155, 2010. ISSN 1877-265X. doi: 10.1007/s12649-010-9015-9. URL http://dx.doi.org/10.1007/s12649-010-9015-9.

[34] Brant Walkley, Rackel San Nicolas, Marc-Antoine Sani, Gregory J. Rees, John V. Hanna, Jannie S.J. van Deventer, and John L. Provis. Phase evolution of c-(n)-a-s-h/n-a-s-h gel blends investigated via alkali-activation of synthetic calcium aluminosilicate precursors. *Cement and Concrete Research*, 89:120 – 135, 2016. ISSN 0008-8846. doi: http://doi.org/10.1016/j.cemconres.2016.08.010. URL http://www.sciencedirect.com/science/article/pii/S0008884616302381.

[35] Claire E. White, John L. Provis, Thomas Proffen, and Jannie S. J. Van Deventer. The effects of temperature on the local structure of metakaolin-based geopolymer binder: A neutron pair distribution function investigation. *Journal of the American Ceramic Society*, 93(10):3486–3492, 2010. ISSN 1551-2916. doi: 10.1111/j.1551-2916.2010.03906.x. URL http://dx.doi.org/10.1111/j.1551-2916.2010.03906.x.

[36] Claire E. White, Katharine Page, Neil J. Henson, and John L. Provis. In situ synchrotron x-ray pair distribution function analysis of the early stages of gel formation in metakaolin-based geopolymers. *Applied Clay Science*, 73(10):17–25, 2013.

[37] Claire E. White, Luke L. Daemen, Monika Hartl, and Katharine Page. Intrinsic differences in atomic ordering of calcium (alumino)silicate hydrates in conventional and alkali-activated cements. *Cement and Concrete Research*, 67:66 – 73, 2015. ISSN

0008-8846. doi: http://doi.org/10.1016/j.cemconres.2014.08.006. URL http://www.sciencedirect.com/science/article/pii/S0008884614001860.

[38] Ping Yu, R. James Kirkpatrick, Brent Poe, Paul F. McMillan, and Xiandong Cong. Structure of calcium silicate hydrate (c-s-h): Near-, mid-, and far-infrared spectroscopy. *Journal of the American Ceramic Society*, 82(3):742–748, 1999. ISSN 1551-2916. doi: 10.1111/j.1151-2916.1999.tb01826.x. URL http://dx.doi.org/10.1111/j.1151-2916.1999.tb01826.x.

A

Appendix A

The following are the full data obtained through the three methods detailed in the Chapter 3 and the PDF data obtained from Argonne National Laboratory for the samples with the specifications detailed below.

This page is intentionally left blank.

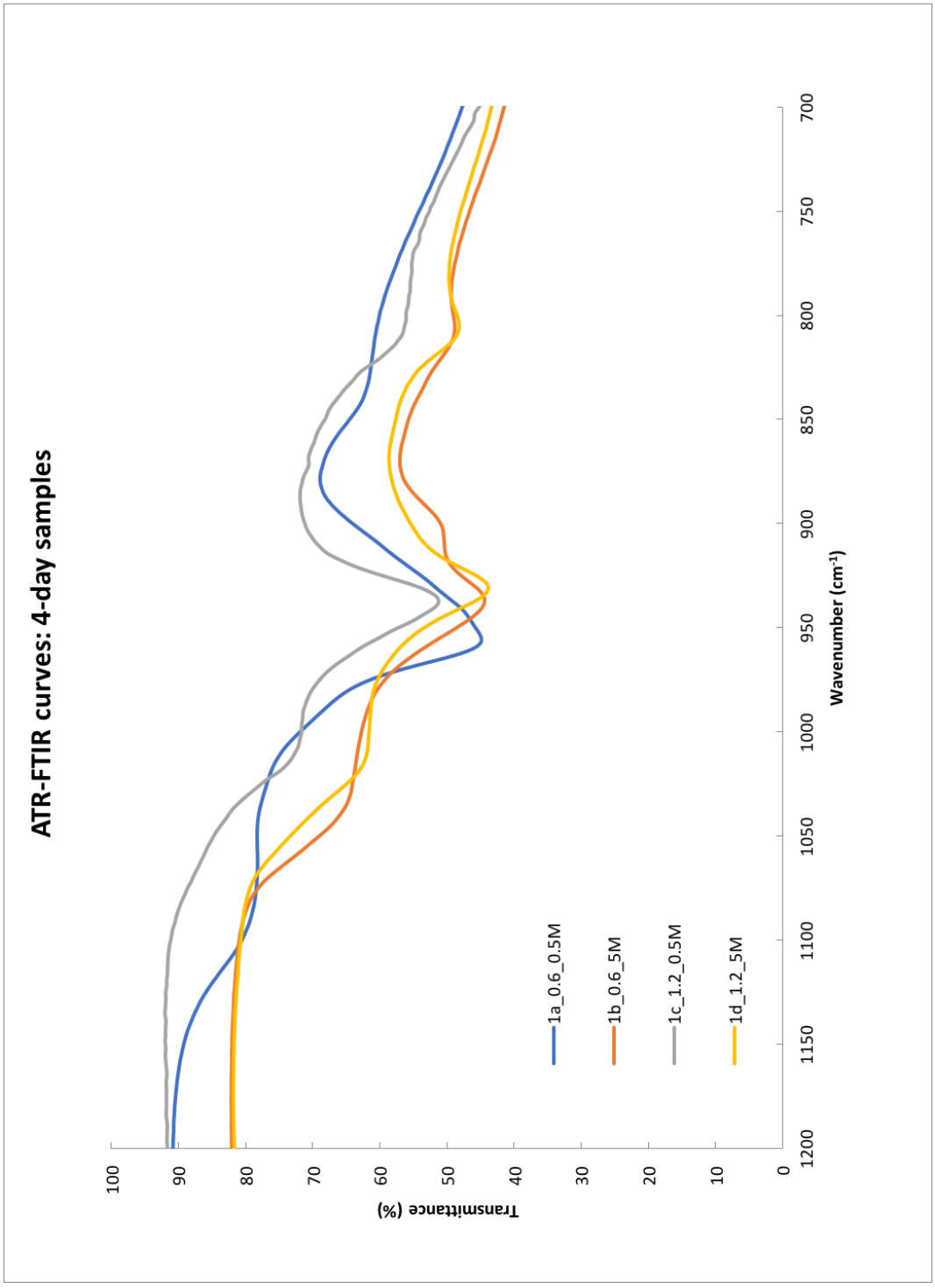

Figure A.1: ATR curves of 4-day C-N-A-S-H gel samples. The sample names follow the system: [timestep number and series letter]_[Ca/Si ratio]_[alkalinity].

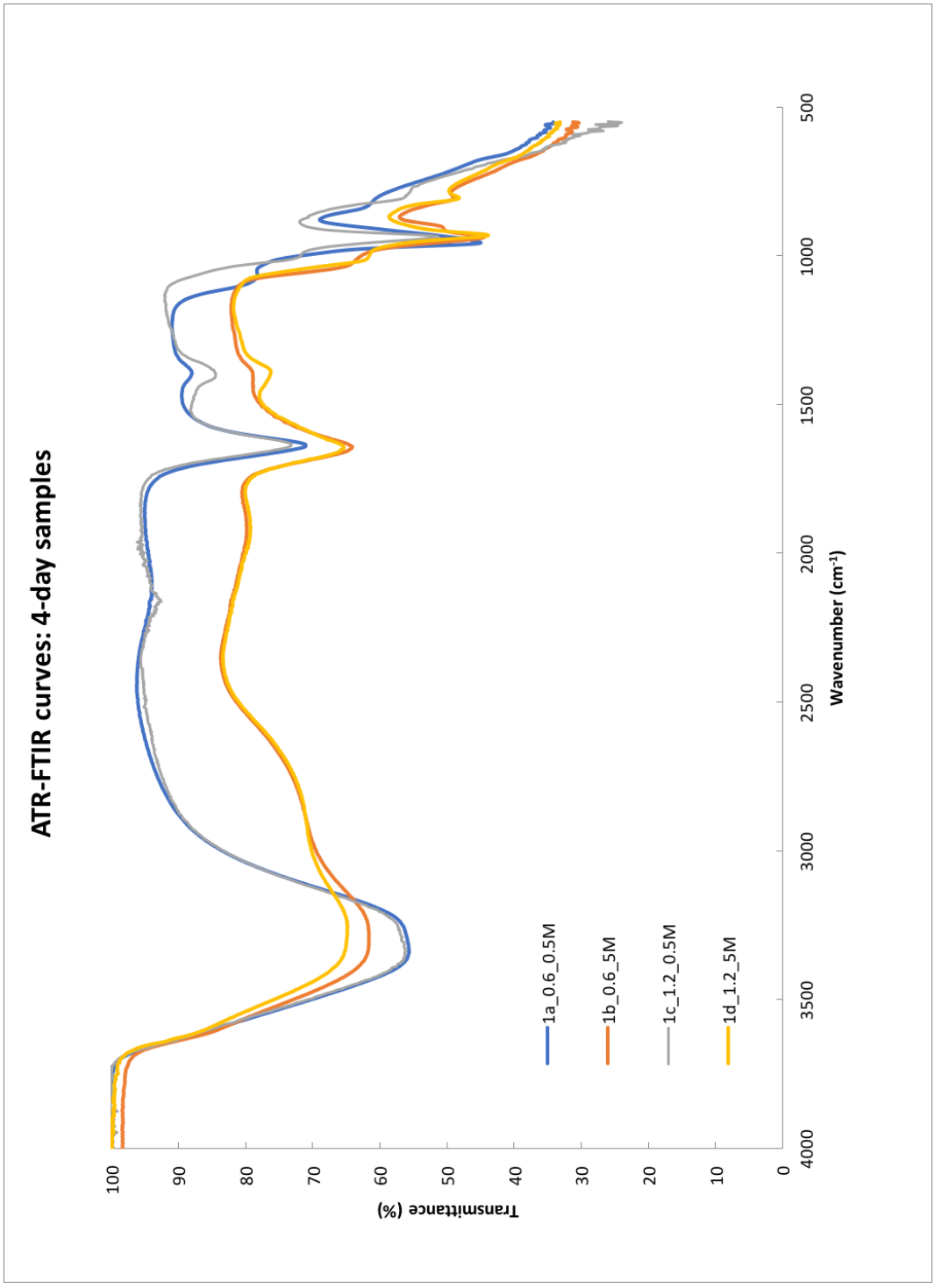

Figure A.2: Full spectrum ATR curves of 4-day C-N-A-S-H gel samples.

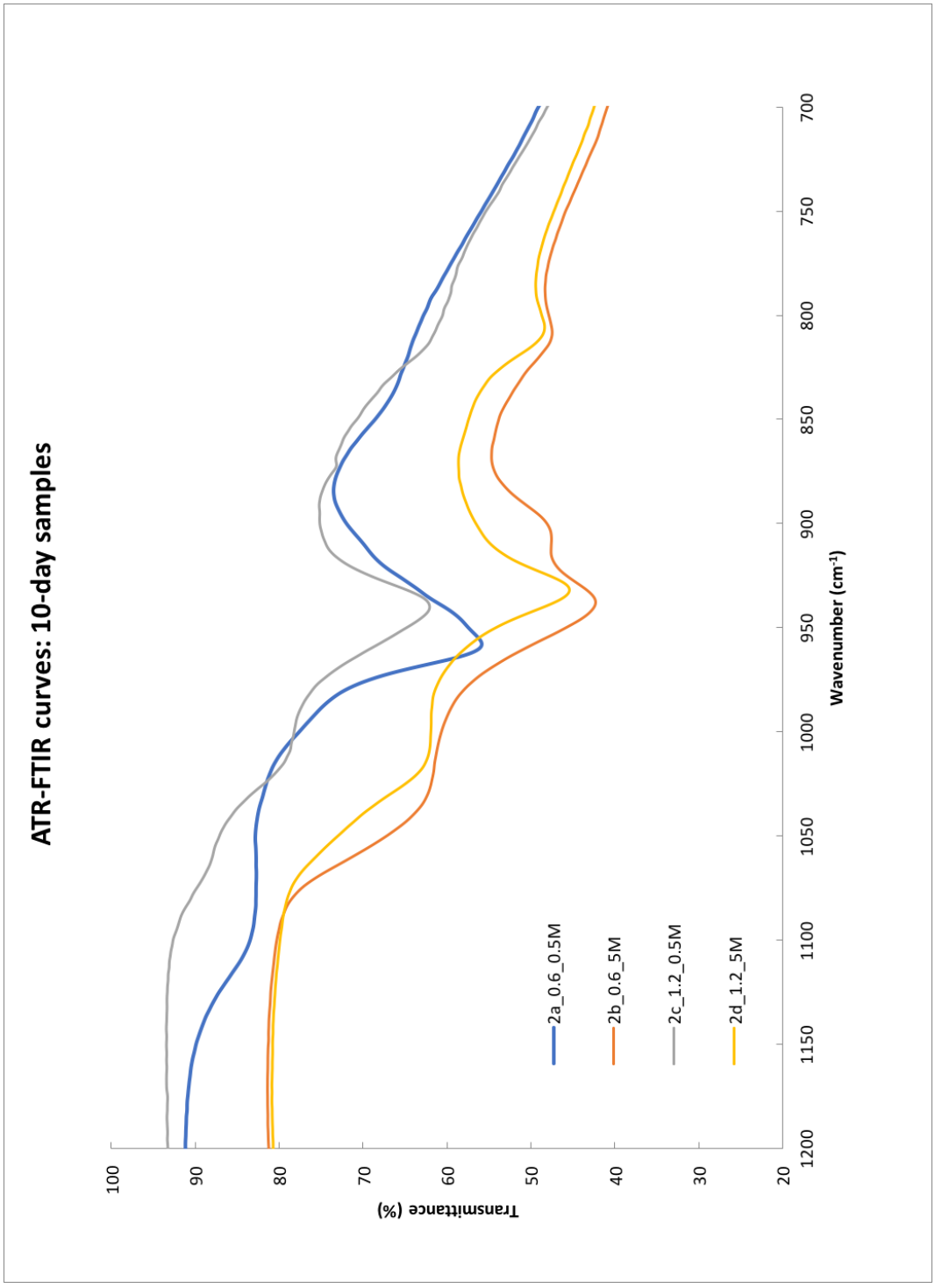

Figure A.3: ATR curves of 10-day C-N-A-S-H gel samples.

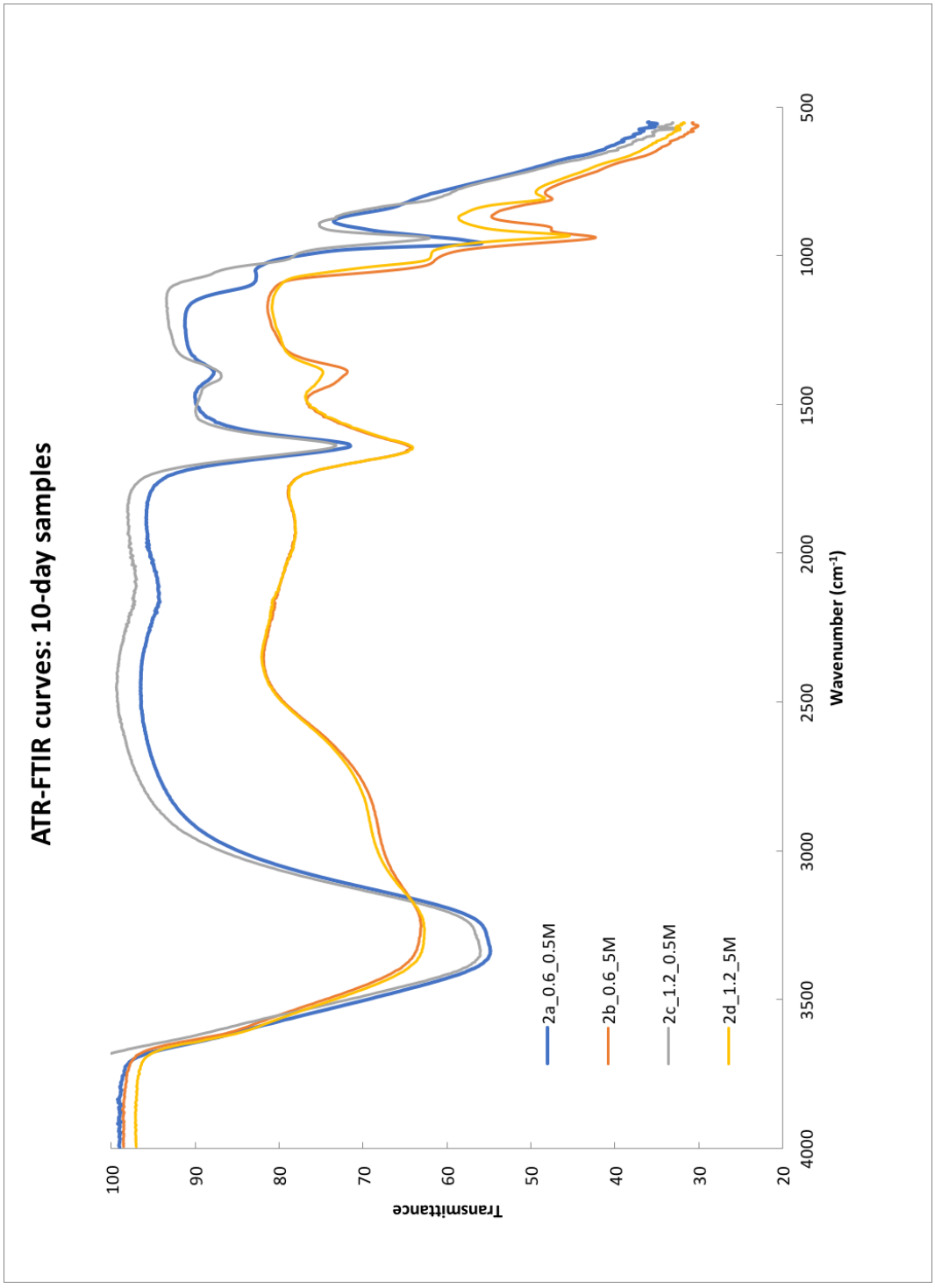

Figure A.4: Full spectrum ATR curves of 10-day C-N-A-S-H gel samples.

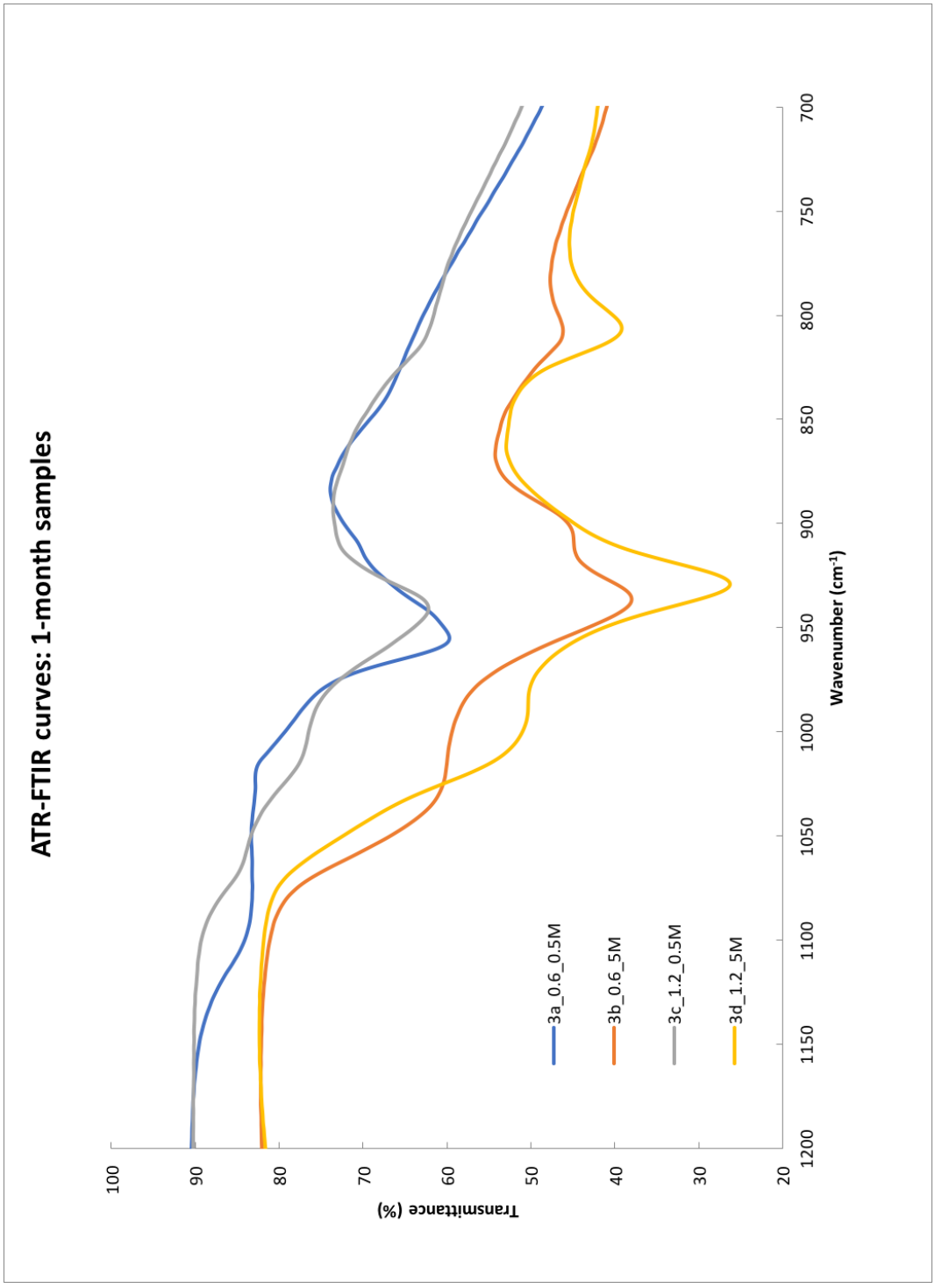

Figure A.5: ATR curves of 1-month C-N-A-S-H gel samples.

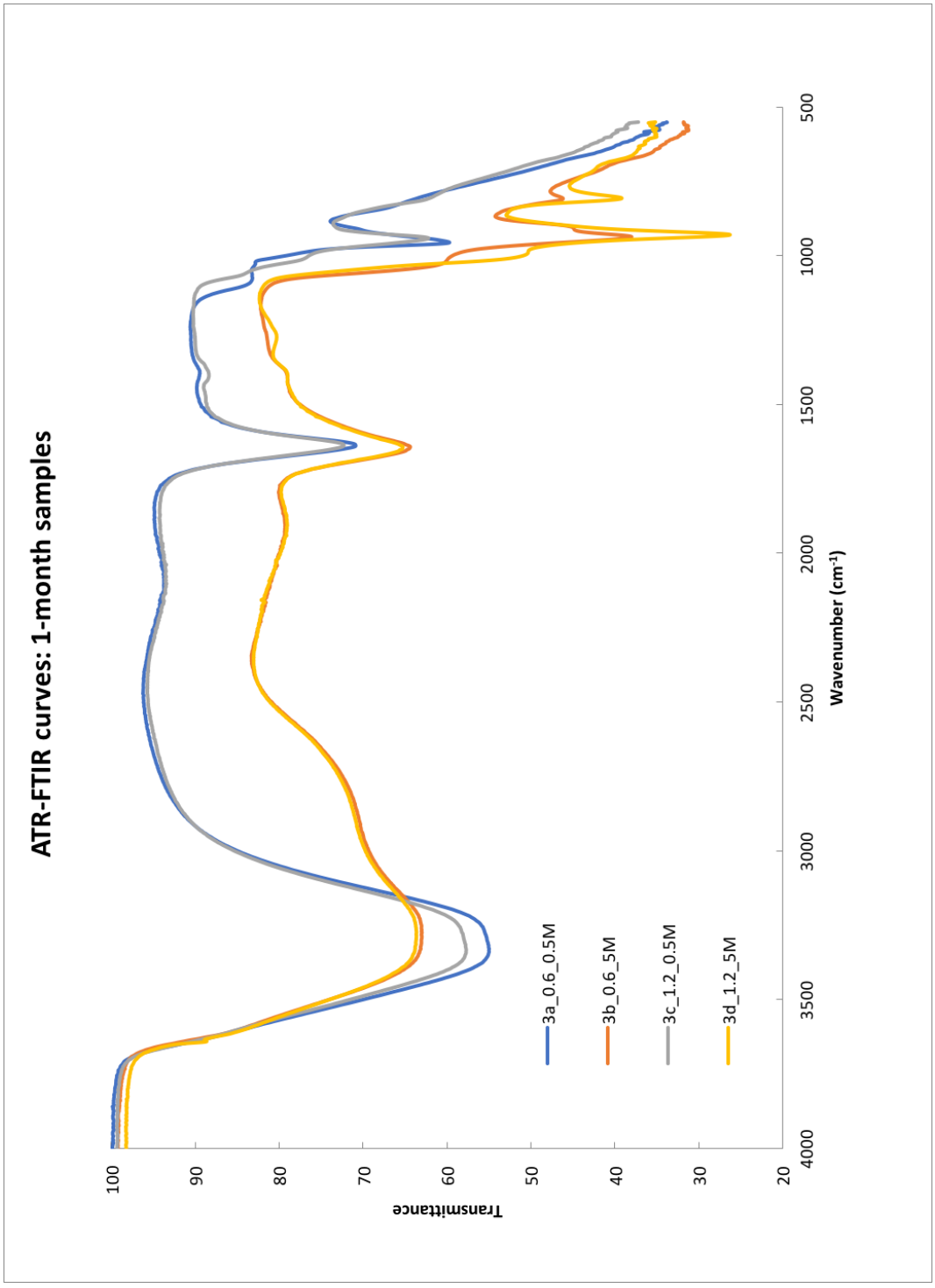

Figure A.6: ATR curves of 1-month C-N-A-S-H gel samples.

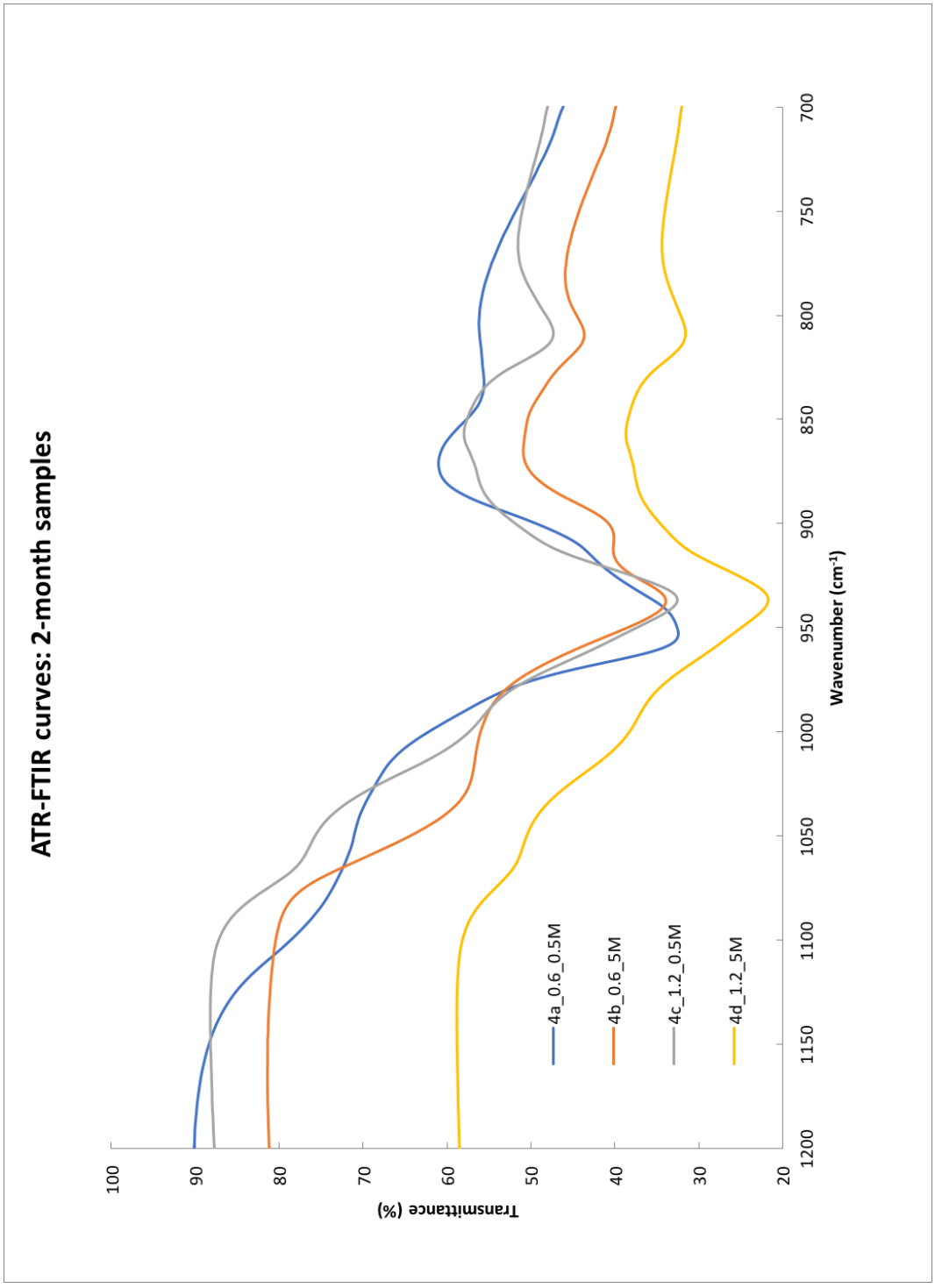

Figure A.7: ATR curves of 2-month C-N-A-S-H gel samples.

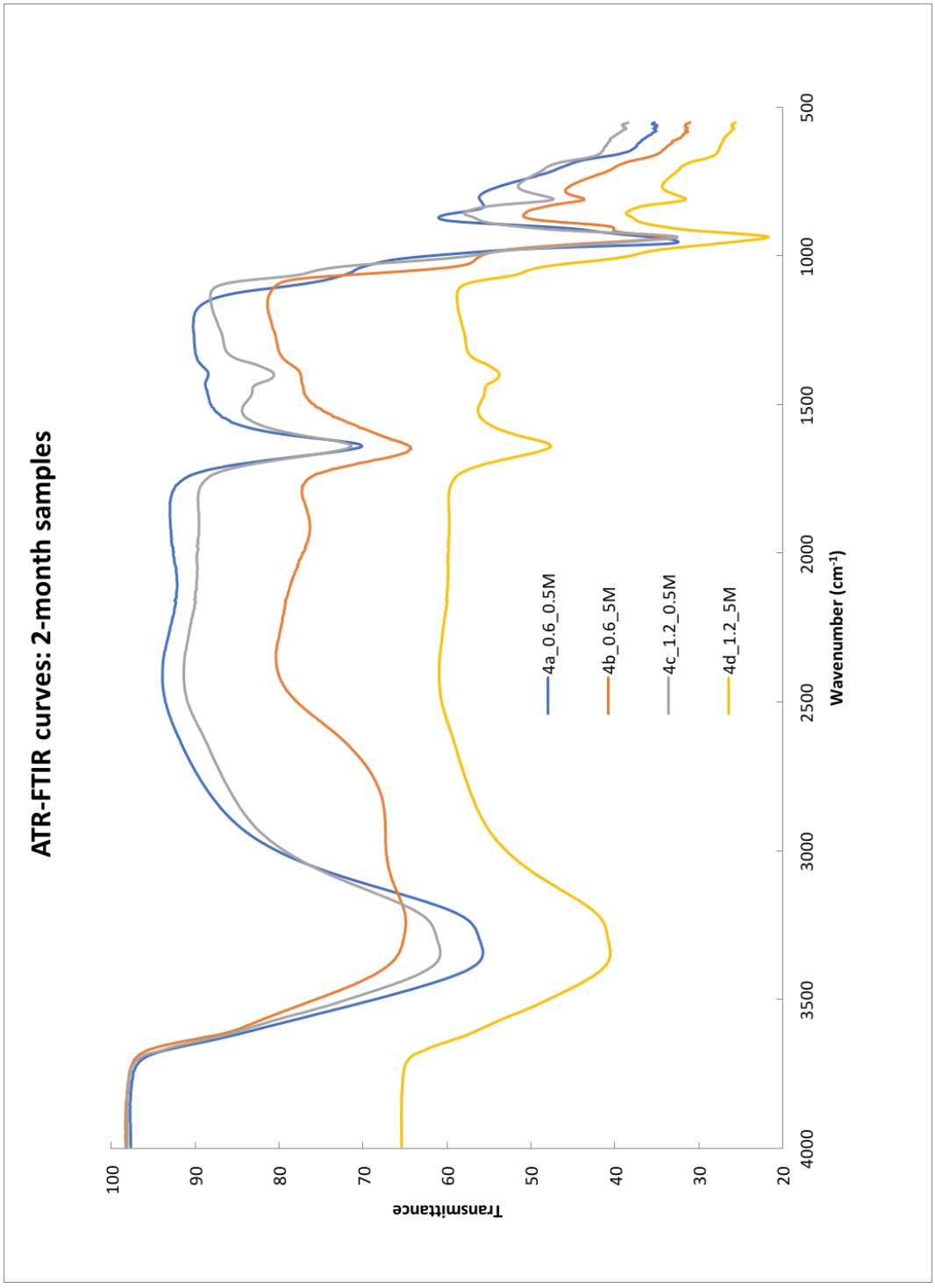

Figure A.8: Full spectrum ATR curves of 2-month C-N-A-S-H gel samples.

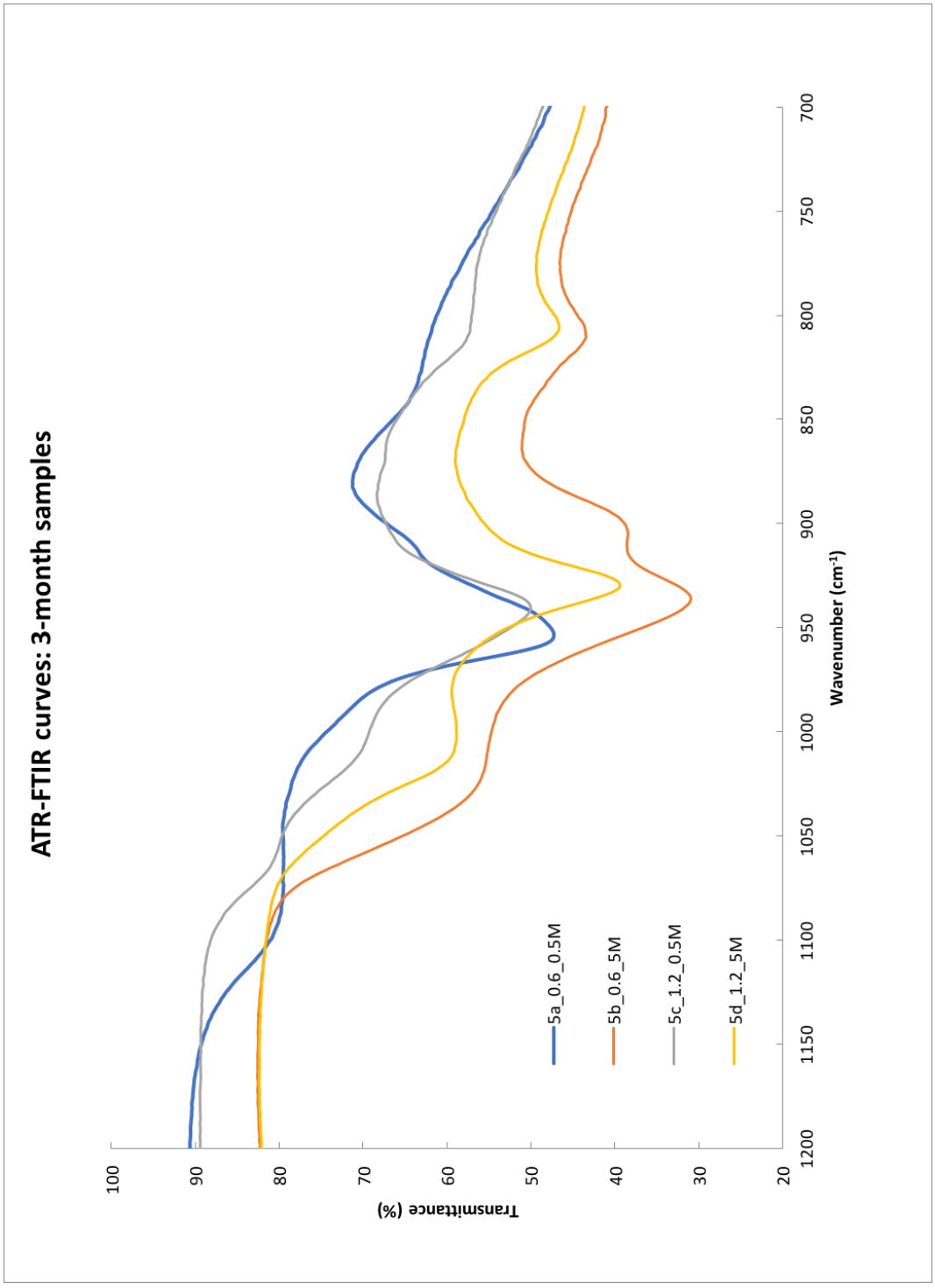

Figure A.9: ATR curves of 3-month C-N-A-S-H gel samples.

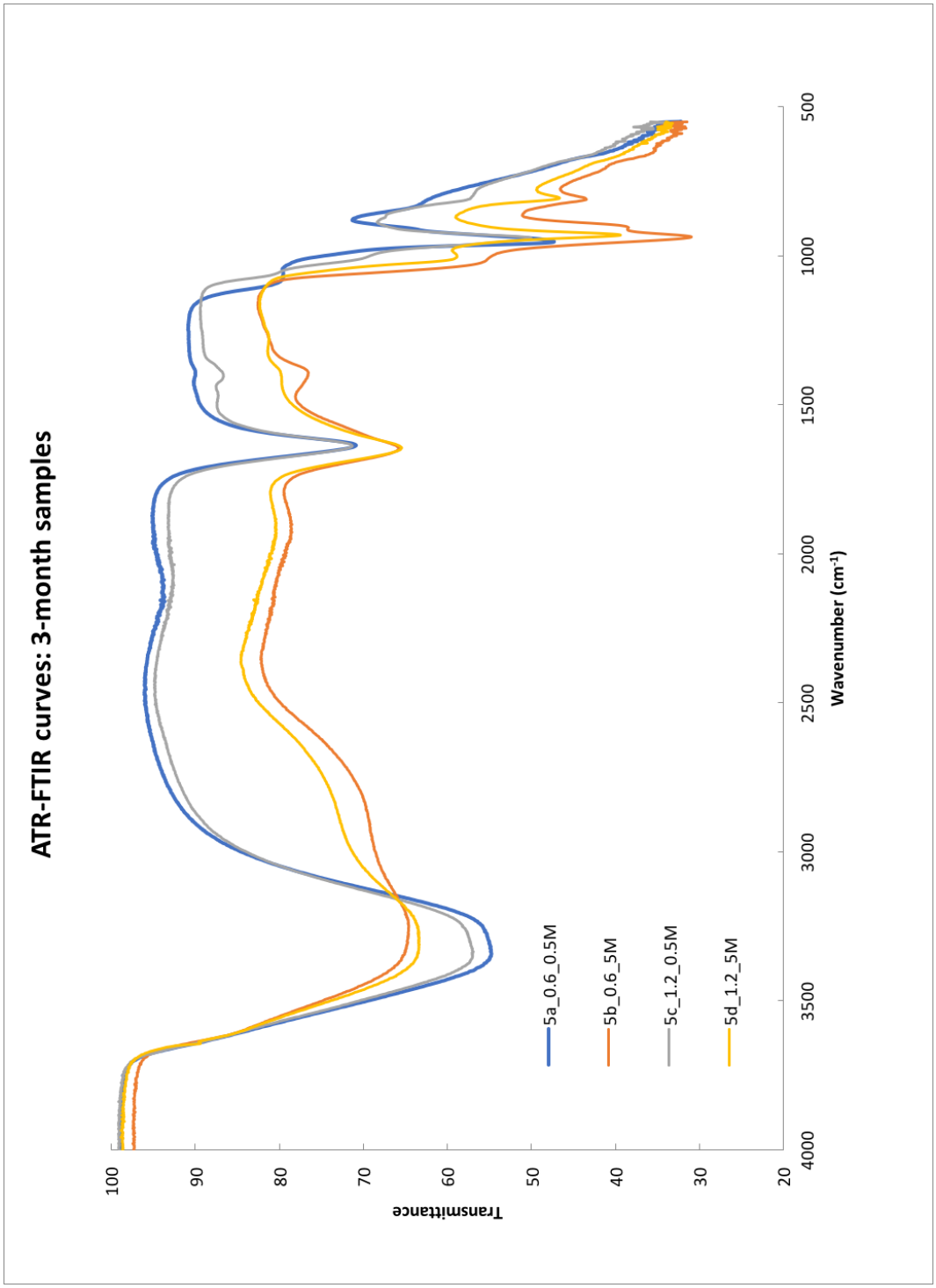

Figure A.10: Full spectrum ATR curves of 3-month C-N-A-S-H gel samples.

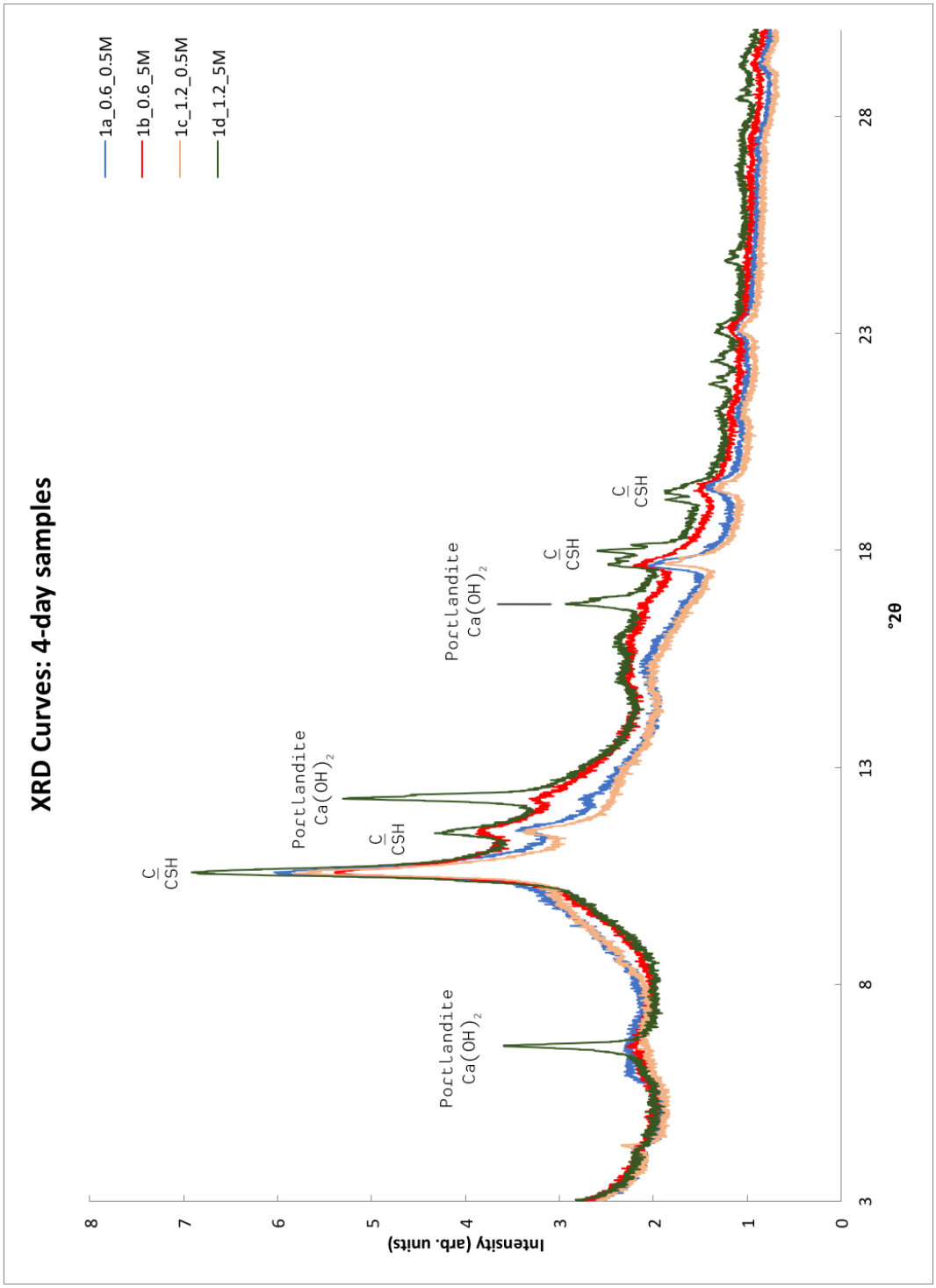

Figure A.11: XRD curves of 4-day C-N-A-S-H gel samples.

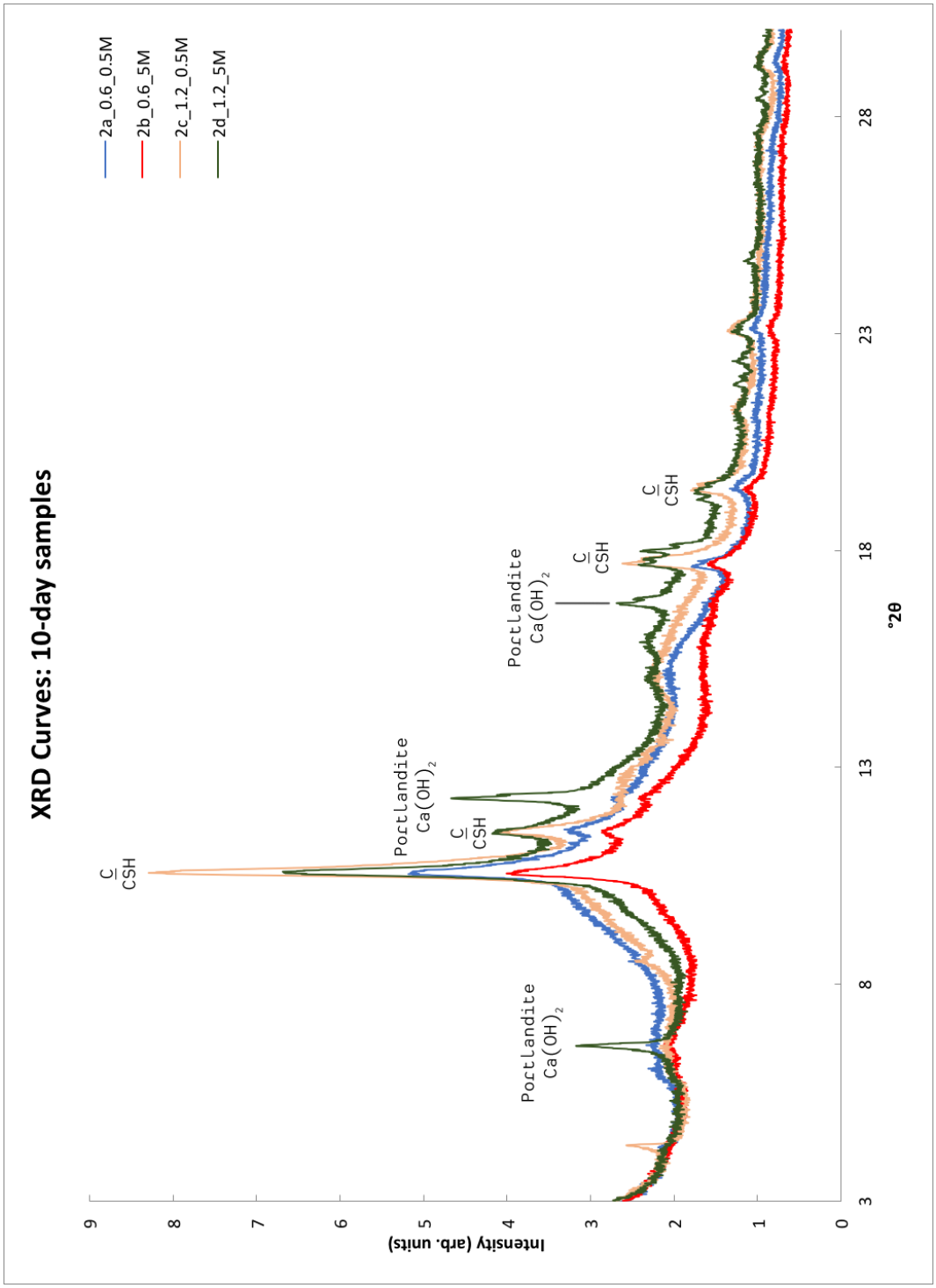

Figure A.12: XRD curves of 10-day C-N-A-S-H gel samples.

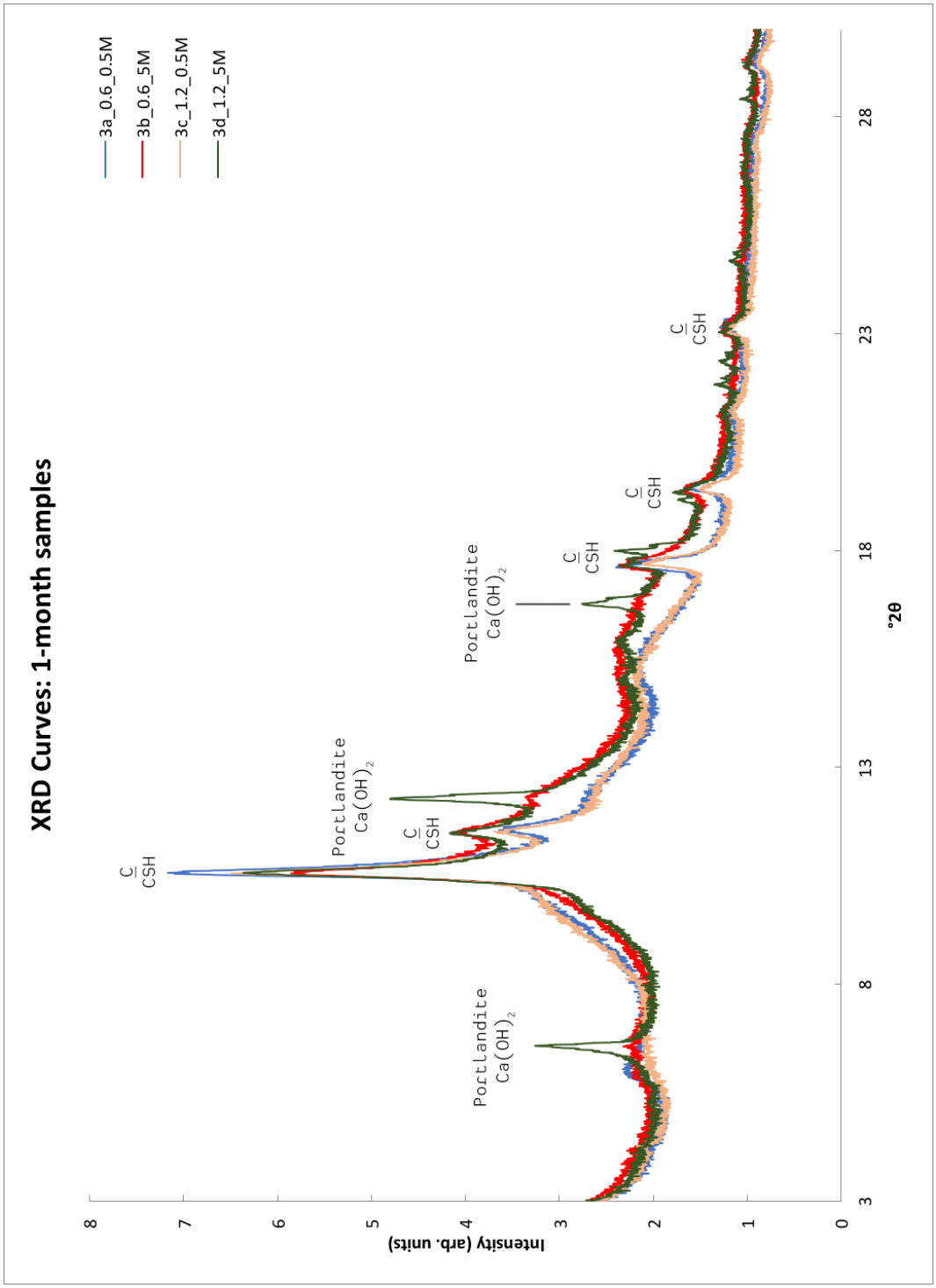

Figure A.13: XRD curves of 1-month C-N-A-S-H gel samples.

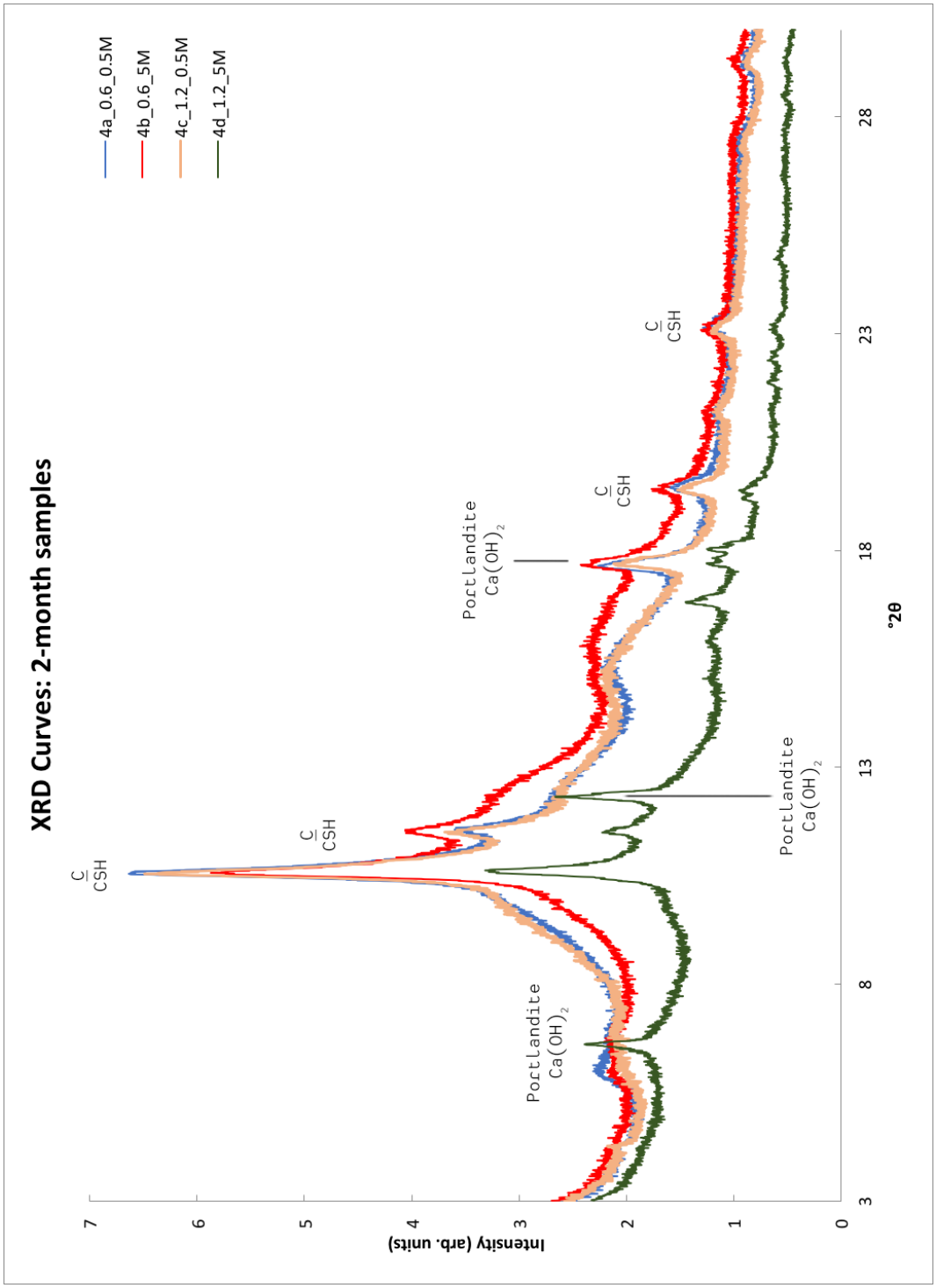

Figure A.14: XRD curves of 2-month C-N-A-S-H gel samples.

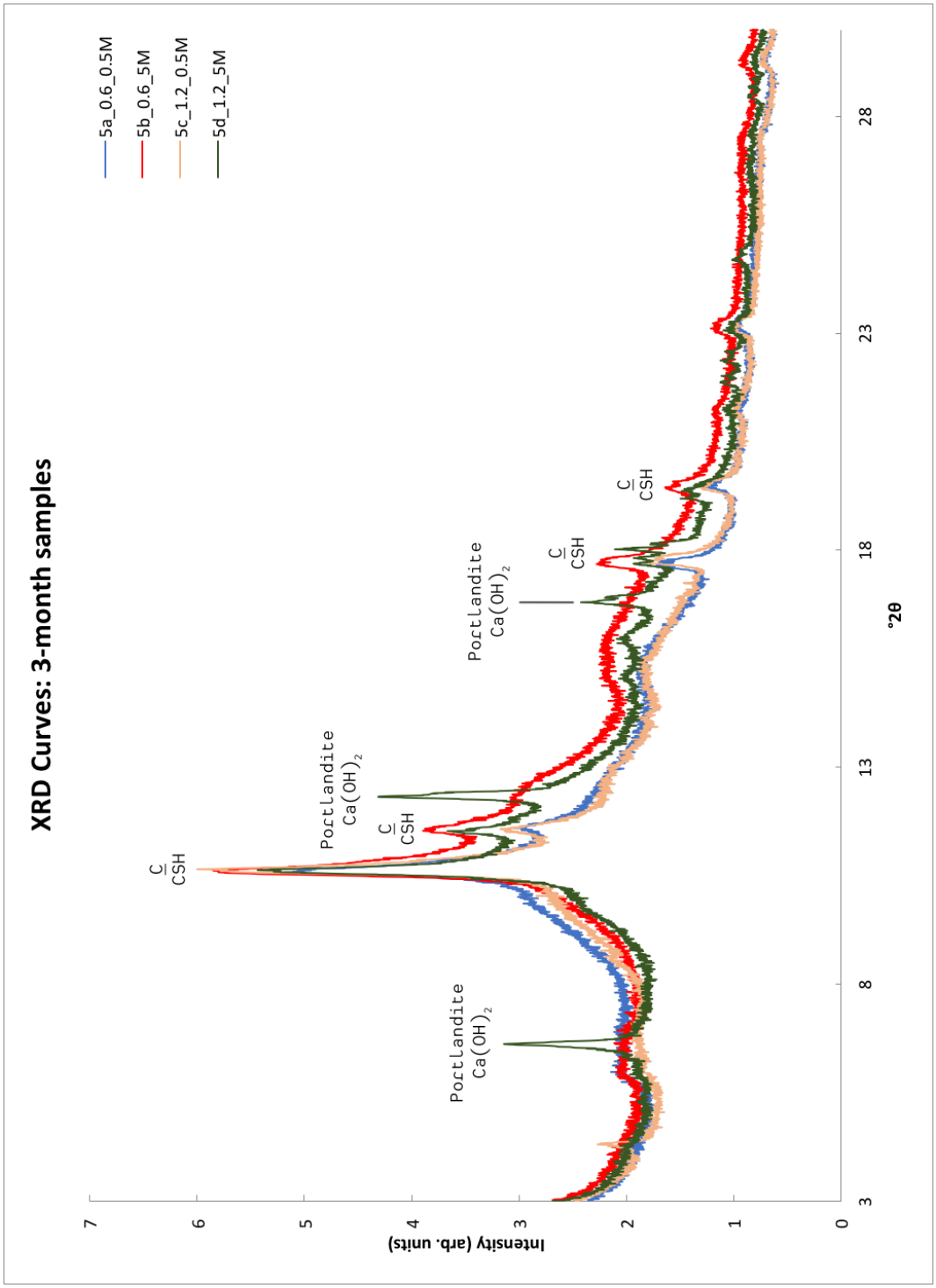

Figure A.15: XRD curves of 3-month C-N-A-S-H gel samples.

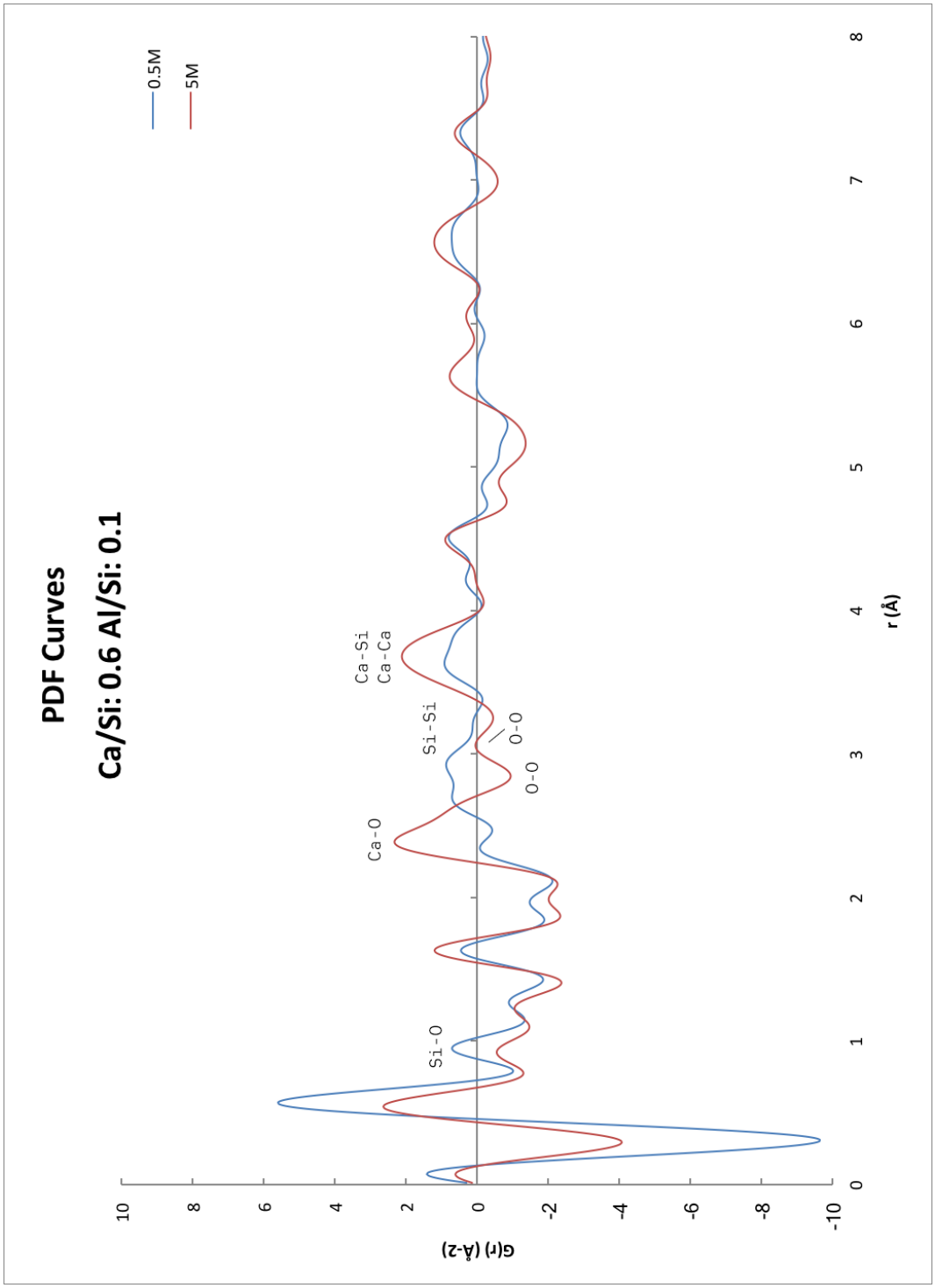

Figure A.16: Detail of PDF curve of C-N-A-S-H gel sample.

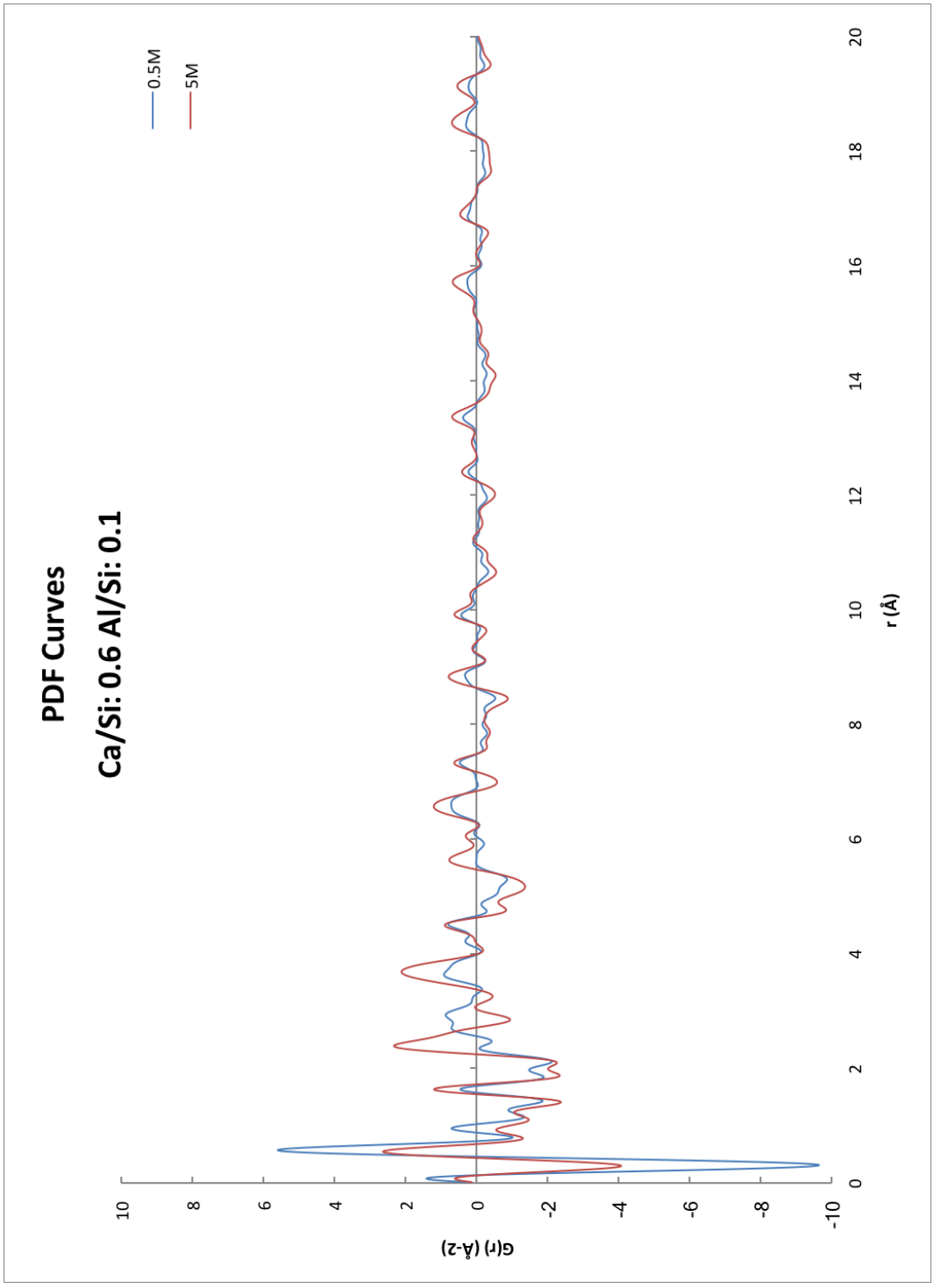

Figure A.17: Half-spectrum PDF curve of C-N-A-S-H gel sample.

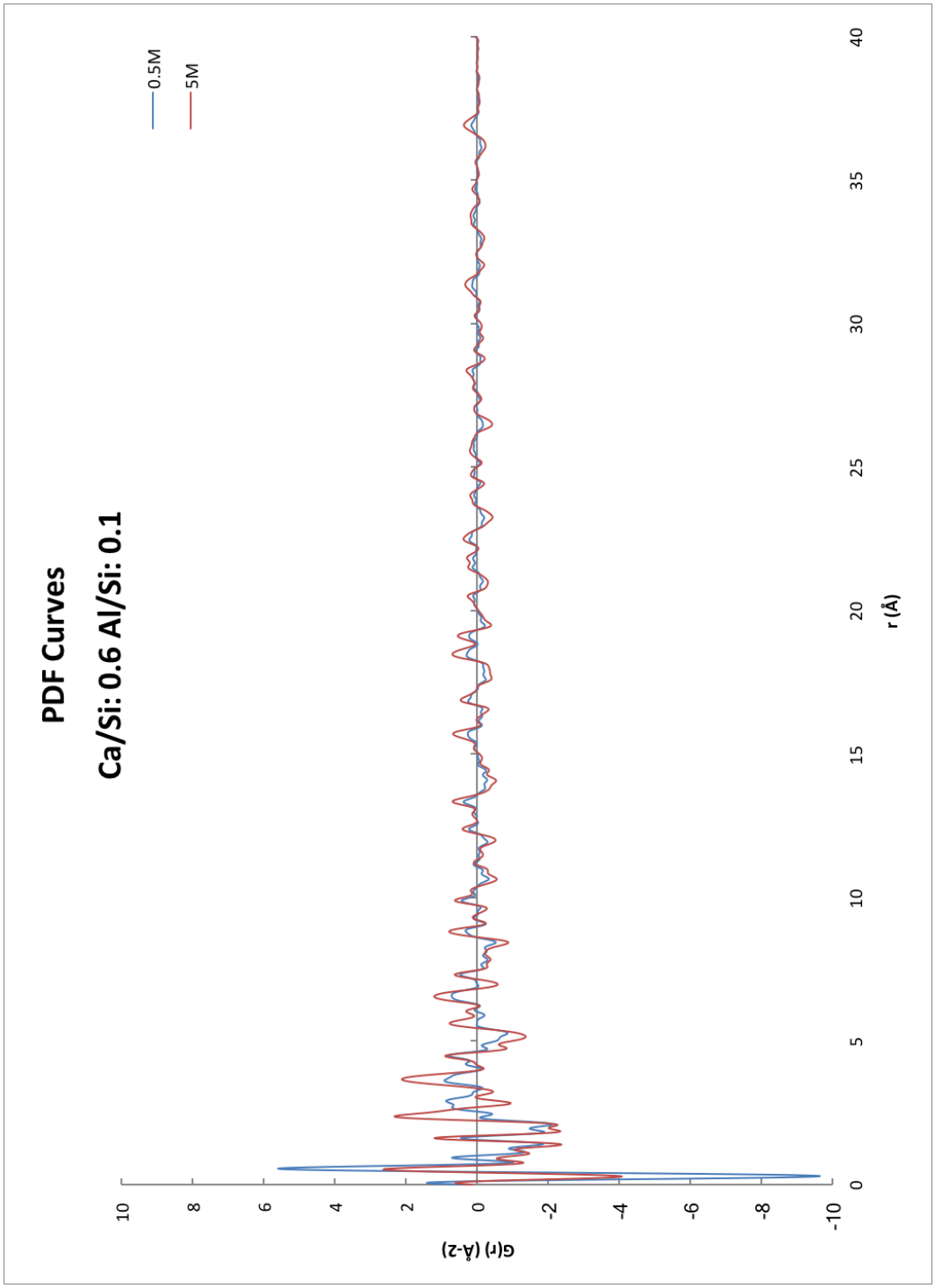

Figure A.18: Full PDF curve of C-N-A-S-H gel sample.

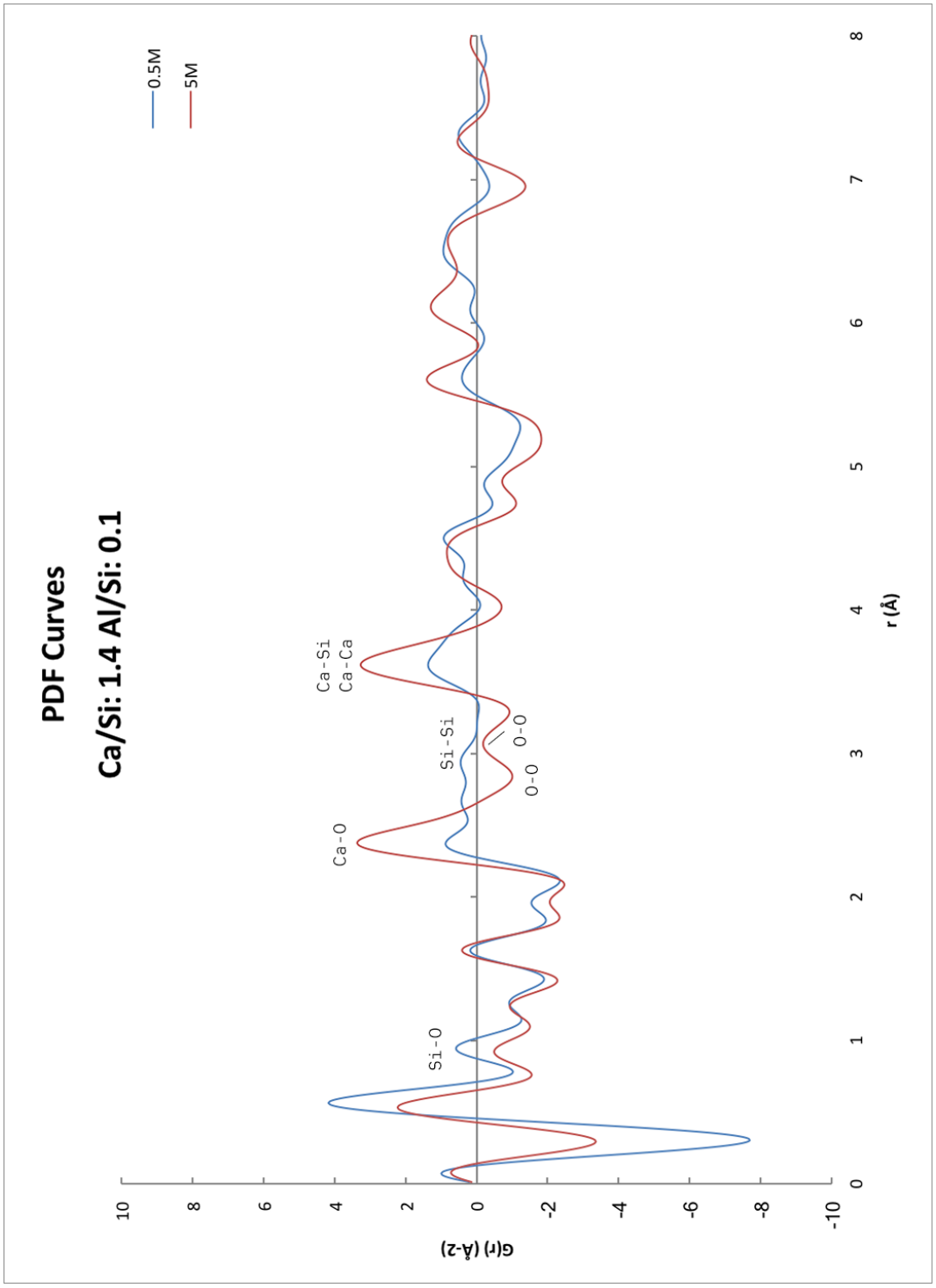

Figure A.19: Detail of PDF curve of C-N-A-S-H gel sample.

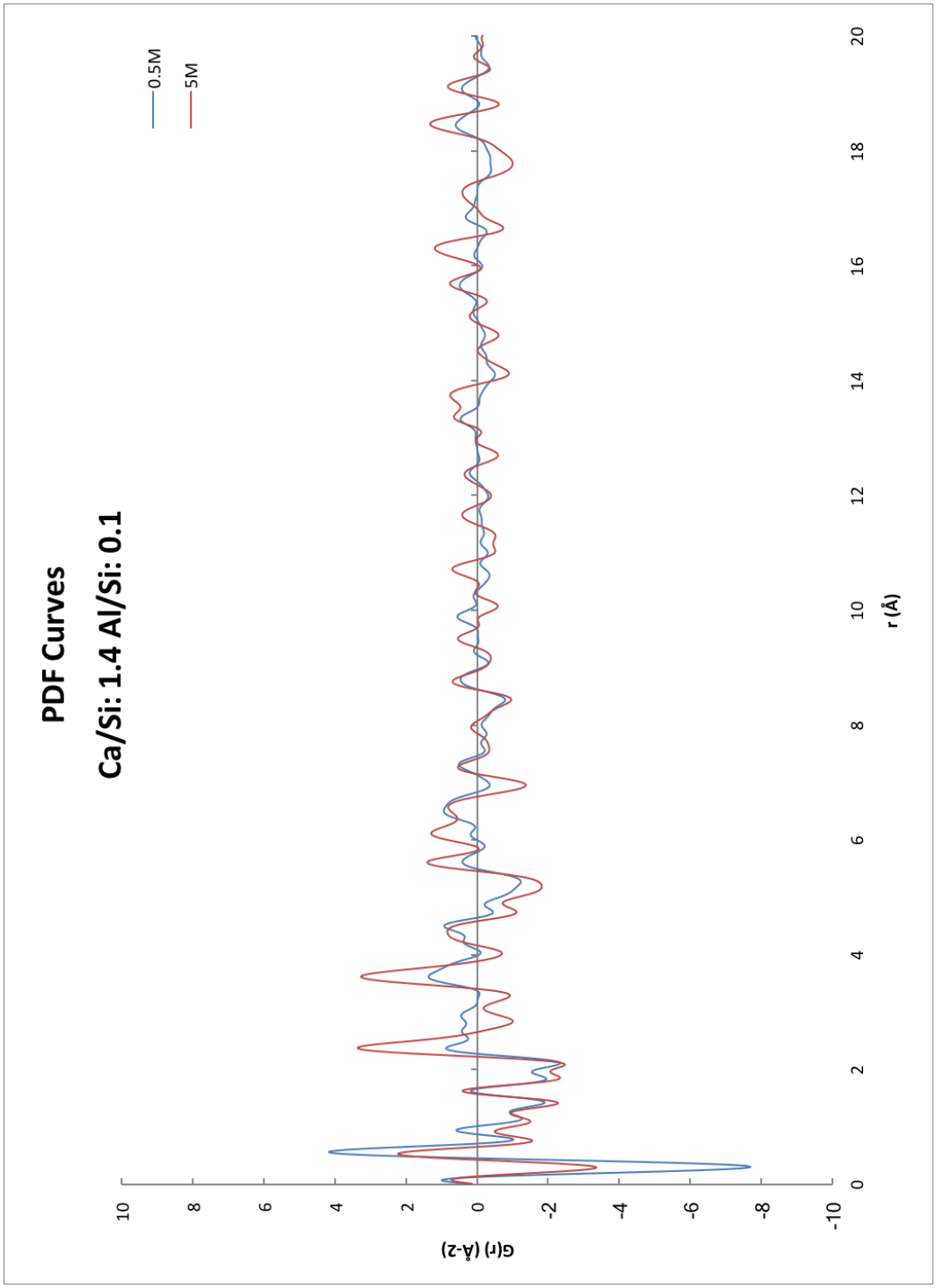

Figure A.20: Half-spectrum PDF curve of C-N-A-S-H gel sample.

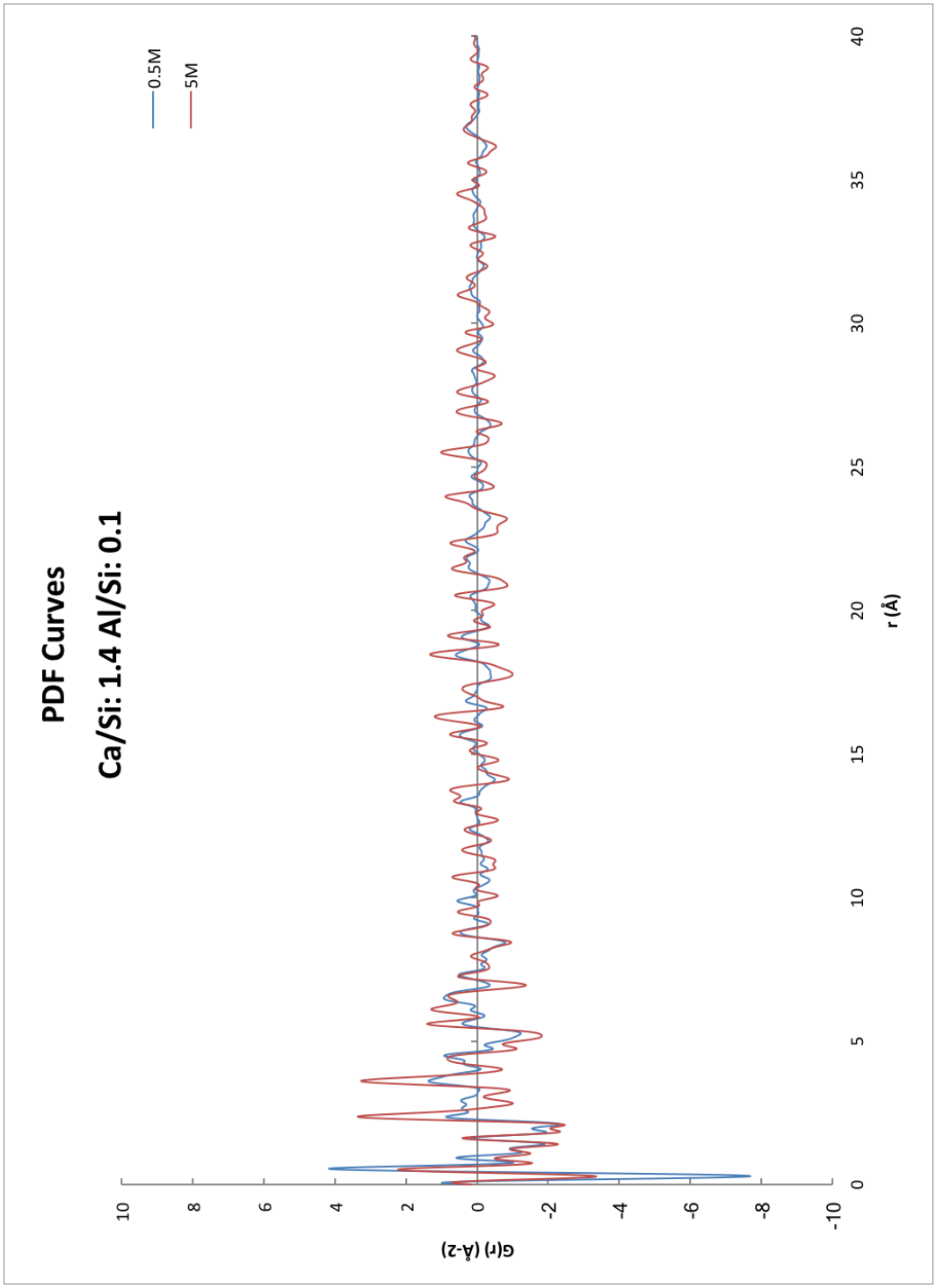

Figure A.21: Full PDF curve of C-N-A-S-H gel sample.

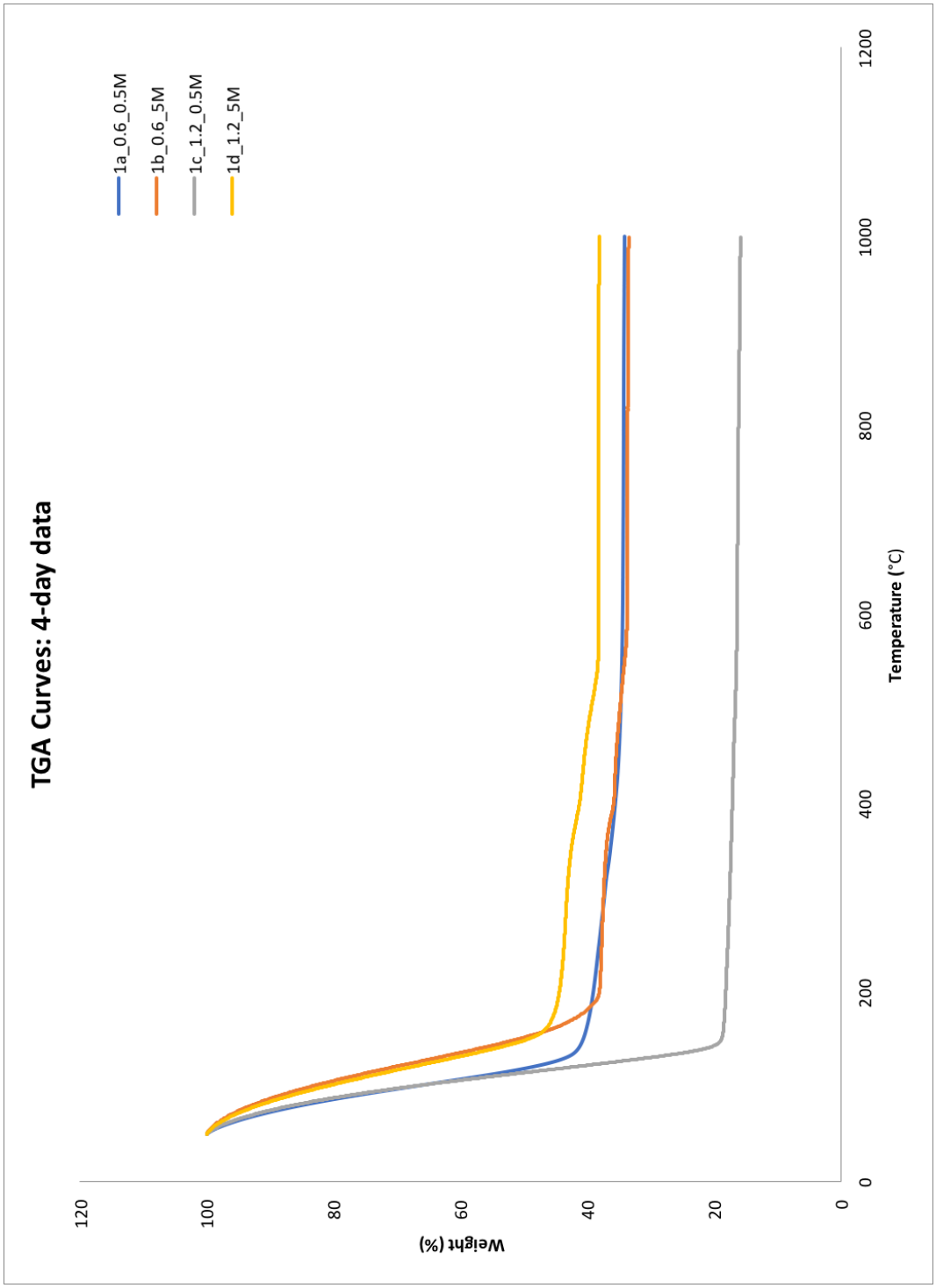

Figure A.22: TGA curves of 4-day C-N-A-S-H gel sample.

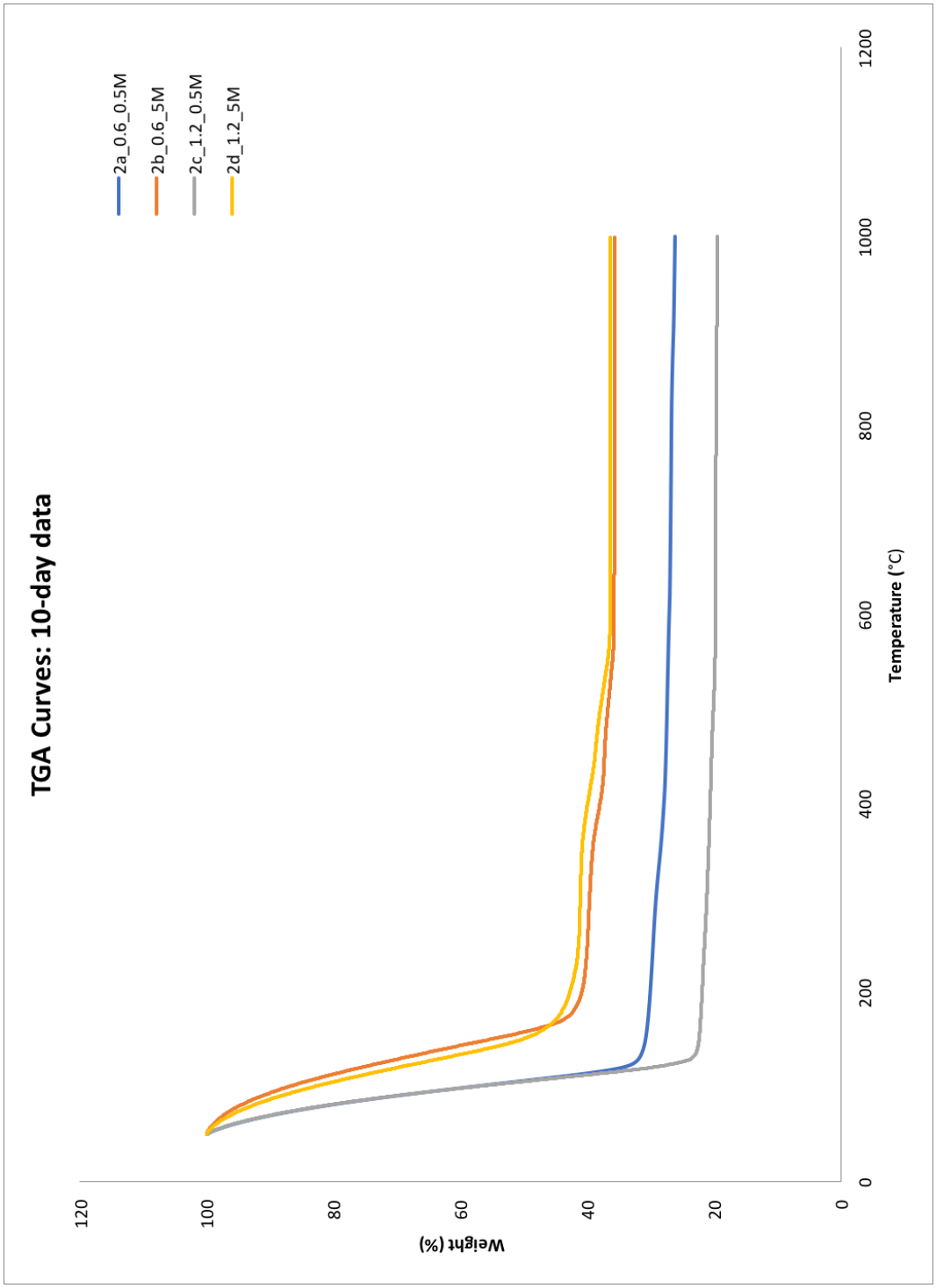

Figure A.23: TGA curves of 10-day C-N-A-S-H gel sample.

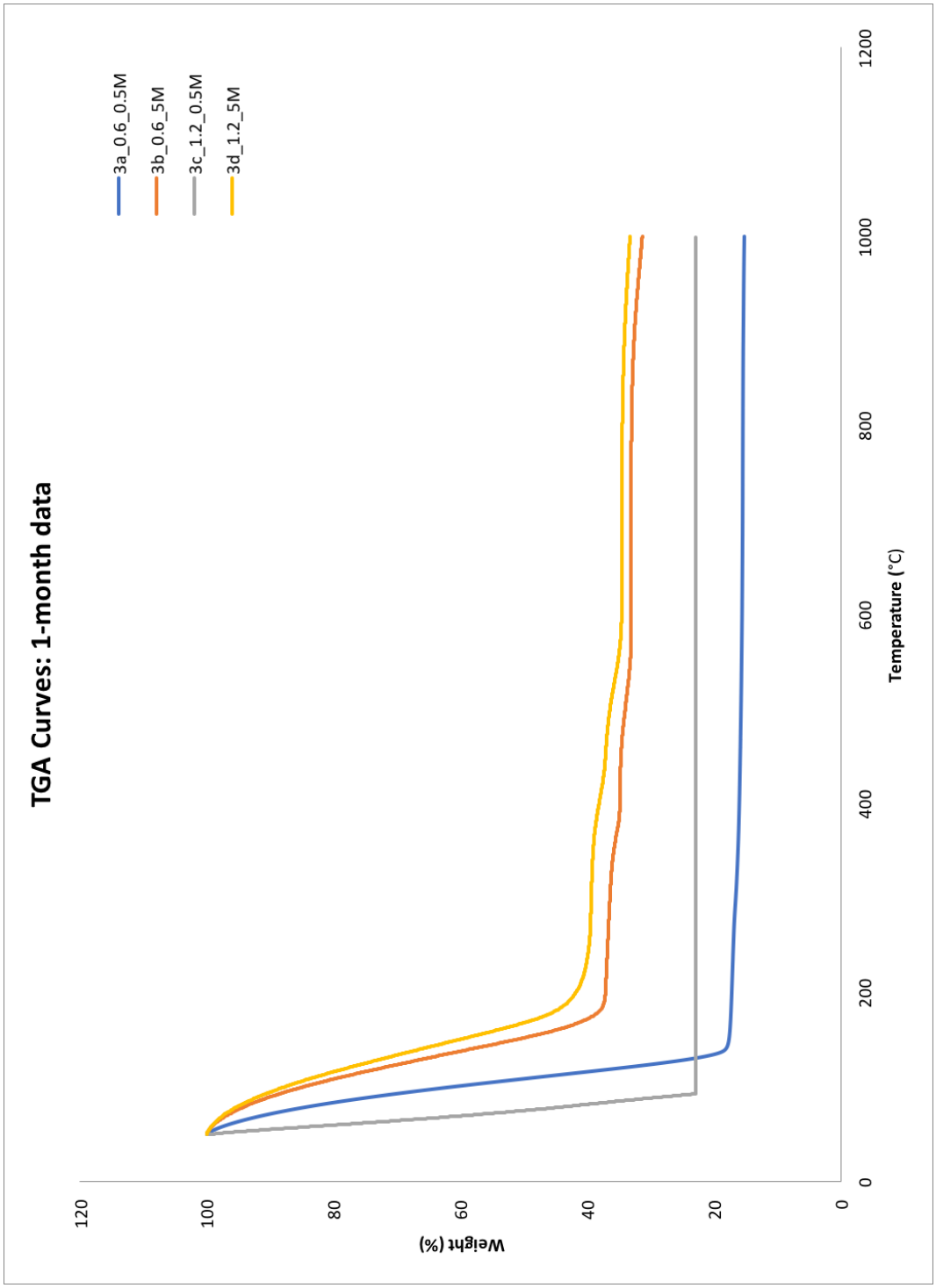

Figure A.24: TGA curves of 1-month C-N-A-S-H gel sample.

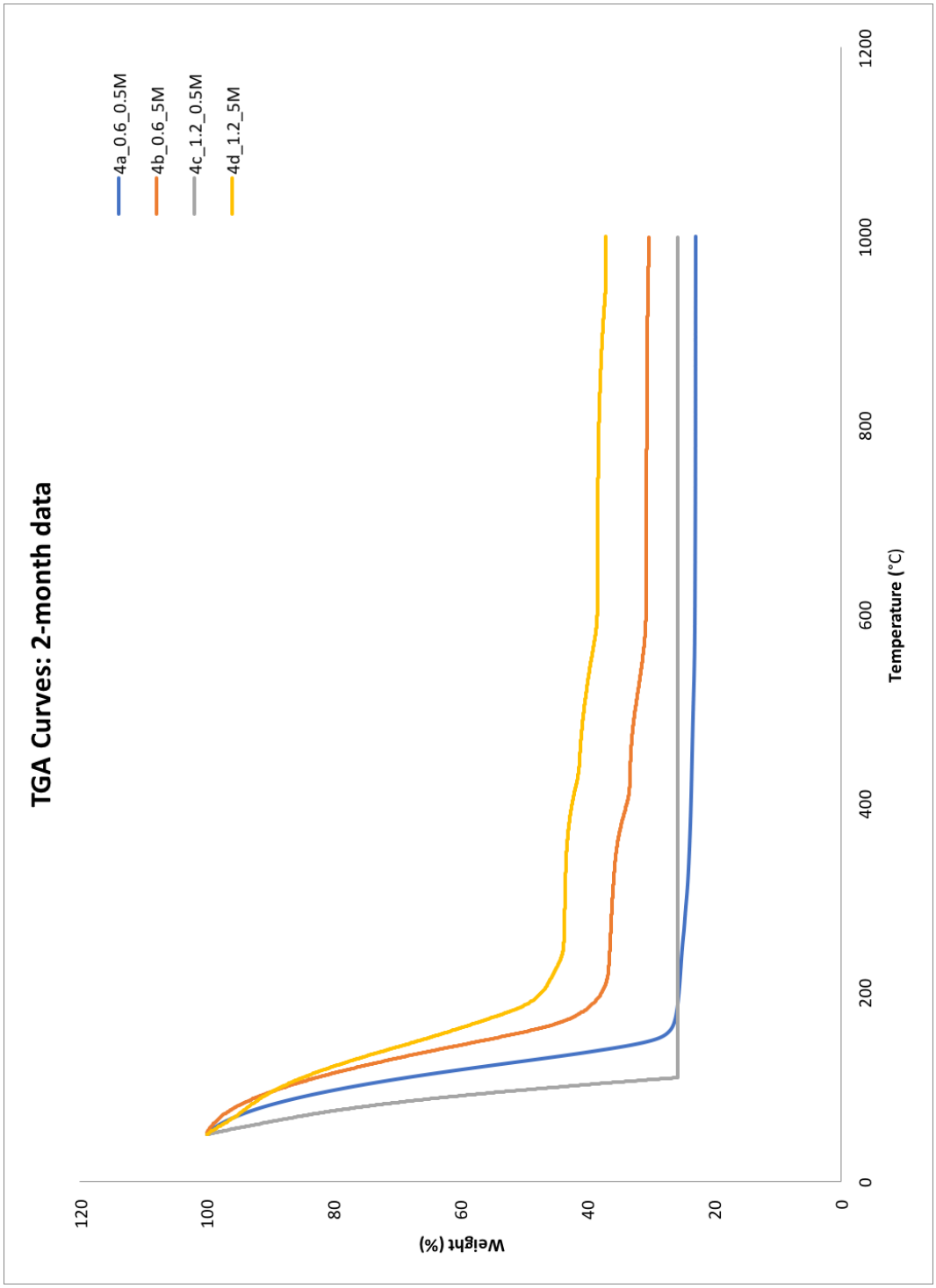

Figure A.25: TGA curves of 2-month C-N-A-S-H gel sample.

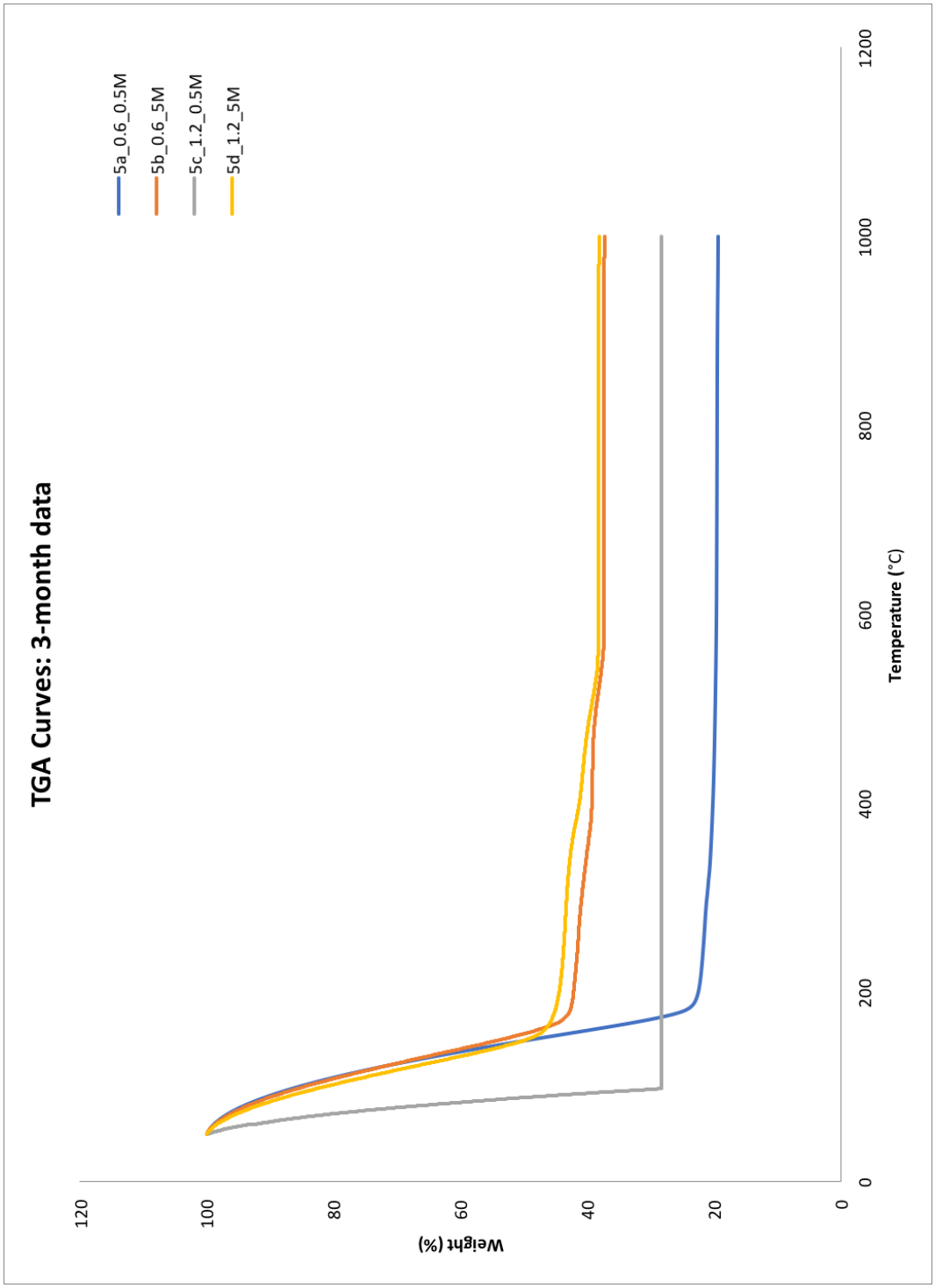

Figure A.26: TGA curves of 3-month C-N-A-S-H gel sample.

The following are guidelines on how to use the sample changer at 11-ID-B, obtained from the X-ray Science Division at Argonne National Laboratory:

Capillaries:

- The sample changer accepts Kapton tubing with 0.0435" OD. These are available through Cole-Parmer or Fisher Scientific (EW-95820-09).
- The Kapton tubing can be cut to length and one end sealed with quick setting epoxy before loading the sample. The outside of the tube must be wiped cleaned or it will not fit in the holder.
- Note for air sensitive materials: Kapton is only resistant to moisture/air in the short term. If your samples are sensitive, we recommend enclosing the sealed capillaries in an air-tight package that will be open immediately prior to measurements. Flame sealed glass capillaries will require a different experimental set up.

Sample loading:

- Samples should be fine powders, without distinguishable crystallites. Tip: Check under a microscope to be certain.
- If necessary, grind the sample in a mortar and pestle. Tip: It is easier to ensure that a sample is uniformly ground if you grind the smallest amount necessary.

- The X-ray beam hits the capillary 5-6 mm from the bottom of the tube. To ensure the sample is in the beam, fill a >10 mm length of the capillary. Tap the capillary on the bench to ensure the powder is densely packed. Tip: For smaller samples, seal the bottom of the tube with a longer epoxy plug, load 2-3 mm sample, and trim the bottom of the tube to center the sample at the beam height.

- Once your sample is loaded, the open end of the capillary should be sealed. We recommend using epoxy. While clay is convenient in the short term, it often becomes dislodged during handling. Tip: A little epoxy can be sucked into the open end of the tube by pinching then releasing the tube while dragging the end through an inverted pool of epoxy.

- Capillaries should be individually labeled.

- Sample sequence: Sample 1 should always be your most weakly scattering and/or lowest crystallinity sample, with subsequent samples in order of increasing scattering strength/crystallinity.